DIFFERENTIAL REPRESENTATION OF DRUG-SEEKING WITHIN VENTRAL PALLIDAL SUBREGIONS

By

DAVID HAMILTON ROOT

A Dissertation submitted to the

Graduate School-New Brunswick

Rutgers, The State University of New Jersey

in partial fulfillment of the requirements

for the degree of

Doctor of Philosophy

Graduate Program in Psychology

written under the direction of

Mark O. West, Ph.D.

and approved by

_____

_____

_____

_____

New Brunswick, New Jersey

January 2012

ABSTRACT OF THE DISSERTATION

Differential representation of drug-seeking within ventral pallidal subregions

By DAVID HAMILTON ROOT

Dissertation Director:

Professor Mark O. West

Ventral pallidum (VP) neurons exhibit changes in firing rate (FR) immediately prior to and/or following cocaine-reinforced responses. We first aimed to determine whether the changes in FR surrounding cocaine-seeking responses were coincident with behaviors such as approaching the manipulandum, responding on the manipulandum, and retreating away from the manipulandum. Second, we aimed to determine whether changes in FR during cocaine-seeking behaviors differed between VP subregions. Prior to recordings, animals exhibited both task and skill learning, replicating previous results using this operant. 171 single-units in the ventromedial VP (VPvm) and 48 in the dorsolateral VP (VPdl) were recorded in well-trained animals during cocaine self-administration. Baseline FR and waveform characteristics did not differ between subregions. VPdl neurons exhibited a greater absolute change in FR over VPvm neurons during approaches as well as approaches divided into cued and uncued conditions. VPdl neurons exhibited a greater absolute change in FR over the VPvm during responses as well as responses divided into those cued/reinforced and uncued/unreinforced conditions. VPdl neurons were more likely to exhibit a similar change in FR during approach and

response than VPvm neurons. VPvm neurons were heterogeneous, changing FRs during approach or response alone, or both. No differences were found between subregions during retreat behavior. VPdl neurons exhibited a greater absolute change in FR over the VPvm for retreats in which the pump was activated prior to or during a retreat, but not for retreats when the pump was not activated. Given that VPdl neurons exhibited a greater change in FR than VPvm neurons during approach and response, VPdl may be involved in the expression of drug-seeking behaviors through projections to "motoric" regions such as subthalamic nucleus and substantia nigra. Furthermore, because VPdl neurons were more likely to continue their change of FR from approach through response while VPvm were more selective (e.g., approach alone, response alone), it is suggested that cocaine-seeking behaviors are differentially represented within VP subregions. The VPvm projects primarily to the mediodorsal thalamus and ventral tegmental area. Heterogeneous firing patterns within the VPvm may be involved in maintaining a representation of behavioral characteristics or sequences of self-administration behaviors.

ACKNOWLEDGEMENTS

I have been privileged with the support of many people over this journey towards the Ph.D. degree. First and foremost I thank my parents, Glenn and Dr. Sharon Root. Quite simply, this achievement would never have been possible without their infinite love, support, and encouragement. Second, I thank my wonderful fiancé Lauren for her love and support. I am fortunate to be able to share my life with you. Third, I am grateful for the support of many friends from several groups. Thank you to my home group, Bryan Beil, Jeff Beagley, Juan Sichon, Heather Reed, Beth Gibson, and Jen Rich. Thank you to my lab mates, David Barker, Sisi Ma, Kevin Coffey, and Tony Pawlak, Thomas Grace Sr, and Jackie Thomas. Special thanks to David Barker, for always intellectually rich discussions and hard work as well as Sisi Ma for teaching me Matlab, revolutionizing data analysis forever. Thank you to colleagues/friends Pete Pantelis, and Drs. Ken Light and Jen Czerniowski. Thank you to undergraduates who trained me early on (Courtney Harding, Alayna Berkowitz, and Smruti Patel) as well as those critical for the analysis of the present experiment (Laura Megehee, Brendan Striano, and Carla Ralston).

If I have found professional success, it has been because I truly stood on the shoulders of giants. My interest in neuroscience blossomed from the teachings of Dr. Sheri Tershner at Western New England College (now University). Her decision to allow me into her lab and be added to their poster presented at Society for Neuroscience was wholly responsible for getting to the next step of my career (grad school). Furthermore, my own interest in the neural mechanisms of learning with regard to drugs of abuse directly stemmed from her. I am grateful to the faculty at Seton Hall University, including Drs. Michael Vigorito, Amy Hunter, and Sulie Chang.

Dr. Michael Vigorito taught me what it meant to be a scientist and teacher. His teaching of soldering, programming, chamber-building, and course material have proven invaluable. I am indebted to Drs. Amy Hunter and Tonio Fabbricatore (Rutgers) for teaching me stereotaxic surgery. Thank you to Dr. Sulie Chang, who taught me valuable lessons on grant writing and biological techniques. Thank you Drs. David Smith and Donald Stehouwer at the University of Florida for their support during a difficult time and beyond. Thank you to Linda King, who taught me perfusions and immunohistochemistry. Your contribution to this research project was vital and would not have been completed with you.

To Dr. Mark West, my mentor and advisor, thank you for your continued support, endless wisdom, experimental training in every aspect of this experiment and others, and general advancement of my career. I am continually inspired by your kind demeanor, never-ending patience, and ability to seemingly solve any problem or know any answer with ease. I hope to be as great a mentor to others as you have been to me. Thank you to Drs. Alex Kusnecov, Elizabeth Torres, Laszlo Záborszky, and Celeste Napier for stimulating discussions and imparting neurobiological wisdom. Thank you to Dr. Danielle McCarthy for her knowledge and teachings regarding human addiction.

Lastly, thank you to the bands listed below for entertaining me while spending endless nights and weekends at the lab: a wilhelm scream, anberlin, andy mckee, antoine dufour, arsis, beloved, between the buried and me, burnt by the sun, comeback kid, darkest hour, defeater, foo fighters, hopesfall, into the moat, ion dissonance, it prevails, mindless self indulgence, name taken, protest the hero, shai hulud, silent drive, silverchair, spineshank, steel train, the arusha accord, the carrier,

the ghost inside, the snake the cross the crown, this is hell, tool, twelve tribes, verse, with honor, and vision of disorder.

TABLE OF CONTENTS

INTRODUCTION

The mesolimbic dopamine system is critical for cocaine self-administration (Roberts et al. 1977, 1980; Roberts and Koob, 1982). The primary target of mesolimbic dopaminergic neurons is the nucleus accumbens (NAcc) and lesions or GABAergic agonists injected into the NAcc decrease cocaine-seeking in rats (Roberts et al. 1977; McFarland and Kalivas, 2001; McFarland et al. 2004). NAcc single unit recordings have revealed rapid phasic changes (increases or decreases) in firing rate (FR) within seconds of cocaine-related cue presentations (Ghitza et al. 2003; Hollander and Carelli, 2005) as well as cocaine-seeking behaviors (Carelli and Deadwyler, 1994; Ghitza et al. 2004, 2006). Subsets of NAcc neurons are sensitive to movements such as approaching and responding on a cocaine-reinforced manipulandum but not during similar movements away from the manipulandum within the same session (Chang et al. 1994). Given that changes in firing rate of NAcc neurons prior to the cocaine-reinforced response are specifically correlated with approach and lever-press behavior rather than the infusion alone (Chang et al. 1994; Peoples et al. 1997), these phasic changes in firing rate likely reflect appetitive neural processing related to drug-seeking.

The nucleus accumbens contains two subregions, core and shell (Záborszky et al. 1985; Zahm and Heimer, 1990; Heimer et al. 1991). These subregions serve different functions in cocaine-seeking behavior. During abstinent drug-seeking behavior, NAcc shell neurons exhibit a greater change in FR following cocaine-predictive cues than neurons in the NAcc core (Ghitza et al. 2003). During cocaine self-administration and abstinent drug-seeking behavior, NAcc core neurons exhibit a greater change in FR prior to and following cocaine-reinforced or unreinforced responses (Ghitza et al. 2004, 2006; Hollander and Carelli, 2005).

The primary target of NAcc efferents is the ventral pallidum (VP), which also integrates projections from the basolateral amygdala (BLA) and ventral tegmental area (VTA) (Heimer and Wilson, 1975; Nauta et al. 1978; Heimer, 1978; Haber and Nauta 1983; O'Donnell et al. 1997; Zahm and Heimer, 1990; Fuller et al. 1987; Sesack et al. 1989; Klitenick et al. 1992). VP contains two subregions which receive topographic projections from the NAcc and project to unique targets. The ventromedial VP (VPvm) receives projections from the NAcc shell and projects predominantly to the mediodorsal thalamus (MDT) and VTA (Zahm and Heimer, 1990; Groenewegen et al. 1993; Kalivas et al. 1993; Zahm et al. 1996; Churchill et al. 1996; Heimer et al. 1997; O'Donnell et al. 1997). The dorsolateral VP (VPdl) receives projections from the NAcc core and projects predominantly to the substantia nigra and subthalamic nucleus, and weakly to mediodorsal thalamus (Zahm and Heimer, 1990; Groenewegen et al. 1993; Bell et al. 1995; Zahm et al. 1996; O'Donnell et al. 1997).

The VP is necessary for cocaine-seeking behaviors. VP lesions or pharmacological challenges block cocaine-induced conditioned place preference (Gong et al. 1997), self-administration (Hubner and Koob, 1990; Robledo and Koob, 1993), and reinstatement (McFarland and Kalivas, 2001; McFarland et al. 2004; Tang et al. 2005). Human cocaine abusers exhibit changes in VP neuropeptide expression post mortem (Frankel et al, 2008). However, it is unclear how VP neurons participate in cocaine-seeking behaviors. We previously demonstrated that single VP neurons exhibit rapid phasic changes in FR prior to as well as following cocaine-reinforced responses (Root et al. 2010). The present examination aimed to determine which cocaine-seeking behaviors were coincident with rapid phasic

changes in FR. These behaviors included approaching the manipulandum, the response itself, and retreating away from the manipulandum.

A second goal of the present experiment was to evaluate whether neurons within different VP subregions exhibited differences in their changes in FR during drug-seeking behaviors. While the VP subregions were delineated over twenty years ago (Zahm and Heimer, 1988; Heimer et al 1991), to our knowledge no study has examined the possibility of differential function ascribed to these subregions. Given that 1) changes in FR within seconds of the cocaine-seeking response are greater in the NAcc core than in the medial NAcc shell (Ghitza et al. 2004, 2006; Fabbricatore et al. 2010) and 2) NAcc core projects to the VPdl while NAcc shell projects to the VPvm, it was predicted that the VPdl would exhibit greater changes in FR during approach, response, and retreat behaviors than the VPvm.

METHODS

Subjects and surgery

Male Long–Evans rats (n = 25; 320–340g; Charles River, Wilmington, MA) were anesthetized with sodium pentobarbital (approximately 50 mg/kg, i.p.). Prior to surgery, subjects received injections of atropine methyl nitrate (10 mg/kg, i.p.) and penicillin G (75,000 U/0.25 ml, i.m.) to reduce the risk of pulmonary edema and bacterial infection, respectively. To block post-surgery pain sensitivity, animals were injected subcutaneously with 0.25 ml bupivaccaine HCl (0.25%) (Abbott Laboratories, North Chicago, IL) spread over 8 injection sites of the incisions on the head and neck. Anesthesia was maintained with periodic i.p. injections of ketamine hydrochloride (approximately 60 mg/kg, i.p.) and sodium pentobarbital

(approximately 15 mg/kg, i.p.). Following catheter implantation into the right jugular vein, a 2x4 array (Microwire Technologies, Heightstown, NJ) of Quad Teflon-coated stainless steel microwires (California Fine Wire, Grover Beach, CA) was implanted bilaterally into the VP (between ± 0.7 to -0.9 AP, ± 0.8 to ± 3.1 ML, -8.0 DV; Paxinos and Watson, 1997) and secured with dental cement. The diameter of each uninsulated microwire tip was 50 μm and wires were separated by 0.30 - 0.40 mm (center-center). An insulated 0.01 inch ground wire, stripped 5 mm from the tip, was implanted 5.5 mm ventral from the skull. The micro connector strip (Omnetics, Minneapolis, MN) was positioned mediolaterally (ear to ear), anterior to the interaural line. After surgery, rats were individually housed with access to food and water in the cocaine self-administration chambers to recover for at least one week. Animals lived in the self-administration chambers and maintained at 320-350g body weight with ad lib access to water following self-administration. Animals received infusions of heparinized saline every 25 minutes other than during self-administration sessions to preserve catheter patency. Protocols were performed in compliance with the Guide for the Care and Use of Laboratory Animals (NIH, Publications 865–23) and approved by the Institutional Animal Care and Use Committee, Rutgers University.

Electrophysiological procedures

Sixteen neural signals were led through four quad-channel operational amplifiers (TLC2264, Texas Instruments, Dallas, TX) inside a custom recording harness (MB Turnkey Designs, Hillsborough, NJ) and fluid/electronic swivel (CAY-675–24, Airflyte Electronics, Bayonne, NJ) to a preamplifier (MB Turnkey Designs, Hillsborough, NJ) that differentially amplified (10x) the signal on the recording

electrode against another microwire that did not exhibit a single unit. The signal was then band-pass filtered (450 Hz to 10 kHz; roll off 1.5 dB/octave at 1 kHz and -6 dB/octave at 11 kHz) and amplified 700x between rollovers (MB Turnkey Designs, Hillsborough, NJ). Using software and hardware of DataWave Technologies (Longmont, CO), electrical signals were sampled (50 kHz sampling frequency per wire) and stored for offline analysis.

One recording of all microwires per animal occurred between days 14 and 24 of self-administration training. The rationale for recording at this time point was several fold. First, we have previously demonstrated rapid phasic changes in FR surrounding cocaine-reinforced responses during this time period (Root et al. 2010). Second, this time point corresponds with the development of escalated drug intake, posited to exemplify "addiction-like behavior" in rats (Ahmed and Koob, 1998; Deroche-Gamonet et al, 2004). Third, recording at this time point also corresponded to fully manifested drug-induced alterations in VP receptor expression (Hammer, 1989). Fourth, well-trained animals quickly load to a relatively stable asymptotic drug level that exhibits little variability during the recording session, mitigating pharmacological differences between responses (Root et al. 2011).

Isolation and separation of individual neural waveforms from background noise and waveforms of other neurons recorded from the same microwire, were conducted post-hoc using spike sorting and separation software (DataWave Technologies, Longmont, CO). First, neural discharges were sorted in terms of waveform parameters, including principal components one and two, valley voltage, peak voltage, voltages at user-defined time cursors, spike height, and peak voltage time. Scatter plots of any 2 waveform parameters were displayed in a window, with all windows' parameter combinations displayed on one screen simultaneously. Each

point plotted on the scatter plot corresponded to one recorded waveform. Each cluster of dots represented similar waveforms, which were separated from other clusters by enclosing it within a circular “cutting box”. All waveforms of the putative individual neuron during the entire session (6-10 hours) were then replayed on a computer-simulated oscilloscope in order to assess the stability of neural waveforms. Waveforms whose parameters did not remain stable were discarded. Second, an interspike interval (ISI) histogram was constructed. If discharges occurred within the first 2 ms in the ISI, corresponding to a neuron’s natural refractory period, the recording was not considered that of a single neuron and discarded. When more than a single population of neural waveforms appeared to have been recorded from a given wire, cross-correlation was used to confirm that the populations corresponded to distinct neurons. Specifically, if discharges occurred within the first 2 ms in the cross-correlation and both neurons contained 0 discharges within their ISI's, both neurons were considered independent single units. Neurons exhibiting signal-to-noise ratios less than 2:1 were discarded.

Head movement task

Using head movement as the operant was selected for its relative ease in shaping self-administration behavior as well as its wide range of motor parameters previously characterized in our laboratory (Tang et al. 2007; Root et al. 2011). Vertical head movements were tracked with infrared-emitting diodes capable of transistor-transistor logic (HOA6299, Honeywell, Morristown, NJ). The light of the photocell was contained within a 5.59 mm diameter beam at 880 nm wavelength, outside the visual spectrum of the rat retina under normal illuminated conditions (Green, 1971; Pardue et al. 2001). Six photocells were arranged along a 50 degree

arc over 69 mm in the corner of the self-administration chamber in order to approximate the learned vertical head movements in a prior water self-administration task (Tang et al. 2007). The head movement apparatus is shown in Figure 1 (A - front view, B - side view, C - view from back of chamber with apparatus mounted). Numbers refer to photocell number in array and are located on the receiving photocells. The lowest photocell beam, photocell one, was positioned 13 mm above the floor. For behavioral vertical movement analyses, movement onset was defined as a photocell beam break for which at least the next photocell beam break was 1 larger than the previous photocell beam break and less than one second in duration from the original photocell beam break. Offset was defined as the last instance for which the previous photocell beam break was 1 larger than the previous photocell beam break and less than one second in duration from the onset. For neuronal analysis of vertical head movements, timestamps of photocell beam breaks were collected using DataWave Technologies (Longmont, CA), which allowed a unique decimal code for simultaneous beam breaks (i.e. photocells beams 1 and 2 broken at the same time). Two simultaneously photocell beam breaks of consecutive photocells were considered as half steps, equally between two photocells. For example, simultaneously breaking photocells 2 and 3 was considered 2.5. For neuronal analyses of responses, movement onset was defined as a photocell beam break for which at least the next photocell beam break was 0.5, 1, or 1.5 larger than the previous photocell beam break and less than one second in duration from the original photocell beam break. Offset was defined as the last instance for which the previous photocell beam break was 0.5, 1, or 1.5 larger than the previous photocell beam break and less than one second in duration from the onset. For both behavioral and neuronal analyses, all photocell beam breaks were recorded for

offline analysis of different movements (1 millisecond resolution). A criterion head movement was defined as a vertical head movement breaking photocells two, three, four, and five consecutively within one second (schematized in Figure 2B). The criterion head movement required at least a 43 mm movement starting at or below the 2nd photocell beam and crossing at least the fifth photocell. Since the photocells were arranged in the corner of the chamber, slanted movements were restricted.

Self-administration began daily with the onset of the house light. Self-administration sessions were controlled by custom programs written in MED-PC (MED-Associates, St. Albans, VT). At the beginning of the first day, vertical head movements in the "head movement corner" were shaped via delivery of cocaine infusion (0.24 mg/0.2 ml/7.5 sec inf) by the experimenter in the presence of the S^D (3.5 kHz, 70 dB). During the first day of training, the S^D was continuously sounded until a criterion head movement was made, at which time the S^D was terminated, cocaine was delivered, and a 40 second time out period began. The S^D was sounded again following the time out period. Criterion movements within the time out period were recorded but had no programmed consequences. Operant responses were readily shaped within the first day in most rats. The shaping process began with rewarding breaking photocell 2 for ten rewards, then rewarding breaking photocells 2 and 3 consecutively within one second for five rewards. Shaping continued with rewarding breaking photocells 2, 3, and 4 consecutively within one second for five rewards and lastly rewarding the final contingency of breaking photocells 2, 3, 4, and 5 within one second consecutively. For most rats, animals self-administered at the final contingency for two additional days under the same S^D duration, infusion dose, time out duration, and contingency.

Following acquisition (starting typically on day 4), animals began normal training. Normal training consisted of the same FR1 schedule of reinforcement during S^D presentations. To allow for rapid "load" infusions, the S^D was sounded for 30 sec and the time out following each of the first ten infusions was fixed to 5 sec. All subsequent time outs and S^D durations were fixed to 30 sec with a dose of 0.06 mg/0.50 ml/1.875 sec inf in order to increase the number of responses for neuronal analysis. This schedule of reinforcement allowed the capability of attaining a maximum of 7.16 mg/kg instantaneous calculated drug level, which was above the level self-administered by all rats. That is, each rat was able to self-administer its “preferred” level, or satiety threshold level of drug (Root et al, 2011). If the rat emitted a criterion head movement while the S^D was sounded, the cue was turned off, cocaine was delivered, and the time out began. If the rat did not make a criterion head movement during the S^D presentation, the cue ended after 30 sec and the time out began. Criterion head movements that occurred when the S^D was off (time out) were recorded but had no programmed consequence. During training, self-administration sessions ended after 6 hours elapsed or 280 rewards were earned, whichever occurred first. During the recording session, the self-administration session ended six hours following the tenth self-infusion of cocaine. Overnight between self-administration sessions, a rectangular 2 in x 2 in x 8 in Plexiglas block was fastened into the head movement corner to block extinction learning.

Histological procedures

At least one hour following the final self-administration session, animals were injected subcutaneously -18 h and -4 h prior to perfusion with 2 mg/kg of haloperidol in order to enhance subsequent immunohistochemical staining in the VP (Eggerman

and Zahm, 1988; Zahm and Heimer, 1990; Geisler and Zahm, 2006). At 0 h, animals were anesthetized with an overdose of sodium pentobarbital (150-200 mg/kg, i.p.). Anodal current (50 μA for 3 sec) was passed through each microwire and the animal was perfused with saline followed by 4% paraformaldehyde. The brain was removed and fixed in a solution of 4% paraformaldehyde overnight. Subsequently, the brain was stored in a 30% sucrose-phosphate buffer solution. Brains were coronally sliced at a thickness of 40 μm through VP and placed in phosphate buffer filled 10 mL net wells for immunohistochemistry.

All immunohistochemical steps were carried out under gentle agitation on a horizontal rotator (Laboratory-Line, Fisher, Pittsburgh, PA, USA). Free-floating sections were rinsed in 0.1 M phosphate buffer (pH 7.4), placed into 1% sodium borohydride for 15 min, thoroughly rinsed in 0.1 M phosphate buffer again, pretreated with 0.1 M phosphate buffer containing 0.1% Triton X-100 and 3% normal goat serum for 1 h, and then transferred into a solution containing a primary antibody, either rabbit anti-neurotensin (ImmunoStar, Inc., Hudson, WI) at a dilution of 1 : 6500, rabbit anti-calbindin d28k (ImmunoStar) at a dilution of 1 : 6000, or rabbit anti-substance P (ImmunoStar) at 1 : 6500 in 0.1 M phosphate buffer with 0.1% Triton X-100 and 3% normal goat serum overnight. The following day, after thorough rinsing in 0.1 M phosphate buffer with 0.1% Triton X-100, sections were placed in a solution containing biotinylated antibody against rabbit immunoglobulin's (Vector Laboratories Inc., Burlingame, CA, USA), at a dilution of 1 : 200 in 0.1 M phosphate buffer with 0.1% Triton X-100 for 1 h. The sections were again rinsed in 0.1 M phosphate buffer with 0.1% Triton X-100 and immersed in a solution containing avidin-biotin-peroxidase complex (Vector; 1 : 200 in 0.1 M phosphate buffer containing 0.1% Triton X-100) for another hour. After thorough rinsing in 0.1 M

phosphate buffer, a color reaction was developed by immersing the sections for 6 min in a solution of 0.01 M phosphate buffer containing 0.05% 3,3'-diaminobenzidine. Sections were mounted onto gelatin-coated slides, incubated in a solution of 5% potassium ferrocyanide and 10% HCl to stain the iron deposits left at the lesioned microwire recording tip. Sections were then dehydrated through a graded series of alcohol, transferred into xylene, and coverslipped with Permount (Fisher, Pittsburgh, PA, USA). Pilot invesitgations observed no staining when any of the primary antibodies were omitted.

Designation of single-units to subregions of the VP was made by a scorer blind to changes in FR during self-administration. In order to be designated into the ventromedial VP, single-units belonging to potassium ferrocyanide-stained tissue from microwire tips were localized: i) within substance P stain; ii) within neurotensin stain; and iii) absent from calbindin d28k stain. In order to be designated into the dorsolateral VP, single-units belonging to potassium ferrocyanide-stained tissue from microwire tips were localized: i) within substance P stain; ii) within calbindin d28k stain; iii) and absent from neurotensin stain.

Training analysis

Outcome variables, e.g., criterion head movements, self-administered mg/kg/day, etc., were analyzed as a function of fourteen training days using repeated measures ANOVAs (PASW 18.0.0, SPSS, Chicago, IL). When the assumption of sphericity was not confirmed (Levine's test), a Greenhouse-Geiser correction was used. Fourteen training days was selected because it was the time of the earliest recording session. Alpha criterion for all tests was 0.05.

Video analysis

A video frame-counter (Thalner Electronics VC-436), connected to the neuronal clock (CTR05, Measurement Computing, Norton, MA), timestamped each frame in a videocassette recorder (JVC HR-DD84OU), which was used to monitor and record additional behaviors (approach and retreat, Figure 2A and C, respectively) for off-line analysis (33 ms resolution).

Approach onset was determined by the start of a change in direction exhibited by the animal towards the photocell corner and culminated in a vertical head movement in the photocell corner. This was typically a leftward or rightward head turn or a vertical head movement prior to head turning, consistent with the approach behaviors described by Chang and colleagues (1994, 1997, 2000). In the minority of cases for which animals initially faced the photocell corner while engaged in focused stereotypy, approach onset was determined as the start of the alternating limb movements toward the photocell corner and culminated in a vertical head movement in the photocell corner. Approach offset was determined by the first photocell break following the approach onset. Approaches and retreats in which the approach onset was less than 150 ms from a previous retreat offset (described below) were removed from analysis due to ambiguity in the offset of retreat and onset of approach. Approaches greater than three seconds in duration were excluded from analysis.

Retreat onset was determined by the start of a change in direction exhibited by the animal away from the photocell corner. In the vast majority of cases, this was a leftward or rightward head turn but in a minority of cases was a backwards movement. The retreat offset was determined by the start of an additional change in direction exhibited by the animal or the start of a pause in locomotion of at least 66

ms (two video frames). For cases in which the animals movement following retreat onset exhibited slight head bobbing or circular head movements during a continuous movement away from the photocell, these slight head movements were not used as the retreat offset. Retreats greater than five seconds in duration were excluded from analysis. Four example approach, response, and retreat nodes are displayed in Supplemental Movie File 1.

Neuronal analysis

Changes in FR were examined with respect to four events: cue, approach, response, and retreat. For each event, all of its occurrences within a session were grouped and an average FR was determined. For the cue event, the objective was to minimize any contribution of movement to the assessment of FR. The average FR was calculated between S^D onset to S^D + 150 ms. For the approach event, the average FR was calculated between approach onset and approach offset (detailed in Video Analysis section). For the response event, the average FR was calculated between criterion movement onset and offset (detailed in Head movement task section). For the retreat event, the average FR was calculated between retreat onset and retreat offset (detailed in Video Analysis section). Changes in FR were visualized in Matlab (The Mathworks, Cambridge, MA) with raster and peri-event time histograms, the code of which was modified from Ma (2010).

Firing during the time points described above were considered potential "signals" during behavior. These signals were compared to a baseline period for standardized "signal:baseline" ratios using a 'B/(A+B)' formula, termed the *directional change in FR,* where 'B' was the signal and 'A' was the baseline. For the cue event, the baseline was the average FR during the 150 ms prior to cue onset, as previously

used (Ghitza et al. 2003). Pre-cue FR was not likely related to any particular movement because behavior was “randomized” in that cues were presented non-contingently. Similarly, cue-evoked movements were prevented from influencing post-cue FR assessments because their onset latency after S^D onset is >150 ms (Ghitza et al. 2003). For approach, response, and retreat events the baseline was the average FR during the period from -6 to -3 sec prior to criterion movements, as previously used (Ghitza et al. 2004, 2006). If within the baseline periods any photocell beam break, approach onset or offset, retreat onset or offset, or pump onset or offset occurred, that particular trial was omitted from calculating the baseline. The standardized, directional change in FR ranged between 0 and 1, with a value of 0.5 indicating no change from baseline, values less than 0.5 a decrease in FR from baseline, and values greater than 0.5 an increase in FR from baseline. Neurons that exhibited a 20% change from baseline in distinct behaviors (approach, response, retreat) were categorized with respect to increases, decreases, or mixed changes in firing rate. Since VP neurons exhibit changes in FR surrounding cocaine-reinforced responses with heterogeneous decreases or increases in FR (Root et al. 2010), a second analysis was conducted on all events termed the *absolute change in FR*. The absolute change in FR was calculated using the formula '| directional change in FR - 0.5 |'. The absolute change in FR ranged between 0 and 0.5 and represents change in FR from baseline regardless of whether the change was a decrease or increase in FR. For all analyses (cues, responses, approaches, and retreats), events that occurred during the initial 10 rapidly-spaced “loading” self-infusions were excluded from all analyses in order to remove minimize the influence of pharmacological differences.

To evaluate subregional differences in changes in FR between VPvm and VPdl neurons, Mann-Whitney U tests evaluated the directional change in FR and the absolute change in FR for cue, approach, response, and retreat events, as previously used (Ghitza et al. 2004, 2006; Fabbricatore et al. 2010). Mann-Whitney U tests were used because these data did not fit a normal distribution. To analyze differential relationships between subregions, correlation coefficients of directional changes in FR values were compared using a z-test as described by Morse (1999). To analyze subregional differences in the prevalence of recorded neurons in left versus right hemisphere, biphasic versus triphasic waveform profiles, and propensity to record from multisingle-unit microwires, Fisher's exact test was used.

RESULTS

Behavior

Prior to recordings, animals exhibited both task and skill learning. With regard to task learning, reaction time in response to the S^D decreased over days, $F(4.040,96.970) = 99.468$, $p < 10^{-32}$ (Figure 3A). Over training sessions, probability of self-infusion upon S^D presentation, $F(4.424, 106.173) = 24.792$, $p < 10^{-14}$ (Figure 3B), and total drug intake (mg/kg), $F(4.980,119.530) = 8.647$, $p < 10^{-6}$ (Figure 3C), increased over days. Animals escalated their intake of cocaine over days, decreasing the latency to reach the 10th self-infusion, $F(3.886,85.487) = 5.133$, $p < 0.001$ (Figure 3D).

In regard to skill learning, the number of criterion movements increased over days, $F(4.948,118.759) = 33.18$, $p < 10^{-20}$ (Figure 3E), while the number of inverse criterion movements (downward movements starting at or above photocell 5 and

ending at photocell 2 or below, but without programmed consequence) did not change, $F(1.907, 45.762) = 2.116$, $p > 0.05$. Over the last three days of training, the latency for the subsequent movement following a criterion movement was 19.26 ± 2.77, 17.80 ± 2.97, and 16.76 ± 2.75 sec. The average velocity of criterion movements increased over days, $F(3.532, 84.775) = 9.480$, $p < 10^{-5}$ (Figure 4A), as a function of decreased duration, $F(2.816, 67.583) = 20.747$, $p < 10^{-8}$ (Figure 4B), but not distance, $F(13,312) = 27.116$, $p > 0.05$ (Figure 4C). The probability of starting the criterion movement at the most optimal photocell position, photocell 2, increased over days, $F(6.193, 154.828) = 2.533$, $p < 0.05$ (Figure 4D). The probability of ending a criterion movement at the most optimal photocell position, photocell 5, did not change, $F(4.686, 112.469) = 1.045$, $p > 0.05$ (Figure 4E).

Neuronal

Animals were recorded typically on day 16 of training (average), ranging between days 14 and 26. Of the 400 microwires implanted within the basal forebrain of 25 rats, 202 microwires were localized to the VP. Of these, 38 microwires were localized to the VPdl (Figure 5), recording 48 single-units. A total of 140 microwires were localized to the VPvm (Figure 6), recording 171 single-units. Twenty-four microwires recording 24 single-units were removed due to histological localization to all three stains, which typically occurred at the most caudal aspects of VP. The amplitude and signal-to-noise ratio of VP neurons (Table 1) did not differ between subregions (all $|z| < 1.84$, $p > 0.05$). The prevalence of recording from multiple single-unit microwires, 9/38 (23.68%) of VPdl and 24/140 (17.14%) of VPvm microwires, did not differ between subregions (Fisher's exact test, $p > 0.05$). A minority of single-units exhibited an initial positivity prior to the valley of the

waveform (triphasic profile), 4/48 (8.33%) in VPdl and 20/171 (11.70%) in VPvm, the prevalence of which did not differ between subregions (Fisher's exact test, $p > 0.05$). The prevalence of single-units recorded from microwires within the right hemisphere, 20/48 (41.67%) of VPdl and 88/171 (51.46%) of VPvm single-units, did not differ between subregions (Fisher's exact test, $p > 0.05$). The cue baseline FRs (Table 1) and movement baseline FRs (Table 1) did not differ between subregions (all $|z| < 0.28$, $p > 0.05$). Overall, these results demonstrate that waveforms and baseline FRs of recorded neurons were statistically not different between VP subregions and hemispheres.

Clear examples of changes in FR following S^D presentation were not observed. Nor were significant differences found between subregions, with respect to the paucity of directional or absolute changes in FR in response to the cue (all $|z| < 0.99$, $p > 0.05$) (Figure 7A,7B). After sorting cue trials into those in which the animal self-administered cocaine (hits) versus those in which the animal did not self-administer cocaine (miss), no differences between subregions were found for either the directional or absolute changes in FR (all $|z| < 1.20$, $p > 0.05$).

The most common changes in FR involved the approach alone, response alone, or approach and response (see Table 2 for behavioral characteristics used in electrophysiological analyses). Two examples of approach-related firing are shown in Figure 8 (VPdl neuron) and Figure 9 (VPvm neuron). In each case, changes in FR occur at the onset of approach (Figure 8A, 9A) and exhibit no change in FR during response (Figure 8B, 9B) or retreat (Figure 8C, 8C). Of neurons exhibiting a 20% change in firing rate during approach alone, 10.42% (5/48) were located in VPdl and 8.19% (14/171) were located in the VPvm (Table 3). As a population, during the approach, the VPdl exhibited a significantly larger absolute change in FR than the

VPvm ($z = -3.30$, $p < 0.001$) but did not differ in terms of the directional change in FR ($z = -0.85$, $p > 0.05$) (Figure 10A, 10B).

Two examples of response-related firing are shown in Figure 11 (VPdl neuron) and Figure 12 (VPvm neuron). In both cases, FRs were altered during the response (Figure 11B, 12B) but not the retreat (Figure 11C, 12C). The VPvm neuron was not altered during the approach (Figure 12A) but the VPdl neuron (Figure 11A) exhibited an increase in FR just prior to the approach offset. Of neurons exhibiting a 20% change in firing rate during approach alone, 25.00% (12/48) were located in VPdl and 22.81% (39/171) were located in the VPvm (Table 3). As a population, during the criterion movement (response), the VPdl exhibited a significantly larger absolute change in FR than the VPvm ($z = -2.78$, $p < 0.01$) which also differed using the directional ($z = -2.18$, $p < 0.05$) change in FR (Figure 13A, 13B). No neurons exhibited any significant relationship of FR with movement properties including distance (Figure 14A), duration (Figure 14B), velocity (Figure 14C), start position/valley (Figure 14D), or end position/peak (Figure 14E).

When a change in FR occurred during the approach, VPdl neurons were highly likely to continue this change in FR through the duration of the response (discussed briefly above for the VPdl neuron in Figure 12; clear VPdl neuron examples shown in Figures 15 and 16). Within the VPdl, a significant correlation was observed between the directional changes in FR during the approach and response, $r = 0.69$, $p < 10^{-7}$ (Figure 17A). While a significant correlation was also observed in the VPvm, $r = 0.32$, $p < 10^{-4}$ (Figure 17B), the correlation was significantly larger in VPdl, $z = 3.11$, $p < 10^{-3}$. That is, although some VPvm neurons also continued to change their FRs through approach and response (example VPvm neuron in Figure 18), VPvm neurons were more selective and thus more heterogeneous in their firing

patterns, including approach-only or response-only changes in FR. Table 3 displays the number and percent of neurons in each subregion exhibiting a 20% change from baseline firing rate for approach and response but not retreat.

Approaches were sorted into cued and uncued trials. The VPdl exhibited larger cued and uncued approach absolute changes in FR than the VPvm (cued $z = -2.90$, $p < 0.01$; uncued $z = -2.26$, $p < 0.05$) (Figures 19A, 20A). Neither the cued nor uncued approach directional changes in FR differed between subregions (all $|z| < 1.50$, $p > 0.05$) (Figures 19B, 20B). Within each subregion, a significant correlation existed between cued and uncued approach directional changes in FR (VPdl $r = 0.69$, $p < 10^{-7}$; VPvm $r = 0.73$, $p < 10^{-28}$) (Figure 21A, 21B), which did not differ between subregions ($z = -0.45$, $p > 0.05$). In other words, most neurons exhibited a similar change in FR between cued approach (Figure 22A, 23A) and uncued approach (Figures 22B, 23B) conditions. Figure 22 displays a VPdl neuron and Figure 23 displays a VPvm neuron during cued versus uncued approach. On the rare occasion in which a difference existed between cued and uncued approach conditions, these neurons were located in the VPvm (Figure 24) but not the VPdl.

Responses were sorted into cued/reinforced and uncued/unreinforced trials. For cued/reinforced responses, the VPdl exhibited a larger absolute change in FR than the VPvm ($z = -2.36$, $p < 0.05$) but was not different using the directional change in FR ($z = -1.50$, $p > 0.05$) (Figure 25A, 25B). For uncued/unreinforced responses, the VPdl exhibited a larger change in FR than VPvm using both the absolute change in FR ($z = -2.31$, $p < 0.05$) and the directional change in FR ($z = -3.061$, $p < 0.01$) (Figure 26A, 26B). A significant correlation between cued/reinforced responses and uncued/unreinforced responses was observed for the VPvm ($r = 0.31$, $p < 10^{-4}$) and the VPdl ($r = 0.34$, $p < 0.05$) (Figure 27A, 27B), but these

correlations did not significantly differ from each other ($z = 0.36$, $p > 0.05$). The correlation coefficients for both VP subregions were weak, suggesting firing patterns were different between cued/reinforced and uncued/unreinforced response conditions. However, large differences between cued/reinforced and uncued/unreinforced conditions were due to directional change comparisons (B/(A+B)) which exhibited very low FRs in both 'A' and 'B' conditions. For example, the VPdl neuron in Figure 28 and VPvm example in Figure 29 both exhibit a near absence of spikes during the reinforced response and only slightly more spikes in the unreinforced condition. Combined with low baseline firing rates, these and other similar neurons exhibited large differences in the directional change in FR between cued/reinforced and uncued/unreinforced conditions. In contrast, the significant correlation observed within both subregions demonstrates that changes in FR were similar overall between conditions, as exemplified by the VPdl neuron in Figure 30 and VPvm neuron in Figure 31.

Changes in FR were observed during the retreat (Figure 32). No significant differences were found between subregions for the directional or absolute changes in FRs during the retreat (all $|z| < 1.95$, $p > 0.05$) (Figure 33A, 33B). In an attempt to identify the influence of the infusion pump on changes in FR during retreat, retreats were sorted into trials in which a pump was initiated two seconds prior to the onset of retreat through the end of the retreat and all other retreats, termed pump retreats and nonpump retreats respectively.

Both VPdl and VPvm exhibited significant correlations of pump and nonpump retreats (VPdl $r = 0.59$, $p > 10^{-4}$; VPvm $r = 0.40$, $p < 10^{-6}$; Figure 34A, 34B), which did not differ from each other ($z = 1.65$, $p > 0.05$). That is, similar changes in FRs during the retreat were observed whether the pump was activated or not (VPdl neuron

example in Figure 35 and VPvm neuron example in Figure 36). Nevertheless, some neurons exhibited differences in FRs between pump and nonpump retreat conditions in both subregions (VPdl neuron example in Figure 37 and VPvm neuron example in Figure 38). VPdl neurons exhibited a greater directional ($z = -2.29$, $p < 0.05$) and absolute ($z = -2.74$, $p < 0.01$) change in FR over VPvm neurons during the pump retreat (Figure 39A, 39B). For the nonpump retreat, in contrast, no significant differences between subregions was observed for either the absolute or directional changes in firing rate (all $|z| < 1.51$, $p > 0.05$; Figure 40A, 40B).

For neurons that exhibited a change in FR during the retreat, these were nearly always coupled with changes in FR during either the approach, response, or both the approach and response. A significant correlation was observed for the directional changes in FRs during the approach and retreat for the VPdl, $r = 0.51$, $p < 0.001$ (Figure 41A) and VPvm, $r = 0.41$, $p < 10^{-7}$ (Figure 41B). Some neurons exhibited a change in FR during approach, reverted back to baseline during the response, and exhibited another change in FR during the retreat (Figures 42, 43; Table 3). While some VPdl neurons exhibited a 20% change in approach and retreat, but not response (Table 3), clear examples of this type of firing pattern was not observed in VPdl neurons. Few neurons exhibited their only change in FR during the retreat, and these neurons were typically located in the VPvm (Figure 32 neuron was recorded from the VPvm; Table 3).

Some neurons exhibited changes in FR during response and retreat (see VPdl example in Figure 44 and VPvm example in Figure 45; Table 3). A significant correlation was observed for the directional changes in FRs during the response and retreat for the VPdl, $r = 0.37$, $p < 0.01$ (Figure 46A) and VPvm, $r = 0.19$, $p < 0.05$ (Figure 46B). The correlation coefficients for each approach-retreat and response-

retreat did not differ between subregions (all $|z| < 0.74$, $p > 0.05$). Other neurons exhibited changes in FR that began during the approach and continued through the response and retreat (VPdl neuron example in Figure 47 and VPvm neuron example in Figure 48). However, most neurons exhibiting a change in FR during approach, response, and retreat did so with heterogeneous directional changes in FR (Figures 49-52 show VPvm neurons and Figures 53-55 show VPdl neurons; Table 3).

The neuron in Figure 55 exhibited a change in FR (decrease) that began prior to the approach. We examined whether VP neurons exhibited firing patterns prior to the approach movement. Visual inspection of all neurons' firing patterns revealed only two additional neurons with changes in FR that began prior to the approach onset. For the neuron in Figure 55, we returned to analyze the recorded videos from self-administration behavior. This rat exhibited a stereotypical movement to one corner of the chamber just prior to the approach toward the photocell corner, which was termed the pre-approach movement (Supplemental Movie 2). Figure 56A displays the approach change in FR, with time 0 as the onset of approach and green dot as the offset of approach. However, plotting the pre-approach movement onset and offset (magenta and cyan dots in Figure 56B, respectively) clearly demonstrates that the decrease in FR prior to approach was due to the pre-approach movement. A simultaneously recorded neuron in the VPvm of this rat also exhibited a change in FR prior to the approach (Figure 57, Figure 58A), which similarly was related to the pre-approach movement (Figure 58B). The final neuron, shown in Figure 59, exhibited a decrease in FR prior to the approach onset. For this neuron, we examined whether previous approaches (Figure 60A), responses (Figure 60B), or retreats (Figure 60C) mediated the decrease in FR prior to the approach. In each case, only trials are shown when the previous behavior (approach, response, retreat)

occurred within the four second firing window prior to the approach onset (time 0). The magenta and cyan dots signify the onset and offset of the previous approach (Figure 60A), response (Figure 60B), or retreat (Figure 60C). Figure 60C demonstrates that this rat often approached the manipulandum quickly following retreat offset, for which a decrease in FR occurred in these trials near the offset of retreat. In summary, with respect to the movements studied in the present report, changes in FR of VP neurons in no case preceded the onset of approach movements but rather occurred strictly *during* movements.

DISCUSSION

Prior to recordings animals exhibited both task and skill learning, replicating previous results using the same operant during cocaine (Root et al. 2011) or water (Tang et al. 2007) self-administration. Indicative of task learning, over training days animals increased the number of criterion movements, reduced their latency to respond following S^D presentation, escalated drug consumption, and increased the probability of self-administering cocaine following S^D presentation. Animals discriminated the vertical head movement as the operant because inverse criterion movements did not change over days. Animals exhibited operant-related behaviors that included approaching the photocell corner, responding, and retreating away from the photocell corner towards their locus of stereotypy. The latency for the subsequent movement to occur following a criterion movement (on average between 16 and 19 seconds over the last three training days) was inconsistent with cocaine-induced head-bobbing in the photocell corner nonspecifically, which occurs at approximately 10 Hz (Fowler et al. 2003, 2007).

With regard to skill learning, although not required, the velocity of criterion movements increased over days as a function of decreasing duration, but not distance. The probability of starting a criterion movement at the most optimal position, photocell two, increased over days while the probability of ending a criterion movement at the most optimal position, photocell five, did not change. Taken together, animals learned the self-administration task and became skilled and efficient in their use of the vertical head movement operant.

Neurons in both VP subregions exhibited firing patterns during different behaviors involved in the process of self-administering cocaine. In fact, over 75% of VPvm and 85% of VPdl neurons exhibited at least a 20% change in firing rate during one or more behaviors of approach, response, retreat (Table 3). On the whole, similar firing patterns were observed between the present experiment utilizing a vertical head movement operant and our prior investigation of VP firing patterns using a lever press operant for cocaine self-infusions (Root et al. 2010). Thus, we suggest that VP cells are responsive to goal-directed movements that involve seeking intravenous self-infusions of cocaine, despite differences in motoric demands. This result is corroborated by the present lack of significant correlations between FR and movement parameters (distance, duration, velocity, valley, apex) in any VP neuron. These results also buttress the findings of Mitchell and colleagues (1987) who reported that VP neurons i) exhibit no changes in FR in response to passive or active movement of any body part prior to conditioning and ii) do not encode information regarding direction and muscle pattern of movements following conditioning.

We observed differential changes in FR within VP subregions during distinct behaviors. The VPdl exhibited a greater absolute change in FR during the approach

and response relative to the VPvm. This was the case for cued and uncued approaches as well as cued/reinforced and uncued/unreinforced responses. Since the NAcc core projects to the VPdl (Heimer et al. 1991), and core neurons exhibit a greater change in FR over NAcc shell neurons during cocaine-seeking behavior (Ghitza et al. 2004), the NAcc core - VPdl subcircuit may be an especially important contributor to the approach/response components of drug-seeking behavior.

The *patterns* in which changes in FR occurred also differed by subregion. VPdl neurons were more rigid in their approach and response firing patterns than VPvm neurons. Changes in FR during the approach often carried through the response in VPdl cells while VPvm cells were more selective, changing FRs during the approach or response alone or sometimes carrying through the approach and response. Taken together with a greater change in firing rate during approach and response by VPdl neurons compared to VPvm neurons, distinct firing patterns during these behaviors suggests a differential representation of drug-seeking between VP subregions.

A differential representation of drug-seeking within VP subregions both supports and extends the classic basal ganglia model (Alexander et al. 1986). Based on their groundbreaking studies of a maintained representation (firing pattern) of body part movements within the "skeletomotor" dorsolateral striatal system (M1+S1 → putamen → globus pallidus → cortex), Alexander and colleagues (1986) predicted that firing patterns are similarly maintained within the "cingulate" system. The cingulate system involves projections from mPFC, BLA, and hippocampus → NAcc → VP → cortex. Seminal studies Woodward and colleagues, recording mPFC (Chang et al. 1997, 2000) and NAcc (Chang et al. 1994, 2000) neurons during cocaine self-administration, taken together with the current VP study, provide critical

insight into the function of this circuit. In their studies, the lever was positioned such that in order to respond, rats had to approach the lever, rear, and position their forelimbs to press the lever downward to respond. The firing patterns observed in their studies were exclusively related to approaching the lever alone or to aspects involving the approach to the lever (rearing) and responding (pressing the lever). First, because the most common firing patterns observed within the VP were related to approaching the manipulandum as well as approaching and responding, the present results support the hypothesis (Alexander et al. 1986) of a maintained representation (firing pattern) of approach and response within the cingulate circuit. Second, the VPvm, with its preferential innervation of the MDT (Zahm and Heimer, 1990; Zahm et al. 1996; O'Donnell et al. 1997) and heterogeneous firing patterns of approach alone, response alone, or approach and response signaling, may enable selective cortical representation of different temporal components or sequences of behaviors during the drug-seeking process. The VPdl on the other hand, with less projections to MDT and its unique efferents to more "motoric" regions than the VPvm, such as subthalamic nucleus and substantia nigra reticulata (Groenewegen et al. 1993; Zahm et al. 1996), may be an important contributor to the expression of drug-seeking motor behaviors during its typical approach and response firing patterns.

In both subregions, we observed changes in FR during the retreat away from the self-administration manipulandum. The change in FR during the retreat did not differ between subregions. It is likely that some of these changes in FR reflect the "post-press" changes in FR observed in our previous examination of VP neurons using a lever press operant (Root et al. 2010). However, some firing patterns occurred after the retreat offset (Figures 11, 15). It is possible that other factors,

such as the activation of the pump, termination of the S^D, or evaluation of successful or unsuccessful (error) responses, contribute to firing patterns during or following the retreat.

Within each subregion, the directional change in FR during retreats involving pump onset significantly predicted the directional change in FR during retreats that did not have pump onset, suggesting on the whole that the pump did not induce a rapid phasic change in FR. Nevertheless, a minority of neurons exhibited differential firing patterns during pump versus nonpump retreats. Moreover, VPdl neurons exhibited a greater absolute change in FR than VPvm neurons during pump retreats. No differences were observed between subregions during nonpump retreats. It is not clear whether retreats differ behaviorally between pump and nonpump conditions, e.g., whether other factors, such as visceral effects of the pump or potential success or error signals contributes to firing during the pump or nonpump retreat conditions. Further experimentation will be necessary to determine the factors involved in producing firing patterns during retreats away from the self-administration manipulandum.

We observed no changes in FR related to S^D presentation. During cocaine self-administration, responses occur when the drug level falls below an internal threshold, above which the animal is satiated and does not respond (Pickens and Thompson 1968, 1971; Yokel and Pickens 1973, 1974; Dougherty and Pickens 1974; Wise 1987; Wise et al. 1995; Markou et al. 1999; Tsibulsky and Norman 1999; Norman et al. 2003; Lynch and Carroll 2001; Norman and Tsibulsky 2006; Olmstead et al. 2000; Panlilio et al. 2006). We have found evidence of such behavior using the head movement paradigm used in the present study. In spite of sounding the S^D during both tests, clamping each animal's drug level slightly above its satiety

threshold eliminated responding while clamping drug level below satiety threshold markedly increased responding (Root et al. 2011). It appears that, during a binge of self-administering cocaine, the S^D has little measurable behavioral influence, and fails to activate ventral striatopallidal neurons. In support of this, we have observed an absence of S^D-induced changes in FR during cocaine self-administration in NAcc shell or core neurons (unpublished observations). The reader is referred to other examinations of NAcc firing evoked by the tone S^D, which does have significant behavioral relevance while the animal is abstinent (Ghitza et al. 2003; Root et al. 2009). Further experimentation will be necessary to determine whether VP exhibits responsiveness to cues related to cocaine self-administration during abstinence.

Of critical importance for drug-abuse research is the determination of which brain regions are responsible for initiating and executing drug-seeking behaviors. Taken at face value, Alexander et al. (1986) implicitly hypothesized NAcc afferents as the origin of firing patterns generating appetitive behavior. In contrast, Mogenson and colleagues (1980) theorized that through projections to the pedunculopontine tegmental mesencephalic locomotor region, VP provides a gateway for limbic/emotional signals sent to NAcc gain access to the motor system.

If VP signals the initiation of appetitive behavior, as hypothesized by Mogenson et al. (1980), one would expect firing pattern changes prior to the onset of approach. Only 3 VP neurons exhibited changes in FR prior to the approach, which upon further inspection were revealed to be due to other factors than a "premotor" firing correlate. Instead of preceding the onset of approach movements, VP FR changes in every case were *coincident* with approach, response, and/or retreat behaviors. Taken together with the arguments of Heimer and colleagues (1997), who contended that previous investigations of VP projections to the mesencephalic

locomotor region "lumped" the VP with the subpallidal parts of the extended amygdala, our results discount the Mogenson et al. (1980) hypothesis of VP as the initiator of appetitive behavior. The present results suggest that VP functions similar to that of the globus pallidus, which is involved in other aspects of appetitive behavior than movement initiation (Aldridge et al. 1980; Alexander et al. 1986; Brotchie et al. 1991a,b; Mink and Thatch 1991a,b,c).

Alexander and colleagues (1986) suggest NAcc afferents may be important for the initiation of appetitive behavior. One region may be the prelimbic cortex, the cortical afferent of NAcc core neurons (Brog et al. 1993), and in which a small number of neurons exhibit changes in FR prior to approaching the cocaine-reinforced manipulandum (Chang et al. 1997, 2000). Prelimbic cortex projects to raphe nuclei and periaqueductal gray (Vertes, 2004), suggesting a role in generating motor behavior. Insight is provided by a study from Chang and colleagues (2000), in which prelimbic cortex and NAcc core neurons were simultaneously recorded during cocaine self-administration. Interestingly, NAcc neurons exhibited their firing patterns during different cocaine-seeking behaviors (approach, response) prior to prelimbic cortex neurons and also led prelimbic neurons in cross-correlation examinations. This intriguing result discounts a role of the prelimbic cortex in the initiation of self-administration of cocaine. Taken together with the present results, prelimbic cortex may be the recipient of approach and response-related firing patterns relayed by the VP projection to MDT.

While the precise brain region responsible for the initiation of drug-seeking behavior has yet to be determined, it is clear that the ventral striatopallidal or "cingulate" system is the recipient of signals related to different drug-seeking behaviors. The present study, although not supporting involvement in initiation,

unequivocally demonstrates that VP subregions are differentially traversed by signals related to the execution of drug-seeking behavior.

REFERENCES

Ahmed SH, Koob GF. (1998). Transition from moderate to excessive drug intake: Change in hedonic set point. Science 282:298–300.

Aldridge JW, Anderson RJ, Murphy JT. (1980). The role of the basal ganglia in controlling a movement initiated by a visually presented cue. Brain Res 192:3-16

Alexander GE, DeLong MR, Strick PL. (1986). Parallel organization of functionally segregated circuits linking basal ganglia and cortex. Annu Rev Neurosci 9:357–381.

Bell K, Churchill L, Kalivas PW. (1995). GABAergic projection from the ventral pallidum and globus pallidus to the subthalamic nucleus. Synapse 20(1):10-18.

Brog JS, Salyapongse A, Deutch AY, Zahm DS. (1993). The patterns of afferent innervation of the core and shell in the "accumbens" part of the rat ventral striatum: immunohistochemical detection of retrogradely transported fluoro-gold. J Comp Neurol 338(2):255-278

Brotchie P, Iansek R, Horne MK. (1991). Motor function of the monkey globus pallidus 1. neuronal discharge and parameters of movement. Brain 114:1667-1683

Brotchie P, Iansek R, Horne MK. (1991). Motor function of the monkey globus pallidus 2. cognitive aspects of movement and phasic neuronal activity. Brain 114:1685-1702.

Carelli RM, Deadwyler SA. (1994). A comparison of nucleus accumbens neuronal firing patterns during cocaine self-administration and water reinforcement in rats. 14(12):7735-7746.

Chang JY, Sawyer SF, Lee RS, Woodward DJ. (1994). Electrophysiological and pharmacological evidence for the role of the nucleus accumbens in cocaine self-administration in freely moving rats. J Neurosci, 14:1224– 1244.

Chang JY, Sawyer SF, Paris JM, Kirillov A, Woodward DJ. (1997). Single neuronal responses in medial prefrontal cortex during cocaine self-administration in freely moving rats. Synapse 26:22-35

Chang JY, Janak PH, and Woodward DJ. (2000). Neuronal and behavioral correlations in the medial prefrontal cortex and nucleus accumbens during cocaine self-administration by rats. Neuroscience 99(3) 433-443

Chrobak JJ and Napier TC. (1993). Opioid and GABA modulation of accumbens-evoked ventral pallidal activity. J Neural Transm, 93:123-143.

Chrobak JJ, Napier TC. (2002). Basal forebrain infusions impair delayed-non-match-to-sample radial arm maze performance. Pharmacol Biochem Behav. 72(1-2):209-212.

Churchill L, Zahm DS, Kalivas PW. (1996). The mediodorsal nucleus of the thalamus in rats--I. forebrain gabaergic innervation. Neuroscience, 70(1):83-102.

Deroche-Gamonet V, Belin D, Piazza PV. (2004). Evidence for addiction-like behavior in the rat. Science 305:1014–1017

Dougherty J, Pickens R (1974). Effects of phenobarbital and SKF525A on cocaine self-administration in rats. Drug Addict 3:135–143

Eggerman KW, Zahm DS. (1988). Numbers of neurotensin-immunoreactive neurons selectively increased in rat ventral striatum following acute haloperidol administration. Neuropeptides 11:125-132

Fabbricatore AT, Ghitza UE, Prokopenko VF, West MO. (2010). Electrophysiological evidence of mediolateral functional dichotomy in the rat nucleus accumbens during cocaine self-administration II: phasic firing patterns. Eur J Neurosci 31(9):1671-1682

Fowler SC, Birkenstrand B, Chen R, Vorontsova E, Zarcone T (2003). Behavioral sensitization toamphetamine in rats: changes in the rhythm of head movements during focused stereotypies. Psychopharmacology 170(2):167–177

Fowler SC, Covington HE, Miczek KA (2007). Stereotyped and complex motor routines expressed during cocaine selfadministration: results from a 24-h binge of unlimited cocaine access in rats. Psychopharmacology 192(4):465–478

Frankel PS, Alburges ME, Bush L, Hanson GR, Kish SJ. (2008). Striatal and ventral pallidum dynorphin concentrations are markedly increased in human chronic cocaine users. Neuropharmacology. 55(1):41-46

Fuller TA, Russchen FT, Price JL. (1987). Sources of presumptive glutamergic/aspartergic afferents to the rat ventral striatopallidal region. J Comp Neurol. 258(3):317-338.

Geisler S, Zahm DS. (2006). Neurotensin afferents of the ventral tegmental area in the rat: [1] re-examination of their origins and [2] responses to acute psychostimulant and antipsychotic drug administration. Eur J Neurosci 24:116-134

Ghitza UE, Fabbricatore AT, Prokopenko V, Pawlak AP, West, MO

(2003). Persistent cue-evoked activity of accumbens neurons after prolonged abstinence from self-administered cocaine. The Journal of Neuroscience, 23 (19), 7239-7245

Ghitza UE, Fabbricatore AT, Prokopenko VF, West MO. (2004). Differences between accumbens core and shell neurons exhibiting phasic firing patterns related to drug-seeking behavior during a discriminative stimulus task. J Neurophysiol, 92:1608–1614.

Ghitza UE, Prokopenko VF, West MO, Fabbricatore AT. (2006). Higher magnitude accumbal phasic firing changes among core neurons exhibiting tonic firing increases during cocaine self-administration. Neuroscience 137: 1075-1085

Gong W, Neill D, Justice JB Jr. (1997). 6-Hydroxydopamine lesion of ventral pallidum blocks acquisition of place preference conditioning to cocaine. Brain Res. 754(1-2):103-112.

Green DG (1971). Light adaptation in the rat retina: evidence for two receptor mechanisms. Science 174(9): 598-600.

Groenewegen HJ, Russchen FT. (1984). Organization of the efferent projections of the nucleus accumbens to pallidal, hypothalamic, and mesencephalic structures: a tracing and immunohistochemical study in the cat. J Comp Neurol. 223(3):347-367.

Groenewegen HJ, Berendse HW, Haber SN. (1993). Organization of the output of the ventral striatopallidal system in the rat: ventral pallidal efferents. Neuroscience. 57(1):113-142.

Haber SN, Nauta WJ. (1983). Ramifications of the globus pallidus in the rat as indicated by patterns of immunohistochemistry. Neuroscience 9(2):245-260.

Hammer RP Jr. (1989). Cocaine alters opiate receptor binding in critical brain reward regions. Synapse. 3(1):55-60.

Heimer L, Harlan RE, Alheid GF, Garcia MM, de Olmos J. (1997). Substantia innominata: a notion which impedes clinical-anatomical correlations in neuropsychiatric disorders. Neuroscience 76(4) 957-1006.

Heimer L, Wilson RD (1975). The subcortical projections of the allocortex: similarities in the neural associations of the hippocampus, the piriform cortex, and the neocortex. In Golgi Centennial Symposium, (Santini M, ed). pp 177-193. Raven Press, New York

Heimer L. (1978). The olfactory cortex and the ventral striatum. In Limbic Mechanisms (Livingston KE, Hornykiewicz O, Eds). pp 95-188. Plenum Press: New York and London

Heimer L, Alheid GF. (1991). Piecing together the puzzle of basal forebrain anatomy. In The Basal Forebrain, Edited by TC Napier et al. Plenum Press, New York NY.

Heimer L, Zahm DS, Churchill L, Kalivas PW, Wohltmann (1991). Specificity in the projection patterns of accumbal core and shell in the rat. Neuroscience 41:89-125

Hollander JA, Carelli RM. (2005). Abstinence from cocaine self-administration heightens neural encoding of goal-directed behaviors in the accumbens. Neuropsychopharmacology 30:146-1474

Hubner CB, Koob GF. (1990). The ventral pallidum plays a role in mediating cocaine and heroin self-administration in the rat. Brain Res. 508(1):20-29.

Kalivas PW, Churchill L, Klitenick MA. (1993). GABA and enkephalin projection from the nucleus accumbens and ventral pallidum to the ventral tegmental area. Neuroscience, 57(4):1047-1060.

Klitenick MA, Deutch AY, Churchill L, Kalivas PW. (1992). Topography and functional role of dopaminergic projections from the ventral mesencephalic tegmentum to the ventral pallidum. Neuroscience 50(2):371-386.

Lynch WJ, Carroll ME (2001). Regulation of drug intake. Exp Clin Psychopharmacol 9(2):131–143

Markou A, Arroyo M, Everitt BJ (1999). Effects of contingent and non-contingent cocaine on drug-seeking behavior measured using a second-order schedule of cocaine reinforcement in rats. Neuropsychopharmacology 20(6):542–555

Ma, S. (2010). Raster and PETH Simple Version. Retrieved from http://www.mathworks.com/matlabcentral/fileexchange/29763-raster-and-peth-simple-version.

McDaid J, Dallimore JE, Mackie AR, Mickiewicz AL, Napier TC. (2006). Changes in accumbal and pallidal pCREB and deltaFosB in morphine-sensitized rats: correlations with receptor-evoked electrophysiological measures in the ventral pallidum. Neuropsychopharmacology 31:1212-1226.

McFarland K, Davidge SB, Lapish CC, Kalivas PW. (2004). Limbic and motor circuitry underlying footshock-induced reinstatement of cocaine-seeking behavior. J Neurosci. 24(7):1551-1560.

McFarland K, Kalivas PW. (2001). The circuitry mediating cocaine-induced reinstatement of drug-seeking behavior. J Neurosci. 21(21):8655-8663.

Mink JW, Thach WT. (1991). Basal ganglia motor control. I. nonexclusion relation of pallidal discharge to five movement modes. J Neurophys 65(2):273-300

Mink JW, Thach WT. (1991). Basal ganglia motor control. II. late pallidal timing relative to movement onset and inconsistent pallidal coding of movement parameters J Neurophys 65(2):301-329

Mink JW, Thach WT. (1991). Basal ganglia motor control. I. pallidal ablation: normal reaction time, muscle cocontraction, and slow movement. J Neurophys 65(2):330-351

Mitchell SJ, Richardson RT, Baker FH, DeLong MR. (1987). The primate globus pallidus: neuronal activity related to direction of movement. Exp Brain Res 68:491-505.

Morse DT. (1999). MINSIZE2: a computer program for determining effect size and minimum sample size for statistical significance for univariate, multivariate, and nonparametric tests. Educ Psychol Meas 59: 518–531.

Napier TC, Mitrovic I, Churchill L, Klitenick MA, Lu XY, Kalivas PW. (1995). Substance P in the ventral pallidum: projection from the ventral striatum, and electrophysiological and behavioral consequences of pallidal substance P. Neuroscience. 69(1):59-70.

Nauta WJ, Smith GP, Faull RL, Domesick VB. (1978). Efferent connections and nigral afferents of the nucleus accumbens septi in the rat. Neuroscience. 3(4-5):385-401.

Norman AB, Tsibulsky VL. (2006). The compulsion zone: a pharmacological theory of acquired cocaine self-administration. Brain Res 1116(1):143–152

Norman AB, Buesing WR, Norman MK, Tabet MR, Tsibulsky VL. (2003). The self-administration of WIN 35,428 and cocacine: comparisons of satiety threshold and elimination half-life in rats. Eur J Pharmacol 483:281–287

O'Donnell P, Lavín A, Enquist LW, Grace AA, Card JP. (1997). Interconnected parallel circuits between rat nucleus accumbens and thalamus revealed by retrograde transynaptic transport of pseudorabies virus. J Neurosci. 17(6):2143-2167.

Olive MF, Anton B, Micevych P, Evans CJ, Maidment NT. (1997). Presynaptic verses postsynaptic localization of mu and -delta opioid receptors in dorsal and ventral striatopallidal pathways. J Neurosci 17(19):7471-7479

Olmstead MC, Parkinson JA, Miles FJ, Everitt BJ, Dickinson A. (2000). Cocaine-seeking by rats: regulation, reinforcement, and activation. Psychopharmacology (Berl) 152(2):123–131

Panlilio LV, Thorndike EB, Schindler CW. (2006). Cocaine self-administration under variable-dose schedules in squirrel monkeys. Pharmacol Biochem Behav 84(2):235–243

Pardue MT, Ball SL, Hetling JR, Chow VY, Chow AY, Peachey NS. (2001). Visual evoked potentials to infrared stimulation in normal cats and rats. Doc Ophthalmol 103(2): 155-162.

Paxinos G and Watson C. (1997). The Rat Brain in Stereotaxic Coordinates. New York: Academic Press, 1997.

Peoples LL, Uzwiak AJ, Gee F, West MO. (1997). Operant behavior during sessions of intravenous cocaine infusion is necessary and sufficient for phasic firing of single nucleus accumbens neurons. Brain Research, 757:280-284.

Pickens R, Thompson T. (1968). Cocaine-reinforced behavior in rats: effects of reinforcement magnitude and fixed-ratio size. J Pharmacol Exp Ther 161:122–129

Pickens R, Thompson T. (1971). Characteristics of stimulant drug reinforcement. In: Thompson T, Pickens R (eds) Stimulus properties of drugs. Appleton, Century, Croft, New York, pp 177–192

Roberts DC, Koob GF. (1982). Disruption of cocaine self-administration following 6-hydroxydopamine lesions of the ventral tegmental area in rats. Pharmacol Biochem Behav. 17(5):901-904.

Roberts DC, Corcoran ME, Fibiger HC. (1977). On the role of ascending catecholaminergic systems in intravenous self-administration of cocaine. Pharmacol Biochem Behav. 6(6):615-620.

Roberts DC, Koob GF, Klonoff P, Fibiger HC. (1980). Extinction and recovery of cocaine self-administration following 6-hydroxydopamine lesions of the nucleus accumbens. Pharmacol Biochem Behav. 12(5):781-787.

Robledo P, Koob GF. (1993). Two discrete nucleus accumbens projection areas differentially mediate cocaine self-administration in the rat. Behav Brain Res. 55(2):159-166.

Root DH, Fabbricatore AT, Barker DJ, Ma S, Pawlak AP, West MO (2009) Evidence for habitual and goal-directed behavior following devaluation of cocaine: a multifaceted interpretation of relapse. PLoS ONE 4(9):e7170

Root DH, Fabbricatore AT, Ma S, Barker DJ, West MO. (2010). Rapid phasic activity of ventral pallidal neurons during cocaine self-administration. Synapse, 64(9):704-713.

Root DH, Barker DJ, Ma S, Coffee KR, West MO. (2011). Evidence for skilled cocaine self-administration in rats. Psychopharmacology (Berl), in press.

Sesack SR, Deutch AY, Roth RH, Bunney BS. (1989). Topographical

organization of the efferent projections of the medial prefrontal cortex in the rat: an anterograde tract-tracing study with Phaseolus vulgaris leucoagglutinin. J Comp Neurol. 290(2):213-242.

Tang XC, McFarland K, Cagle S, Kalivas PW. (2005). Cocaine-induced reinstatement requires endogenous stimulation of mu-opioid receptors in the ventral pallidum. J Neurosci. 25(18):4512-4520.

Tang C, Pawlak AP, Prokopenko V, West MO. (2007). Changes in activity of the striatum during formation of a motor habit. Eur J Neurocsi. 25(4), 1212-1227.

Tsibulsky VL, Norman AB. (1999). Satiety threshold: a quantitative model of maintained cocaine self-administration. Brain Res 839:85–93

Vertes RP. (2004). Differential Projections of the Infralimbic and Prelimbic Cortex in the Rat. Synapse 51:32-58

Wise RA. (1987). Intravenous drug self-administration: a special case of positive reinforcement. In: Bozarth MA (ed) Methods of assessing the reinforcing properties of abused drugs. Springer, New York, pp 117–141

Wise RA, Newton P, Leeb K, Burnette B, Pocock D, Justice JB Jr. (1995). Fluctuations in nucleus accumbens dopamine concentration during intravenous cocaine self-administration in rats. Psychopharmacology (Berl) 120(1):10–20

Yokel RA, Pickens R. (1973). Self-administration of optical isomers of amphetamine and methylamphetamine by rats. J Pharmacol Exp Ther 187(1):27–33

Yokel AR, Pickens R. (1974). Drug level of D- and L-amphetamine during intravenous self-administration. Psychopharmacologia 34:255–264

Záborszky L, Heimer L, Eckenstein F, Leranth C. (1986). GABAergic input to cholinergic forebrain neurons: an ultrastructural study using retrograde tracing of HRP and double immunolabeling. J Comp Neurol 250:282-295.

Záborszky L, Léránth C, Heimer L. (1984). Ultrastructural evidence of amygdalofugal axons terminating on cholinergic cells of the rostral forebrain. Neurosci Lett. 52(3):219-225.

Záborszky, L., Alheid, G.F., Beinfeld, M.C., Eiden, L.E., Heimer, L. & Palkovits, M. (1985). Cholecystokinin innervation of the ventral striatum: a morphological and radioimmunological study. Neuroscience, 14, 427–453.

Záborszky L, Cullinan WE. (1992). Projections from the nucleus accumbens to cholinergic neurons of the ventral pallidum: a correlated light and electron microscopic double-immunolabeling study in rat. Brain Research 570:92-101

Zahm, D.S. & Heimer, L. (1988). Ventral striatopallidal parts of the basal ganglia in the rat: I. Neurochemical compartmentation as reflected by the distributions of neurotensin and substance P immunoreactivity. J. Comp. Neurol., 272, 516–535.

Zahm DS, Heimer L. (1990). Two transpallidal pathways originating in the rat nucleus accumbens. J Comp Neurol. 302(3):437-446.

Zahm DS, Záborszky L, Alones VE, Heimer L. (1985). Evidence for the coexistence of glutamate decarboxylase and Met-enkephalin immunoreactivities in axon terminals of rat ventral pallidum. Brain Res. 325(1-2):317-321.

Zahm DS, Williams E, Wohltmann C. (1996). Ventral striatopallidothalamic projection: IV. Relative involvements of neurochemically distinct subterritories in the ventral pallidum and adjacent parts of the rostroventral forebrain. J Comp Neurol 364(2):340-362.

Zahm DS, Jensen SL, Williams ES, Martin JR 3rd. (1999). Direct comparison of projections from the central amygdaloid region and nucleus accumbens shell. 11(4):1119-26.

FIGURE LEGENDS

Figure 1. Head-movement apparatus. Numbers refer to photocell number and are always located on the "receiving" photocell. Apparatus is shown with a front view (A), side view (B), and mounted to the rear corner of the chamber ("photocell corner") in its operative position outside the chamber (C).

Figure 2. Behaviors schematized for neuronal analysis. Appetitive behaviors included the approach towards the photocell corner (A), criterion head movement operant response (B), and retreat away from the photocell corner (C).

Figure 3. Self-administration and cue learning. Reaction time in response to the S^D (A), probability of self-administering cocaine upon S^D presentation (B), cocaine consumption (C), latency to load up to the tenth infusion (D), number of criterion movements (E). Values are average ± SEM (y axes) per day (x axes).

Figure 4. Skill learning: changes in criterion head movement characteristics with extensive repetition. Changes in velocity (a), duration (b), distance (c), probability of starting at photocell two, the minimum required for a criterion movement (d), and the probability of ending at photocell 5 (e). Values for a, b, and c are average median ± SEM per day for criterion head movements (y axes). Values for d and e are average probability ± SEM. All x axes refer to training day.

Figure 5. Microwires localized to the VPdl. Row A shows five examples of substance P stained tissue. Row B shows five examples of calbindin-d28k stained tissue. Row

C shows five examples of neurotensin stained tissue. Each number refers to a set of three stains used to localize each microwire, visualized as a green/blue dot from a potassium ferrocyanide counterstain. As a model for all VPdl neurons recorded, example 1 (A1, B1, C1) displays two microwire lesions. The medial wire was localized to the substance P stain (A1), calbindin d28k stain (B1), but not the neurotensin stain (C1). The lateral microwire was localized outside of the substance P stain and therefore was not considered in the dataset.

Figure 6. Microwires localized to the VPvm. Row A shows five examples of substance P stained tissue. Row B shows five examples of calbindin-d28k stained tissue. Row C shows five examples of neurotensin stained tissue. Each number refers to a set of three stains used to localize each microwire, visualized as a green/blue dot from a potassium ferrocyanide counterstain. As a model for all VPvm neurons recorded, example 1 (A1, B1, C1) displays a microwire lesion localized to the substance P stain (A1), neurotensin stain (C1), but not the calbindin d28k stain (B1).

Figure 7. Absence of S^D–evoked changes in FR. Cumulative proportion of all neurons' absolute (A) and directional (B) cue changes in FR per subregion. Black and gray lines indicate cumulative proportions for VPdl and VPvm neurons, respectively. Median values (0.50 proportion value) are displayed as square (VPdl) and circle (VPvm). No significant differences were observed between subregions. Note that for these figures, the scales (x-axis) differ for the absolute (A) and directional (B) changes in FR. For absolute changes in FR (A), a value of 0 was no difference from baseline FR and a fifty percent change from baseline FR was 0.1.

For the directional changes in FR (B), a value of 0.5 was no difference from baseline FR and a fifty percent change from baseline FR was 0.6 (increase) or 0.4 (decrease).

Figure 8. Approach VPdl neuron. Rasters and PETHs are centered (time 0) around end of approach (A), end of response (B), and beginning of retreat (C). Blue dot in A and green dot in B indicate the onset of approach and response, respectively. Red dot in C refers to the end of retreat. All rasters have been sorted for movement duration. Y-axis of raster refers to behavioral trial; y-axis of PETH refers to average FR (spikes/sec) per trial. Both x-axes refer to time (ms). This example VPdl neuron exhibited an increase in FR during the approach (A) but not the response (B) or retreat (C).

Figure 9. Approach VPvm neuron. Rasters and PETHs are centered (time 0) around end of approach (A), end of response (B), and beginning of retreat (C). Blue dot in A and green dot in B indicate the onset of approach and response, respectively. Red dot in C refers to the end of retreat. All rasters have been sorted for movement duration. Y-axis of raster refers to behavioral trial; y-axis of PETH refers to average FR (spikes/sec) per trial. Both x-axes refer to time (ms). This example VPvm neuron exhibited an increase in FR during the approach (A) but not the response (B) or retreat (C).

Figure 10. Approach changes in FR. Cumulative proportion of all neurons' absolute (A) and directional (B) approach changes in FR per subregion. Black and gray lines indicate cumulative proportions for VPdl and VPvm neurons, respectively. Median

values (0.50 proportion value) are displayed as square (VPdl) and circle (VPvm). VPdl neurons exhibited a greater absolute change in firing rate compared with VPvm neurons (A).

Figure 11. Response VPdl neuron. Rasters and PETHs are centered (time 0) around end of approach (A), end of response (B), and beginning of retreat (C). Blue dot in A and green dot in B indicate the onset of approach and response, respectively. Red dot in C refers to the end of retreat. All rasters have been sorted for movement duration. Y-axis of raster refers to behavioral trial; y-axis of PETH refers to average FR (spikes/sec) per trial. Both x-axes refer to time (ms). This example VPdl neuron exhibited a small increase in FR just prior to approach offset (A), an increase in FR during the response (B) but no change in FR during the retreat (C).

Figure 12. Response VPvm neuron. Rasters and PETHs are centered (time 0) around end of approach (A), end of response (B), and beginning of retreat (C). Blue dot in A and green dot in B indicate the onset of approach and response, respectively. Red dot in C refers to the end of retreat. All rasters have been sorted for movement duration. Y-axis of raster refers to behavioral trial; y-axis of PETH refers to average FR (spikes/sec) per trial. Both x-axes refer to time (ms). This example VPvm neuron exhibited an increase in FR during the response (B) but not during the approach (A) or retreat (C).

Figure 13. Criterion movement (Response)-induced changes in FR. Cumulative proportion of all neurons' absolute (A) and directional (B) response changes in FR per subregion. Black and gray lines indicate cumulative proportions for VPdl and

VPvm neurons, respectively. Median values (0.50 proportion value) are displayed as square (VPdl) and circle (VPvm). VPdl neurons exhibited a greater absolute change in firing rate compared with VPvm neurons (A). When taking direction of firing rate change into account, VPdl neurons exhibited a significant decrease in firing rate compared with VPvm neurons (B).

Figure 14. Frequency histogram of individual neuron correlation coefficients (x-axis) of response movement characteristics with FR. Given that no significant relationships were observed, all neurons were pooled into graphs of distance (A), duration (B), velocity (C), valley (start position) (D), and peak (end position) (E) regardless of subregion.

Figure 15. Approach-Response VPdl neuron. Rasters and PETHs are centered (time 0) around end of approach (A), end of response (B), and beginning of retreat (C). Blue dot in A and green dot in B indicate the onset of approach and response, respectively. Red dot in C refers to the end of retreat. All rasters have been sorted for movement duration. Y-axis of raster refers to behavioral trial; y-axis of PETH refers to average FR (spikes/sec) per trial. Both x-axes refer to time (ms). This example VPdl neuron exhibited a decrease in FR during both the approach (A) and response (B) but returned to baseline during the retreat (C).

Figure 16. Approach-Response VPdl neuron. Rasters and PETHs are centered (time 0) around end of approach (A), end of response (B), and beginning of retreat (C). Blue dot in A and green dot in B indicate the onset of approach and response, respectively. Red dot in C refers to the end of retreat. All rasters have been sorted

for movement duration. Y-axis of raster refers to behavioral trial; y-axis of PETH refers to average FR (spikes/sec) per trial. Both x-axes refer to time (ms). This example VPdl neuron exhibited a decrease in FR during both the approach (A) and response (B) but returned to baseline during the retreat (C).

Figure 17. Approach-Response relationship. Values on the x-axis refer to directional changes in FR during the response and values on the y-axis refer to directional changes in FR during the approach, for each neuron in the VPdl (A) and VPvm (B).

Figure 18. Approach-Response VPvm neuron. Rasters and PETHs are centered (time 0) around end of approach (A), end of response (B), and beginning of retreat (C). Blue dot in A and green dot in B indicate the onset of approach and response, respectively. Red dot in C refers to the end of retreat. All rasters have been sorted for movement duration. Y-axis of raster refers to behavioral trial; y-axis of PETH refers to average FR (spikes/sec) per trial. Both x-axes refer to time (ms). This example VPvm neuron exhibited a decrease in FR near the approach offset (A) and response (B) but returned to baseline during the retreat (C).

Figure 19. Cued Approach changes in FR. Cumulative proportion of all neurons' absolute (A) and directional (B) cued approach changes in FR per subregion. Black and gray lines indicate cumulative proportions for VPdl and VPvm neurons, respectively. Median values (0.50 proportion value) are displayed as square (VPdl) and circle (VPvm). VPdl neurons exhibited a greater absolute change in firing rate compared with VPvm neurons (A).

Figure 20. Uncued approach changes in FR. Cumulative proportion of all neurons' absolute (A) and directional (B) uncued approach changes in FR per subregion. Black and gray lines indicate cumulative proportions for VPdl and VPvm neurons, respectively. Median values (0.50 proportion value) are displayed as square (VPdl) and circle (VPvm). VPdl neurons exhibited a greater absolute change in firing rate compared with VPvm neurons (A).

Figure 21. Cued Approach-Uncued approach relationship. Values on the x-axis refer to directional changes in FR during the uncued approach and values on the y-axis refer to directional changes in FR during the cued approach, for each neuron (one dot per neuron) in the VPdl (A) and VPvm (B).

Figure 22. Cued/uncued approach VPdl neuron. Rasters and PETHs are centered (time 0) around end of cued approach (A) and uncued approach (B). Green dots refer to the onset of approach. Y-axis of raster refers to behavioral trial; y-axis of PETH refers to average FR (spikes/sec) per trial. Both x-axes refer to time (ms). This example VPdl neuron exhibited similar changes in FR during cued and uncued approaches.

Figure 23. Cued/uncued approach VPvm neuron. Rasters and PETHs are centered (time 0) around end of cued approach (A) and uncued approach (B). Green dots refer to the onset of approach. Y-axis of raster refers to behavioral trial; y-axis of PETH refers to average FR (spikes/sec) per trial. Both x-axes refer to time (ms). This example VPvm neuron exhibited similar changes in FR during cued and uncued approaches.

Figure 24. Cued approach VPvm neuron. Rasters and PETHs are centered (time 0) around end of cued approach (A) and uncued approach (B). Green dots refer to the onset of approach. Y-axis of raster refers to behavioral trial; y-axis of PETH refers to average FR (spikes/sec) per trial. Both x-axes refer to time (ms). This example VPvm neuron exhibited a decrease in FR when the approach was cued but not when the approach was uncued.

Figure 25. Cued/Reinforced response changes in FR. Cumulative proportion of all neurons' absolute (A) and directional (B) cued/reinforced response changes in FR per subregion. Black and gray lines indicate cumulative proportions for VPdl and VPvm neurons, respectively. Median values (0.50 proportion value) are displayed as square (VPdl) and circle (VPvm). VPdl neurons exhibited a greater absolute change in firing rate compared with VPvm neurons (A).

Figure 26. Uncued/Unreinforced response changes in FR. Cumulative proportion of all neurons' absolute (A) and directional (B) uncued/unreinforced changes in FR per subregion. Black and gray lines indicate cumulative proportions for VPdl and VPvm neurons, respectively. Median values (0.50 proportion value) are displayed as square (VPdl) and circle (VPvm). VPdl neurons exhibited a greater absolute change in firing rate compared with VPvm neurons (A). When taking direction of firing rate change into account, VPdl neurons exhibited a significant decrease in firing rate compared with VPvm neurons (B).

Figure 27. Cued/Reinforced response-Uncued/Unreinforced response relationship. Values on the x-axis refer to directional changes in FR during the cued/reinforced response and values on the y-axis refer to directional changes in FR during the uncued/unreinforced, for each neuron in the VPdl (A) and VPvm (B).

Figure 28. VPdl neuron during cued/reinforced and uncued/unreinforced nodes. Rasters and PETHs are centered (time 0) around end of cued/reinforced response (A) and uncued/unreinforced approach (B). Blue dots refer to the onset of response. Y-axis of raster refers to behavioral trial; y-axis of PETH refers to average FR (spikes/sec) per trial. Both x-axes refer to time (ms). While this neuron exhibited a decrease in FR during cued/reinforced responses relative to the uncued/unreinforced response, this was likely due to low FRs observed during behaviors and response nodes rather than a reflection of appetitive processing.

Figure 29. VPvm neuron during cued/reinforced and uncued/unreinforced nodes. Rasters and PETHs are centered (time 0) around end of cued/reinforced response (A) and uncued/unreinforced approach (B). Blue dots refer to the onset of response. Y-axis of raster refers to behavioral trial; y-axis of PETH refers to average FR (spikes/sec) per trial. Both x-axes refer to time (ms). While this neuron exhibited a decrease in FR during cued/reinforced responses relative to the uncued/unreinforced response, this was likely due to low FRs observed during behaviors and response nodes rather than a reflection of appetitive processing.

Figure 30. VPdl neuron during cued/reinforced and uncued/unreinforced nodes. Rasters and PETHs are centered (time 0) around end of cued/reinforced response

(A) and uncued/unreinforced approach (B). Blue dots refer to the onset of response. Y-axis of raster refers to behavioral trial; y-axis of PETH refers to average FR (spikes/sec) per trial. Both x-axes refer to time (ms). This neuron exhibited a decrease in FR during both cued/reinforced and uncued/unreinforced responses.

Figure 31. VPvm neuron during cued/reinforced and uncued/unreinforced nodes. Rasters and PETHs are centered (time 0) around end of cued/reinforced response (A) and uncued/unreinforced approach (B). Blue dots refer to the onset of response. Y-axis of raster refers to behavioral trial; y-axis of PETH refers to average FR (spikes/sec) per trial. Both x-axes refer to time (ms). This neuron exhibited a decrease in FR during both cued/reinforced and uncued/unreinforced responses.

Figure 32. VPvm retreat neuron. Rasters and PETHs are centered (time 0) around end of approach (A), end of response (B), and beginning of retreat (C). Blue dot in A and green dot in B indicate the onset of approach and response, respectively. Red dot in C refers to the end of retreat. All rasters have been sorted for movement duration. Y-axis of raster refers to behavioral trial; y-axis of PETH refers to average FR (spikes/sec) per trial. Both x-axes refer to time (ms). This example VPvm neuron exhibited no change in FR during the approach (A) or response (B) but exhibited changes in FR during the retreat (C).

Figure 33. Retreat changes in FR. Cumulative proportion of all neurons' absolute (A) and directional (B) retreat changes in FR per subregion. Black and gray lines indicate cumulative proportions for VPdl and VPvm neurons, respectively. Median

values (0.50 proportion value) are displayed as square (VPdl) and circle (VPvm). No differences were observed between subregions.

Figure 34. Pump retreat-Nonpump retreat relationship. Values on the x-axis refer to directional changes in FR during the pump retreat and values on the y-axis refer to directional changes in FR during the nonpump retreat, for each neuron (each dot per neuron) in the VPdl (A) and VPvm (B).

Figure 35. VPdl neuron during pump and nonpump retreats. Rasters and PETHs are centered (time 0) around beginning of pump retreats (A) and nonpump retreats (B). Red dots refer to the offset of the retreat. Y-axis of raster refers to behavioral trial; y-axis of PETH refers to average FR (spikes/sec) per trial. Both x-axes refer to time (ms). This neuron exhibited an increase in FR during both pump and nonpump retreats.

Figure 36. VPvm neuron during pump and nonpump retreats. Rasters and PETHs are centered (time 0) around beginning of pump retreats (A) and nonpump retreats (B). Red dots refer to the offset of the retreat. Y-axis of raster refers to behavioral trial; y-axis of PETH refers to average FR (spikes/sec) per trial. Both x-axes refer to time (ms). This neuron exhibited an increase in FR during both pump and nonpump retreats.

Figure 37. VPdl neuron during pump and nonpump retreats. Rasters and PETHs are centered (time 0) around beginning of pump retreats (A) and nonpump retreats (B). Red dots refer to the offset of the retreat. Y-axis of raster refers to behavioral trial; y-

axis of PETH refers to average FR (spikes/sec) per trial. Both x-axes refer to time (ms). This neuron exhibited an increase in FR during only nonpump retreats.

Figure 38. VPvm neuron during pump and nonpump retreats. Rasters and PETHs are centered (time 0) around beginning of pump retreats (A) and nonpump retreats (B). Red dots refer to the offset of the retreat. Y-axis of raster refers to behavioral trial; y-axis of PETH refers to average FR (spikes/sec) per trial. Both x-axes refer to time (ms). This neuron exhibited an increase in FR during only pump retreats.

Figure 39. Pump retreat changes in FR. Cumulative proportion of all neurons' absolute (A) and directional (B) cue changes in FR per subregion. Black and gray lines indicate cumulative proportions for VPdl and VPvm neurons, respectively. Median values (0.50 proportion value) are displayed as square (VPdl) and circle (VPvm). VPdl neurons exhibited a greater absolute change in firing rate compared with VPvm neurons (A). When taking direction of firing rate change into account, VPdl neurons exhibited a significant decrease in firing rate compared with VPvm neurons (B).

Figure 40. Nonpump retreat changes in FR. Cumulative proportion of all neurons' absolute (A) and directional (B) cue changes in FR per subregion. Black and gray lines indicate cumulative proportions for VPdl and VPvm neurons, respectively. Median values (0.50 proportion value) are displayed as square (VPdl) and circle (VPvm). No differences were observed between subregions.

Figure 41. Approach-retreat relationship. Values on the x-axis refer to directional changes in FR during the retreat and values on the y-axis refer to directional changes in FR during the approach, for each neuron (one dot per neuron) in the VPdl (A) and VPvm (B).

Figure 42. VPvm approach-retreat neuron. Rasters and PETHs are centered (time 0) around end of approach (A), end of response (B), and beginning of retreat (C). Blue dot in A and green dot in B indicate the onset of approach and response, respectively. Red dot in C refers to the end of retreat. All rasters have been sorted for movement duration. Y-axis of raster refers to behavioral trial; y-axis of PETH refers to average FR (spikes/sec) per trial. Both x-axes refer to time (ms). This example VPvm neuron exhibited a decrease in FR during the approach (A), returned to baseline during the response (B), and increased in FR during the retreat (C).

Figure 43. VPvm approach-retreat neuron. Rasters and PETHs are centered (time 0) around end of approach (A), end of response (B), and beginning of retreat (C). Blue dot in A and green dot in B indicate the onset of approach and response, respectively. Red dot in C refers to the end of retreat. All rasters have been sorted for movement duration. Y-axis of raster refers to behavioral trial; y-axis of PETH refers to average FR (spikes/sec) per trial. Both x-axes refer to time (ms). This example VPvm neuron exhibited a decrease in FR during the approach (A), returned to baseline during the response (B), and increased in FR during the retreat (C).

Figure 44. VPdl response-retreat neuron. Rasters and PETHs are centered (time 0) around end of approach (A), end of response (B), and beginning of retreat (C). Blue

dot in A and green dot in B indicate the onset of approach and response, respectively. Red dot in C refers to the end of retreat. All rasters have been sorted for movement duration. Y-axis of raster refers to behavioral trial; y-axis of PETH refers to average FR (spikes/sec) per trial. Both x-axes refer to time (ms). This example VPdl neuron exhibited no change in FR during the approach (A), an increase in FR during the response (B), and decreased in FR during the retreat (C).

Figure 45. VPvm response-retreat neuron. Rasters and PETHs are centered (time 0) around end of approach (A), end of response (B), and beginning of retreat (C). Blue dot in A and green dot in B indicate the onset of approach and response, respectively. Red dot in C refers to the end of retreat. All rasters have been sorted for movement duration. Y-axis of raster refers to behavioral trial; y-axis of PETH refers to average FR (spikes/sec) per trial. Both x-axes refer to time (ms). This example VPvm neuron exhibited no change in FR during the approach (A), a decrease in FR during the response (B), and increased in FR during the retreat (C).

Figure 46. Response-retreat relationship. Values on the x-axis refer to directional changes in FR during the retreat and values on the y-axis refer to directional changes in FR during the response, for each neuron (one dot per neuron) in the VPdl (A) and VPvm (B).

Figure 47. VPdl continuous approach-response-retreat neuron. Rasters and PETHs are centered (time 0) around end of approach (A), end of response (B), and beginning of retreat (C). Blue dot in A and green dot in B indicate the onset of approach and response, respectively. Red dot in C refers to the end of retreat. All

rasters have been sorted for movement duration. Y-axis of raster refers to behavioral trial; y-axis of PETH refers to average FR (spikes/sec) per trial. Both x-axes refer to time (ms). This example VPdl neuron exhibited a decrease in FR that began during the approach (A) and continued through the response (B) and retreat (C).

Figure 48. VPvm continuous approach-response-retreat neuron. Rasters and PETHs are centered (time 0) around end of approach (A), end of response (B), and beginning of retreat (C). Blue dot in A and green dot in B indicate the onset of approach and response, respectively. Red dot in C refers to the end of retreat. All rasters have been sorted for movement duration. Y-axis of raster refers to behavioral trial; y-axis of PETH refers to average FR (spikes/sec) per trial. Both x-axes refer to time (ms). This example VPvm neuron exhibited a decrease in FR that began during the approach (A) and continued through the response (B) and retreat (C).

Figure 49. VPvm heterogeneous approach-response-retreat neuron. Rasters and PETHs are centered (time 0) around end of approach (A), end of response (B), and beginning of retreat (C). Blue dot in A and green dot in B indicate the onset of approach and response, respectively. Red dot in C refers to the end of retreat. All rasters have been sorted for movement duration. Y-axis of raster refers to behavioral trial; y-axis of PETH refers to average FR (spikes/sec) per trial. Both x-axes refer to time (ms). This example VPvm neuron exhibited an increase in FR during the approach and a decrease in FR during the response (B) and retreat (C).

Figure 50. VPvm heterogeneous approach-response-retreat neuron. Rasters and PETHs are centered (time 0) around end of approach (A), end of response (B), and

beginning of retreat (C). Blue dot in A and green dot in B indicate the onset of approach and response, respectively. Red dot in C refers to the end of retreat. All rasters have been sorted for movement duration. Y-axis of raster refers to behavioral trial; y-axis of PETH refers to average FR (spikes/sec) per trial. Both x-axes refer to time (ms). This example VPvm neuron exhibited a decrease in FR during the approach and response (B) but increased in FR during the retreat (C).

Figure 51. VPvm heterogeneous approach-response-retreat neuron. Rasters and PETHs are centered (time 0) around end of approach (A), end of response (B), and beginning of retreat (C). Blue dot in A and green dot in B indicate the onset of approach and response, respectively. Red dot in C refers to the end of retreat. All rasters have been sorted for movement duration. Y-axis of raster refers to behavioral trial; y-axis of PETH refers to average FR (spikes/sec) per trial. Both x-axes refer to time (ms). This example VPvm neuron exhibited an increase in FR during the approach and response (B) but decreased in FR during the retreat (C).

Figure 52. VPvm heterogeneous approach-response-retreat neuron. Rasters and PETHs are centered (time 0) around end of approach (A), end of response (B), and beginning of retreat (C). Blue dot in A and green dot in B indicate the onset of approach and response, respectively. Red dot in C refers to the end of retreat. All rasters have been sorted for movement duration. Y-axis of raster refers to behavioral trial; y-axis of PETH refers to average FR (spikes/sec) per trial. Both x-axes refer to time (ms). This example VPvm neuron exhibited a decrease in FR during the approach and response (B) but increased in FR during the retreat (C).

Figure 53. VPdl heterogeneous approach-response-retreat neuron. Rasters and PETHs are centered (time 0) around end of approach (A), end of response (B), and beginning of retreat (C). Blue dot in A and green dot in B indicate the onset of approach and response, respectively. Red dot in C refers to the end of retreat. All rasters have been sorted for movement duration. Y-axis of raster refers to behavioral trial; y-axis of PETH refers to average FR (spikes/sec) per trial. Both x-axes refer to time (ms). This example VPdl neuron exhibited an increase in FR during the approach and a decrease in FR during the response (B) and retreat (C).

Figure 54. VPdl heterogeneous approach-response-retreat neuron. Rasters and PETHs are centered (time 0) around end of approach (A), end of response (B), and beginning of retreat (C). Blue dot in A and green dot in B indicate the onset of approach and response, respectively. Red dot in C refers to the end of retreat. All rasters have been sorted for movement duration. Y-axis of raster refers to behavioral trial; y-axis of PETH refers to average FR (spikes/sec) per trial. Both x-axes refer to time (ms). This example VPdl neuron exhibited a decrease in FR during the approach and an increase in FR during the response (B) and retreat (C).

Figure 55. VPdl heterogeneous approach-response-retreat neuron. Rasters and PETHs are centered (time 0) around end of approach (A), end of response (B), and beginning of retreat (C). Blue dot in A and green dot in B indicate the onset of approach and response, respectively. Red dot in C refers to the end of retreat. All rasters have been sorted for movement duration. Y-axis of raster refers to behavioral trial; y-axis of PETH refers to average FR (spikes/sec) per trial. Both x-axes refer to

time (ms). This example VPdl neuron exhibited an increase in FR during the approach and a decrease in FR during the response (B) and retreat (C).

Figure 56. Pre-approach movement firing correlate of VPdl neuron in Figure 55. In contrast to previous approach graphs, rasters and PETHs are centered (time 0) around the beginning of approach (A and B). Furthermore, in contrast to previous approach figure, the green dot refers to the end of approach. All rasters have been sorted for movement duration. Y-axis of raster refers to behavioral trial; y-axis of PETH refers to average FR (spikes/sec) per trial. Both x-axes refer to time (ms). This neuron exhibited a pre-approach decrease in FR (A). Video analyses revealed that this neuron decreased in FR during the movement prior to the approach (magenta dots are onset and cyan dots in (B) are the offset of the pre-approach movement).

Figure 57. Potential pre-movement neuron. Rasters and PETHs are centered (time 0) around end of approach (A), end of response (B), and beginning of retreat (C). Blue dot in A and green dot in B indicate the onset of approach and response, respectively. Red dot in C refers to the end of retreat. All rasters have been sorted for movement duration. Y-axis of raster refers to behavioral trial; y-axis of PETH refers to average FR (spikes/sec) per trial. Both x-axes refer to time (ms). This example VPvm neuron exhibited an increase in FR prior to the approach, which was examined in Figure 58.

Figure 58. Pre-approach movement firing correlate of VPvm neuron in Figure 57. In contrast to previous approach graphs, rasters and PETHs are centered (time 0) around the beginning of approach (A and B). Furthermore, in contrast to previous

approach figure, the green dot refers to the end of approach. All rasters have been sorted for movement duration. Y-axis of raster refers to behavioral trial; y-axis of PETH refers to average FR (spikes/sec) per trial. Both x-axes refer to time (ms). This neuron exhibited a pre-approach decrease in FR (A). Video analyses revealed that this neuron increased in FR during the movement prior to the approach (magenta dots indicate onset and cyan dots in (B) indicate offset of the pre-approach movement).

Figure 59. Potential pre-movement neuron. Rasters and PETHs are centered (time 0) around end of approach (A), end of response (B), and beginning of retreat (C). Blue dot in A and green dot in B indicate the onset of approach and response, respectively. Red dot in C refers to the end of retreat. All rasters have been sorted for movement duration. Y-axis of raster refers to behavioral trial; y-axis of PETH refers to average FR (spikes/sec) per trial. Both x-axes refer to time (ms). This example VPvm neuron exhibited an increase in FR prior to the approach, which was examined in Figure 60.

Figure 60. Pre-approach movement firing correlate of VPvm neuron in Figure 59. In contrast to previous approach graphs, rasters and PETHs are centered (time 0) around the beginning of approach (A, B, and C). Furthermore, in contrast to previous approach figure, the green dot refers to the end of approach. All rasters have been sorted for movement duration. Y-axis of raster refers to behavioral trial; y-axis of PETH refers to average FR (spikes/sec) per trial. Both x-axes refer to time (ms). Panel (A) shows trials in which a previous approach occurred within the 4 second firing window prior to the current approach. Prior approach onset and offset are

displayed as magenta and cyan dots, respectively. Panel (B) shows trials in which a previous response occurred within the 4 second firing window prior to the approach. Prior response onset and offset are displayed as magenta and cyan dots, respectively. Panel (C) shows trials in which a previous retreat occurred within the 4 second firing window prior to the approach. Prior approach onset and offset are displayed as magenta and cyan dots, respectively. This figure suggests that the decrease in FR observed in Figure 59A prior to the approach was due to a decrease in FR near the offset of the previous retreat which was proximal to the approach onset (60C).

TABLE LEGENDS

Table 1. Data are presented as means ± SEM. *Amplitude of unitary action potentials.

Table 2. Behavioral characteristics used for electrophysiological analyses. Data are presented as means ± SEM.

Table 3. Distribution of neurons within VP subregions exhibiting 20% change from baseline (increase, decrease, or mixed) during distinct behaviors. Numbers in parentheses refer to percent and number of neurons in VPdl or VPvm.

SUPPLEMENTAL MOVIE LEGENDS

Movie 1. This movie provides four examples of approach, response, and retreat nodes used for electrophysiological analysis. Onset and offset times are marked for each behavior.

Movie 2. This movie provides examples of the pre-approach movement and approach nodes exhibited by one rat. Two neurons exhibited changes in FR during these behaviors (Figure 55-58). Onset and offset times are marked for both behaviors.

Table 1. Electrophysiological data by subregion						
Subregion	Units / Microwires (n)	Triphasic (%)	Amplitude (μV)	Signal-to-noise ratio	Baseline FR (cue)	Baseline FR (movements)
VPvm	171 / 140	11.63	139.14 ± 6.33	4.22 ± 0.09	1.49 ± 0.35	1.52 ± 0.36
VPdl	48 / 38	8.33	116.55 ± 7.10	4.49 ± 0.20	0.95 ± 0.2	1.00 ± 0.22
Total	219 / 178					

Table 2. Behavioral nodes used for electrophysiological analyses		
Behavior	Number of events	Duration (ms)
Approach	608.96 ± 72.77	956.60 ± 63.08
Cued Approach	310.60 ± 35.17	955.97 ± 63.83
Uncued Approach	298.36 ± 38.98	960.40 ± 62.55
Criterion Movement (Response)	312.96 ± 41.72	340.20 ± 19.00
Reinforced/Cued Response	88.12 ± 8.57	352.35 ± 19.16
Unreinforced/Uncued Response	165.44 ± 24.44	335.94 ± 20.52
Retreat	630 ± 75.09	694.92 ± 39.00

Table 3. Neurons exhibiting 20% change from baseline during distinct behaviors				
	Increase (% / N)	Decrease (% / N)	Mixed (% / N)	Total (% / N)
Approach VPdl	4.17% / 2	6.25% / 3	NA	10.42% / 5
Approach VPvm	2.92% / 5	5.26% / 9	NA	8.19% / 14
Response VPdl	6.25% / 3	18.75% / 9	NA	25% / 12
Response VPvm	10.53% / 18	12.28% / 21	NA	22.81% / 39
Retreat VPdl	0% / 0	2.08% / 1	NA	2.08% / 1
Retreat VPvm	5.85% / 10	2.92% / 5	NA	8.77% / 15
Approach-Response VPdl	2.08% / 1	10.42% / 5	2.08% / 1	14.58% / 7
Approach-Response VPvm	1.75% / 3	5.85% / 10	1.75% / 3	9.36% / 16
Approach-Retreat VPdl	4.17% / 2	2.08% / 1	0% / 0	6.25% / 3
Approach-Retreat VPvm	2.34% / 4	2.34% / 4	1.17% / 2	5.85% / 10
Response-Retreat VPdl	0% / 0	2.08% / 1	2.08% / 1	4.17% / 2
Response-Retreat VPvm	1.75% / 3	2.34% / 4	7.02% / 12	11.11% / 19
Approach-Response-Retreat VPdl	6.25% / 3	12.5% / 6	4.17% / 2	22.92% / 11
Approach-Response-Retreat VPvm	2.92% / 5	3.51% / 6	3.51% / 6	9.94% / 17
Total VPdl (% / N)	22.92% / 11	54.17% / 26	8.33% / 4	85.42% / 41
Total VPvm (% / N)	28.07% / 48	34.5% / 59	13.45% / 23	76.02% / 130

Figure 1

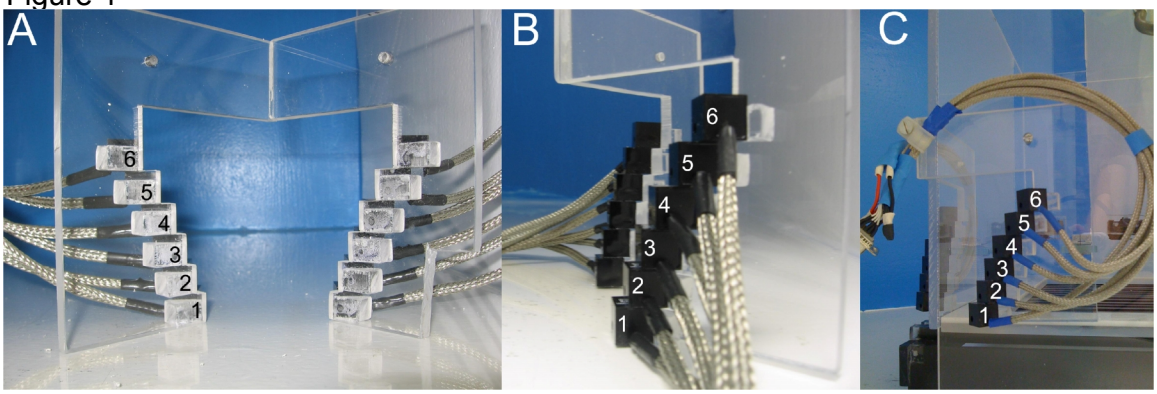

Figure 2

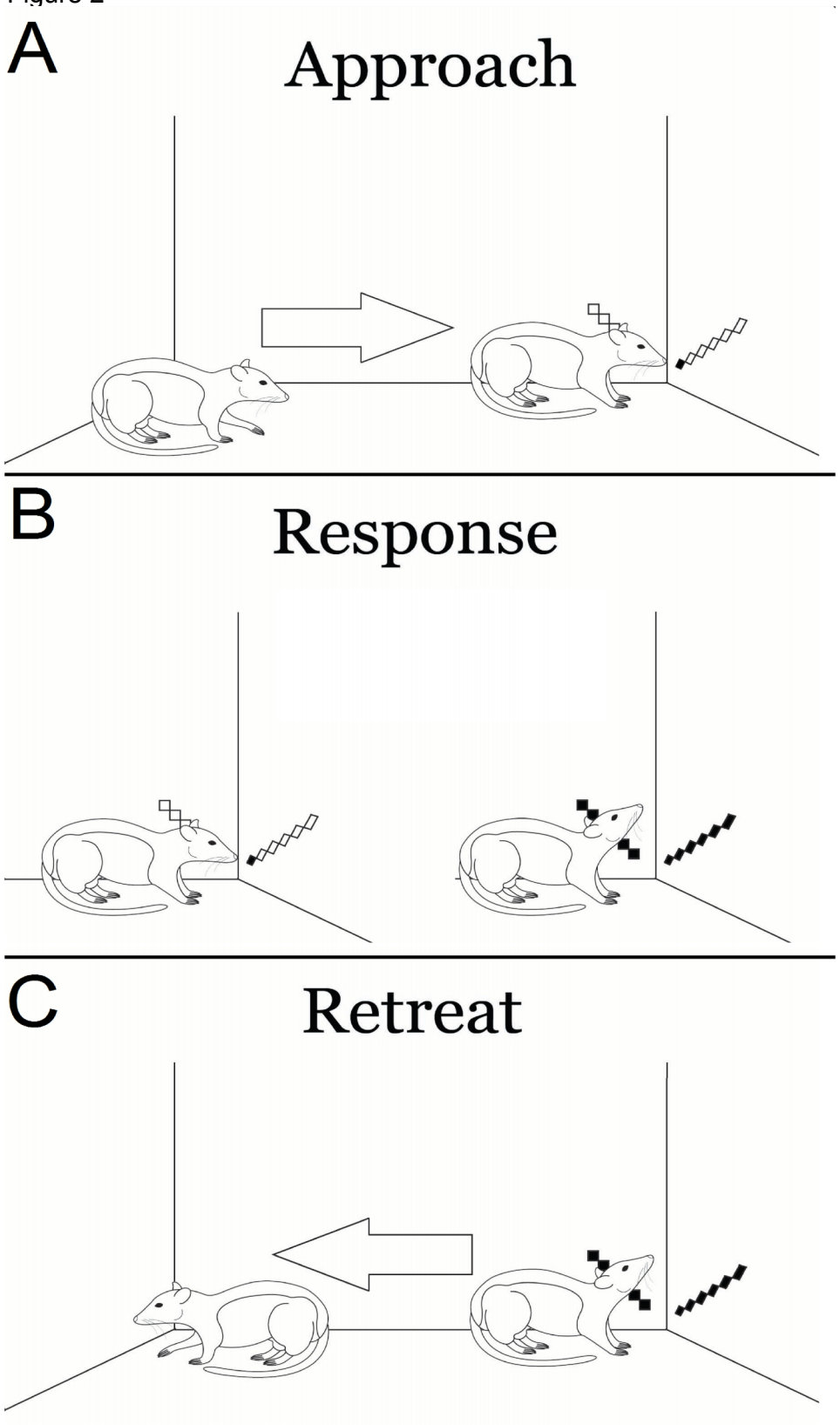

Figure 3

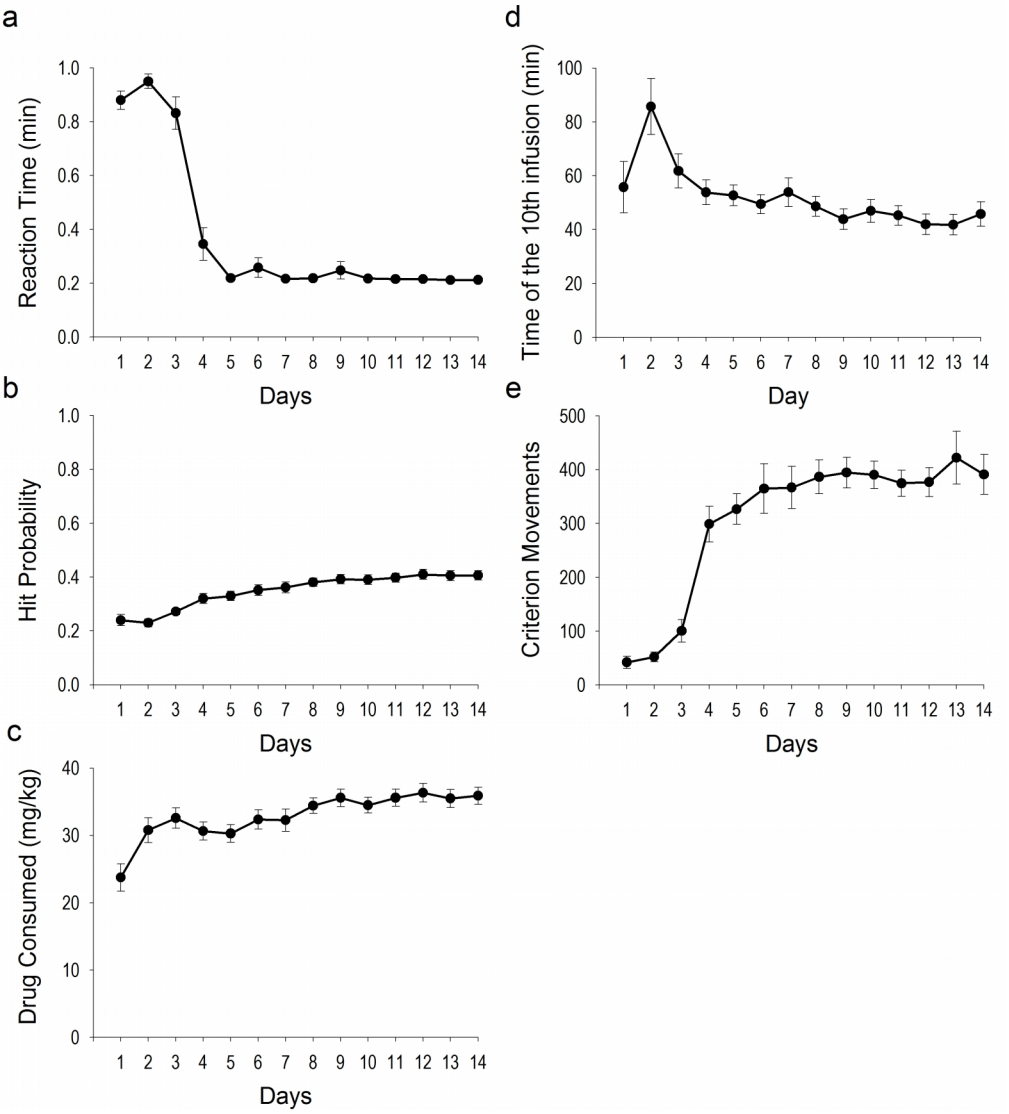
a
Reaction Time (min)
Days
b
Hit Probability
Days
c
Drug Consumed (mg/kg)
Days
d
Time of the 10th infusion (min)
Day
e
Criterion Movements
Days

Figure 4

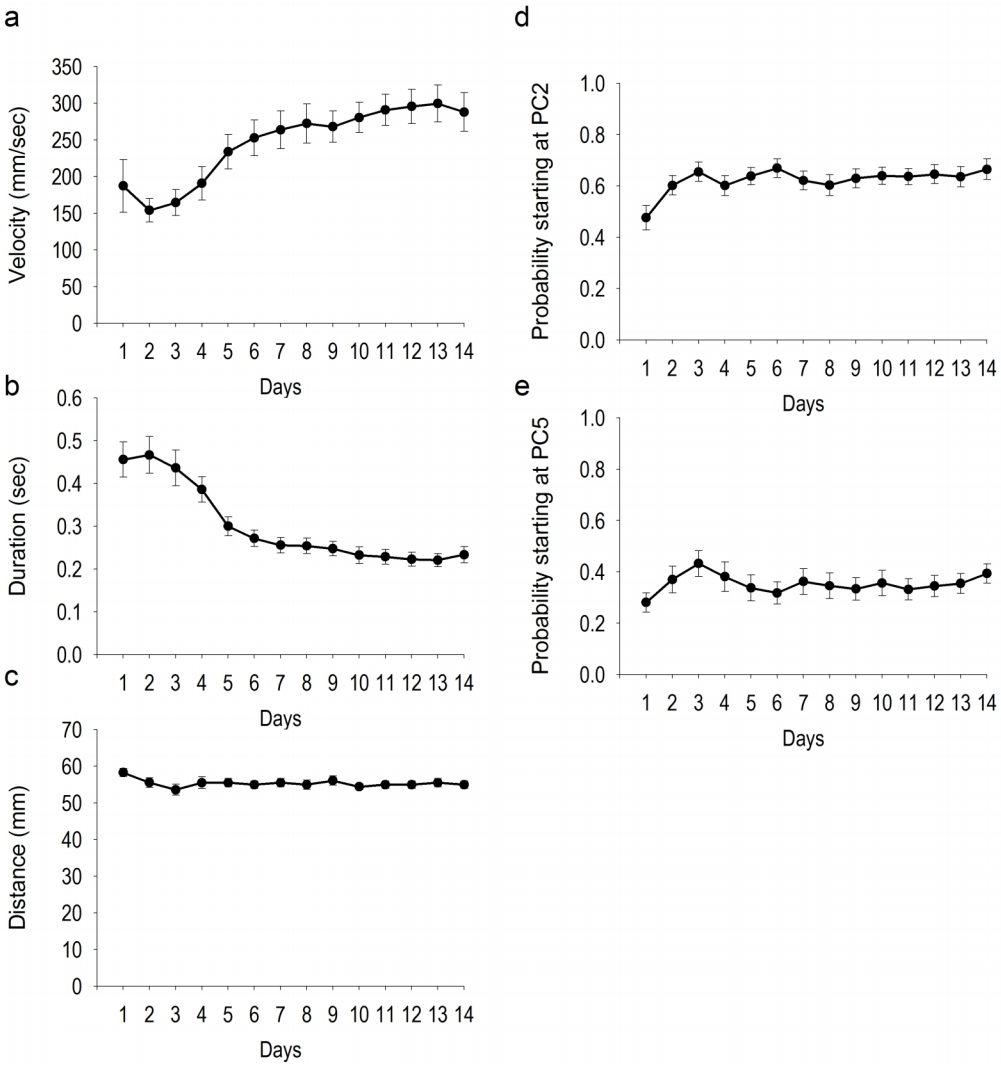
a
Velocity (mm/sec)
Days
b
Duration (sec)
Days
c
Distance (mm)
Days
d
Probability starting at PC2
Days
e
Probability starting at PC5
Days

Figure 5

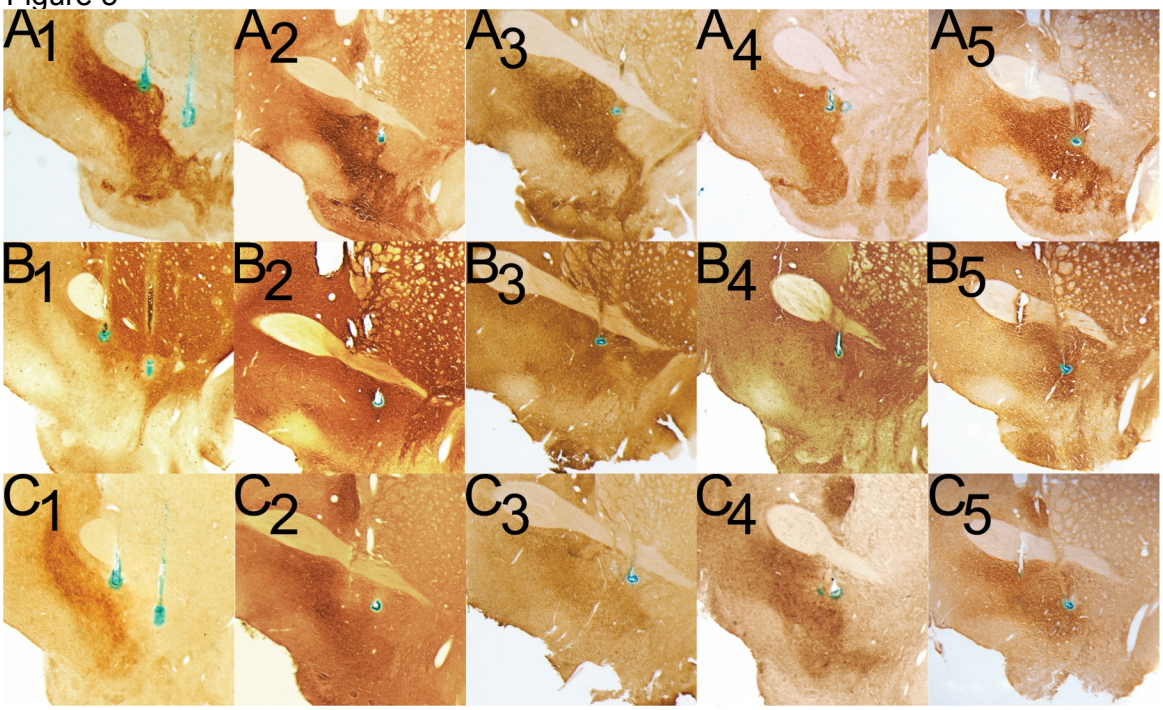

Figure 6

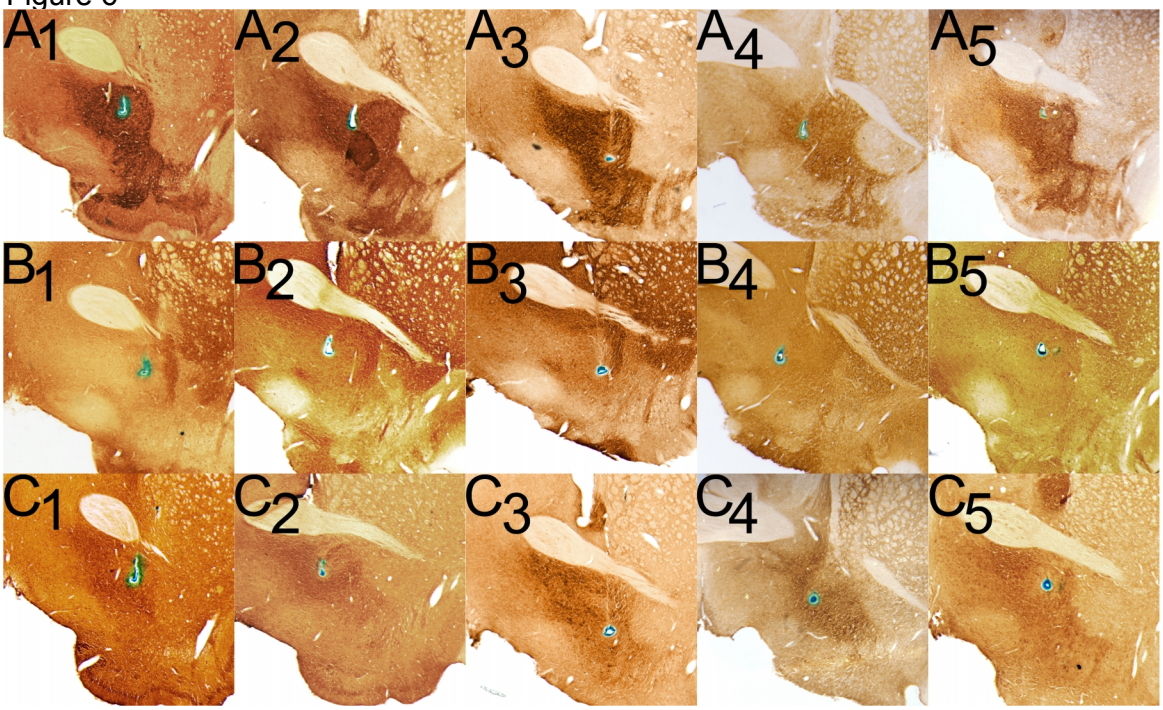

Figure 7

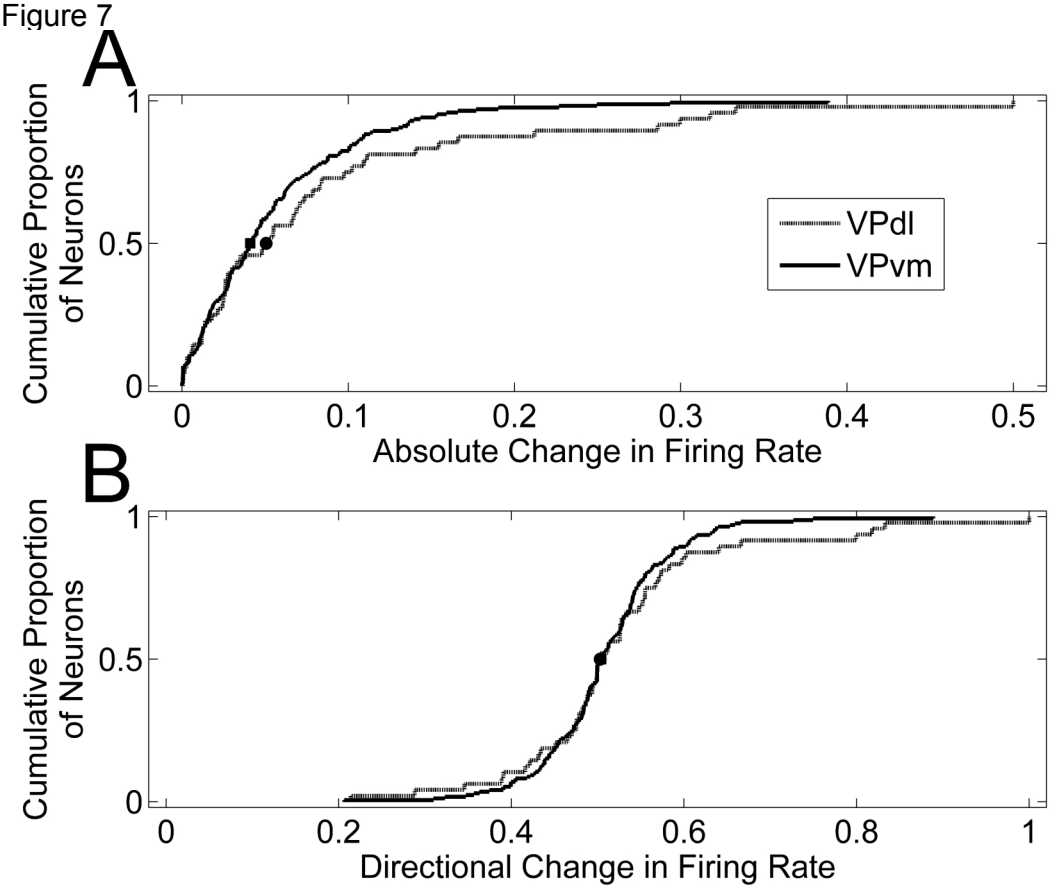
A
Cumulative Proportion of Neurons
1
0.5
0
0
0.1
0.2
0.3
0.4
0.5
Absolute Change in Firing Rate
VPdl
VPvm
B
Cumulative Proportion of Neurons
1
0.5
0
0
0.2
0.4
0.6
0.8
1
Directional Change in Firing Rate

Figure 8

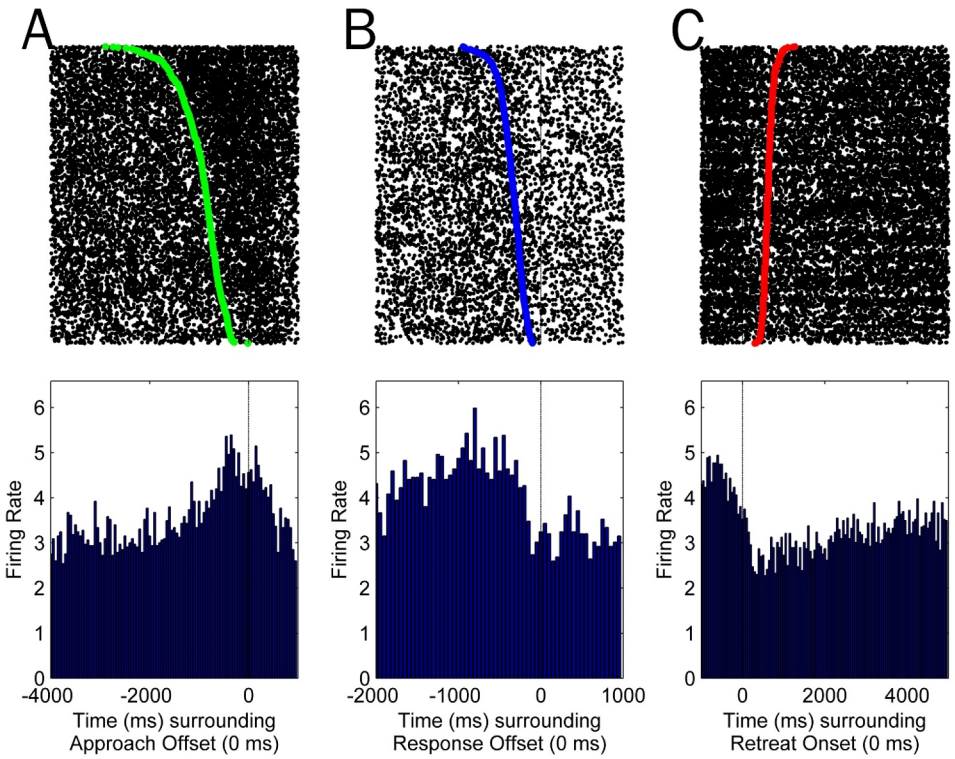
A
B
C
Firing Rate
Time (ms) surrounding
Approach Offset (0 ms)
Time (ms) surrounding
Response Offset (0 ms)
Time (ms) surrounding
Retreat Onset (0 ms)

Figure 9

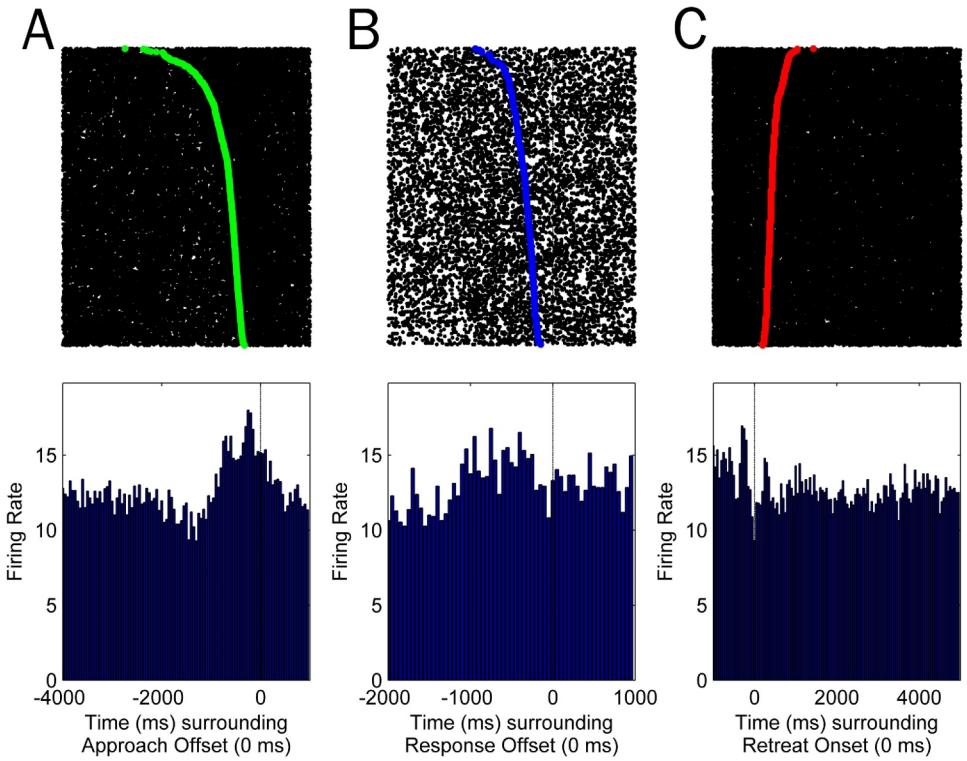
A
B
C
Firing Rate
15
10
5
0
-4000
-2000
0
Time (ms) surrounding
Approach Offset (0 ms)
-2000
-1000
0
1000
Time (ms) surrounding
Response Offset (0 ms)
0
2000
4000
Time (ms) surrounding
Retreat Onset (0 ms)

Figure 10

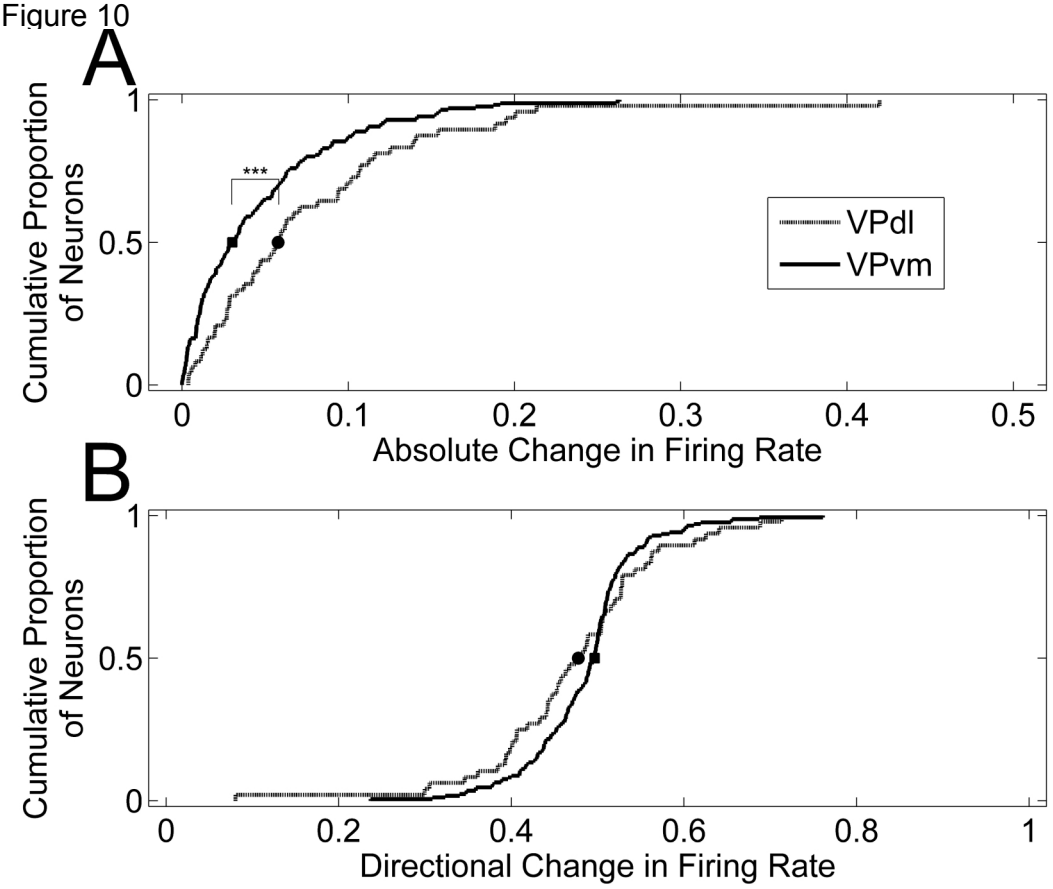
A
Cumulative Proportion of Neurons
1
0.5
0
***
VPdl
VPvm
0
0.1
0.2
0.3
0.4
0.5
Absolute Change in Firing Rate
B
Cumulative Proportion of Neurons
1
0.5
0
0
0.2
0.4
0.6
0.8
1
Directional Change in Firing Rate

Figure 11

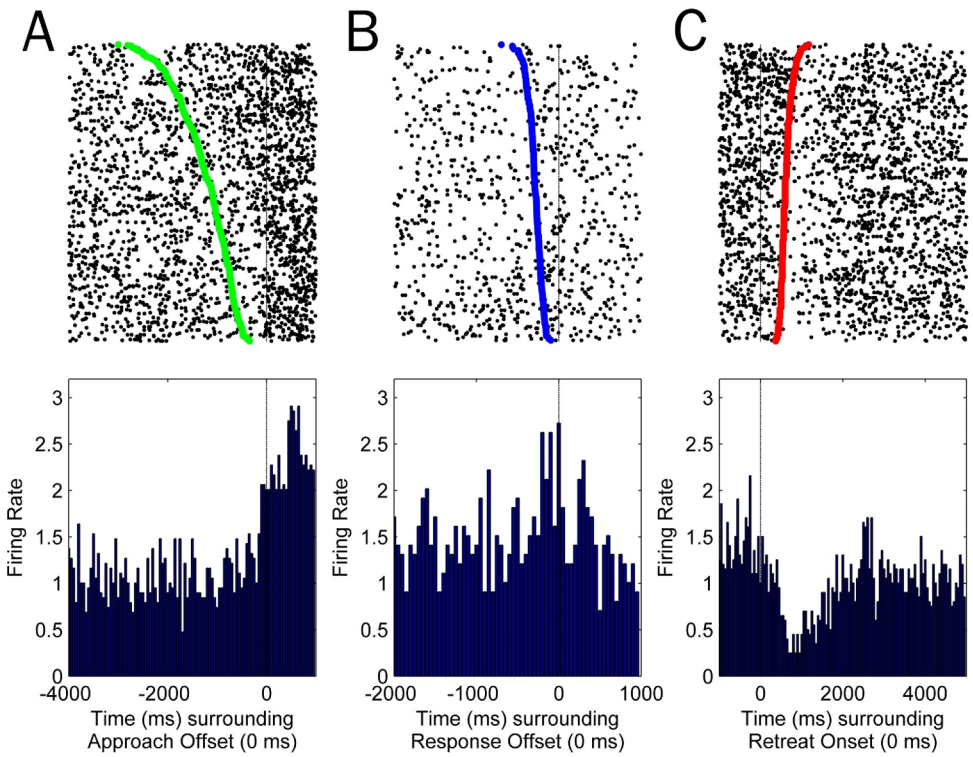
A
B
C
Firing Rate
Time (ms) surrounding
Approach Offset (0 ms)
Time (ms) surrounding
Response Offset (0 ms)
Time (ms) surrounding
Retreat Onset (0 ms)

Figure 12

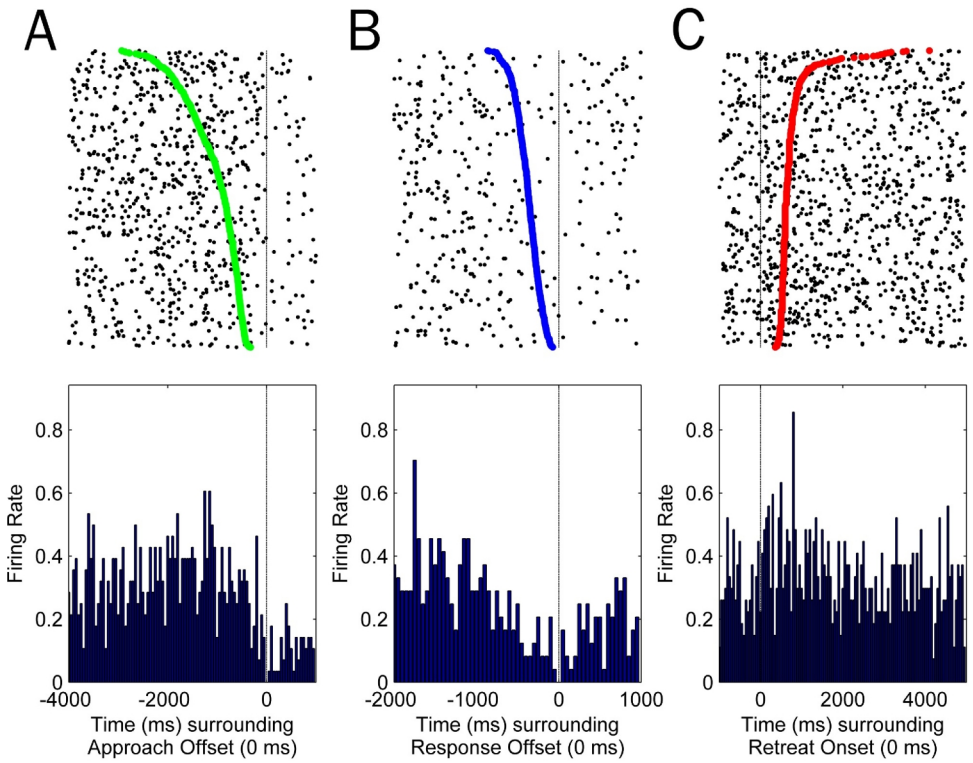
A
B
C
Firing Rate
0
0.2
0.4
0.6
0.8
-4000
-2000
0
Time (ms) surrounding
Approach Offset (0 ms)
-2000
-1000
0
1000
Time (ms) surrounding
Response Offset (0 ms)
0
2000
4000
Time (ms) surrounding
Retreat Onset (0 ms)

Figure 13

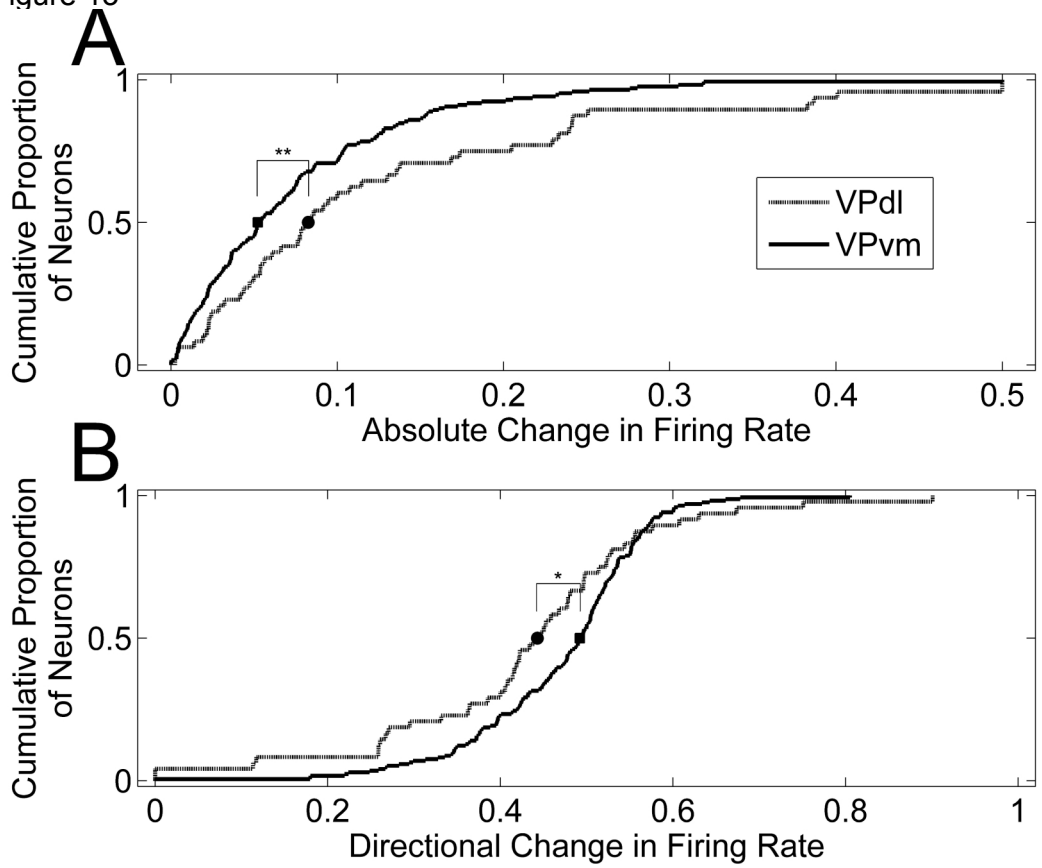
A
Cumulative Proportion of Neurons
1
0.5
0
**
VPdl
VPvm
0
0.1
0.2
0.3
0.4
0.5
Absolute Change in Firing Rate
B
Cumulative Proportion of Neurons
1
0.5
0
*
0
0.2
0.4
0.6
0.8
1
Directional Change in Firing Rate

Figure 14

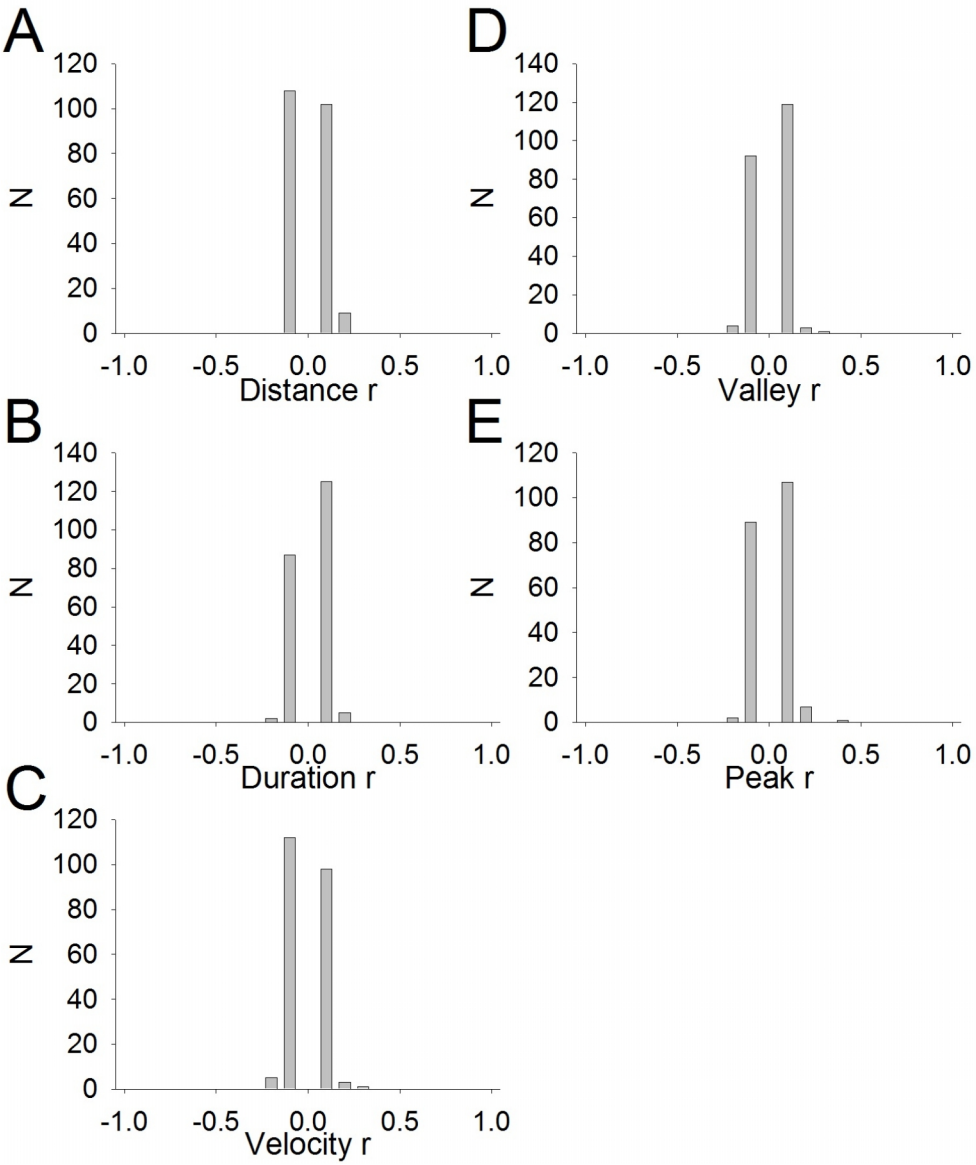

Figure 15

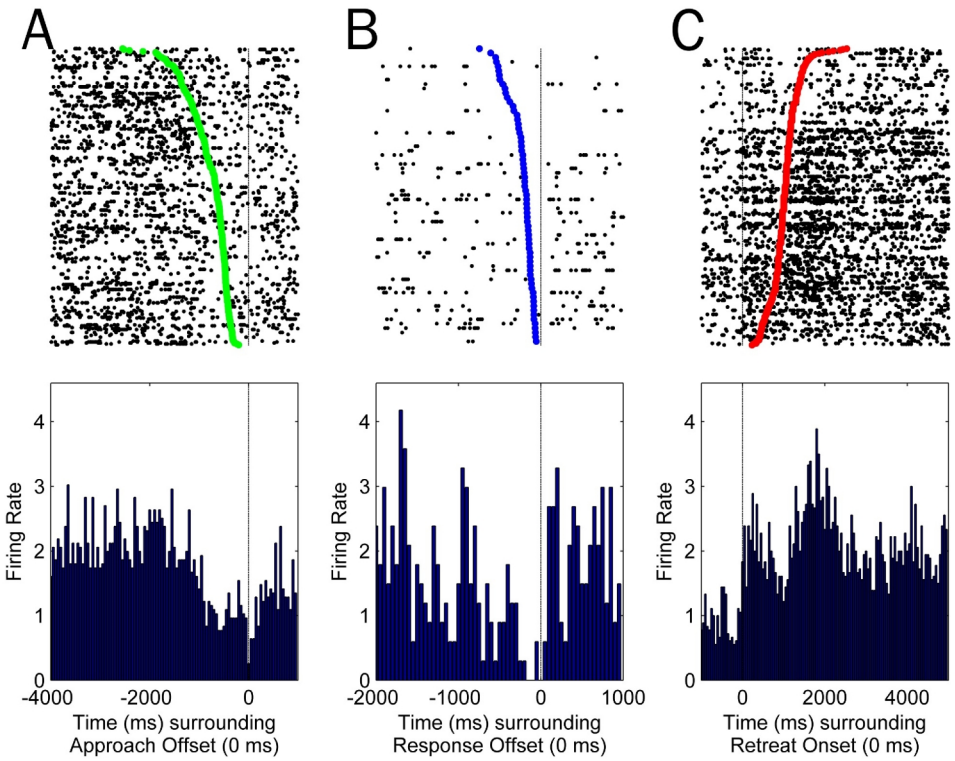
A
B
C
Firing Rate
Time (ms) surrounding
Approach Offset (0 ms)
Time (ms) surrounding
Response Offset (0 ms)
Time (ms) surrounding
Retreat Onset (0 ms)

Figure 16

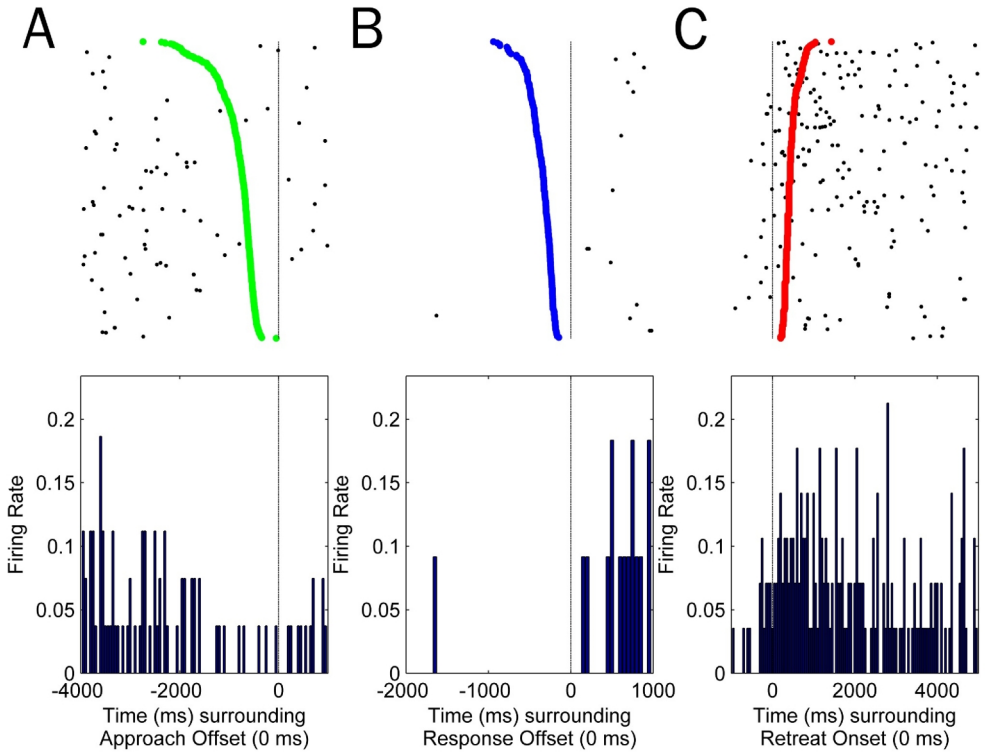
A
B
C
Firing Rate
0.2
0.15
0.1
0.05
0
-4000
-2000
0
Time (ms) surrounding
Approach Offset (0 ms)
-2000
-1000
0
1000
Time (ms) surrounding
Response Offset (0 ms)
2000
4000
Time (ms) surrounding
Retreat Onset (0 ms)

Figure 17

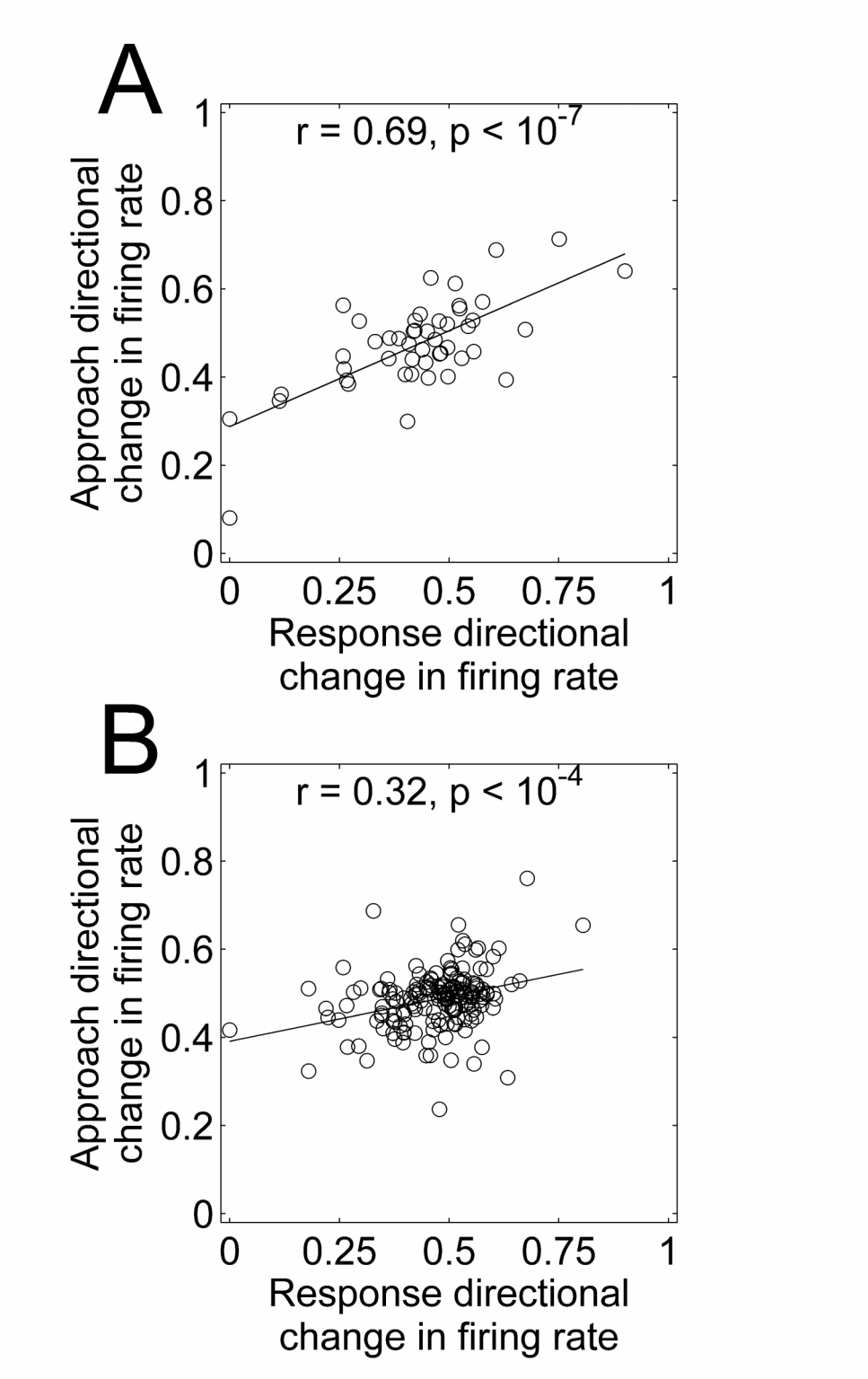
A
r = 0.69, p < 10^-7
Approach directional change in firing rate
Response directional change in firing rate
0
0.2
0.4
0.6
0.8
1
0.25
0.5
0.75
B
r = 0.32, p < 10^-4
Approach directional change in firing rate
Response directional change in firing rate

Figure 18

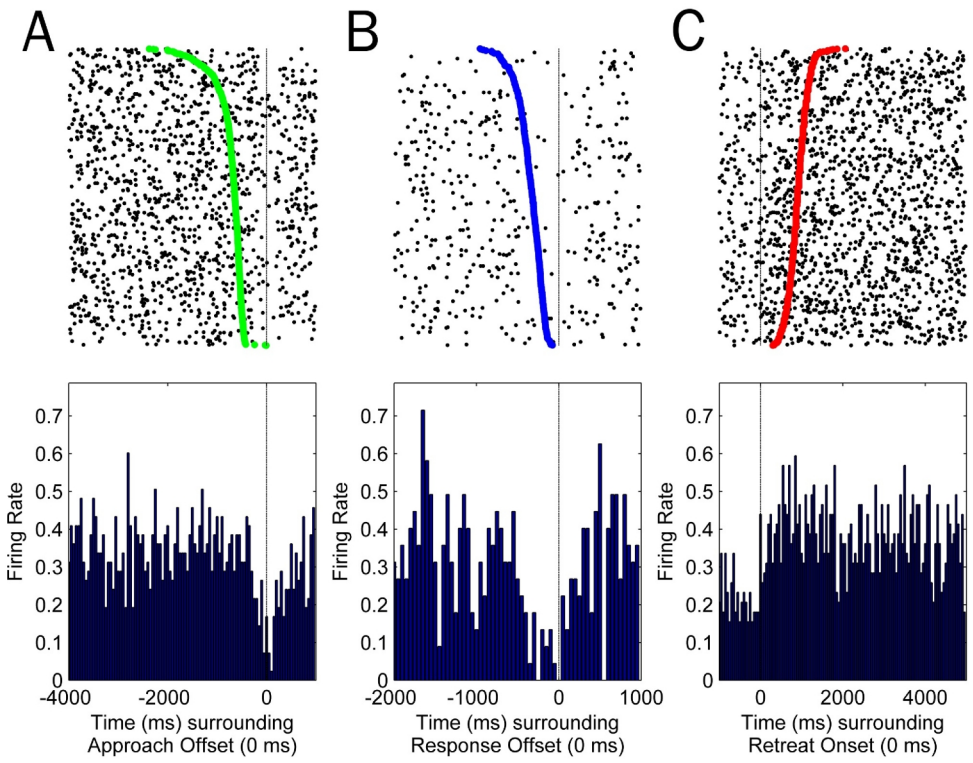
A
B
C
Firing Rate
0.7
0.6
0.5
0.4
0.3
0.2
0.1
0
-4000
-2000
0
Time (ms) surrounding
Approach Offset (0 ms)
-2000
-1000
0
1000
Time (ms) surrounding
Response Offset (0 ms)
0
2000
4000
Time (ms) surrounding
Retreat Onset (0 ms)

Figure 19

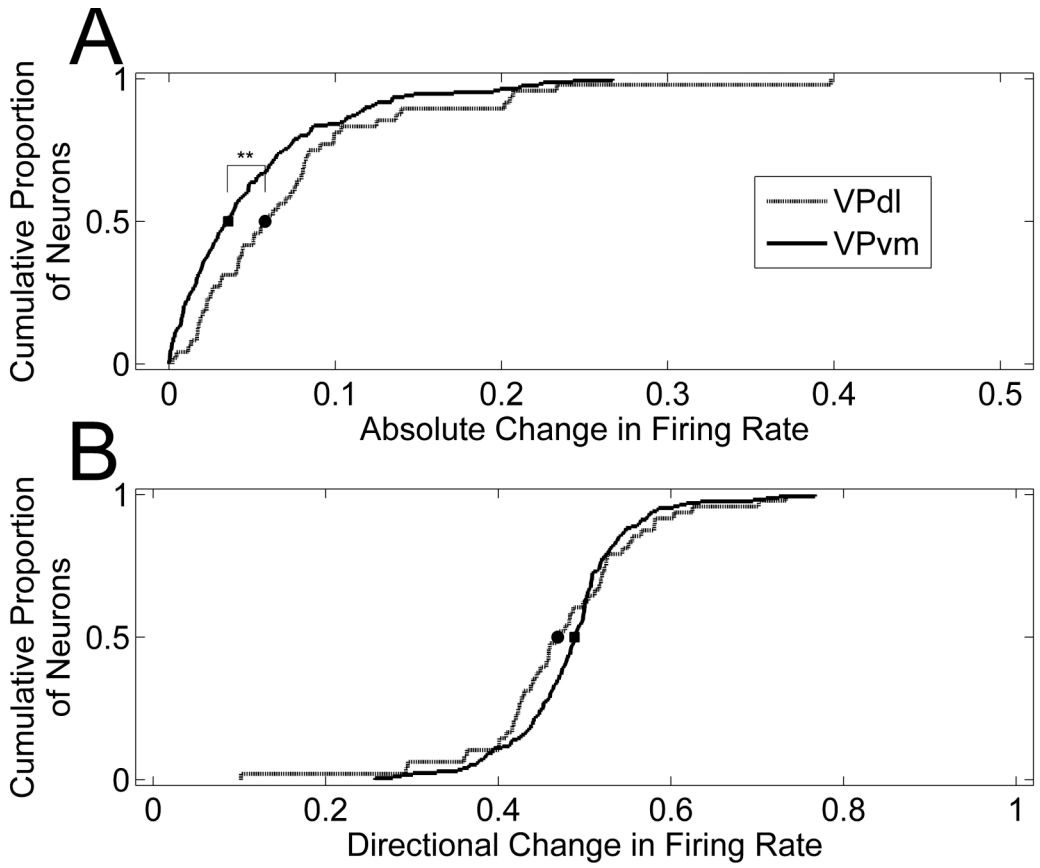
A
Cumulative Proportion of Neurons
1
0.5
0
**
VPdl
VPvm
0
0.1
0.2
0.3
0.4
0.5
Absolute Change in Firing Rate
B
Cumulative Proportion of Neurons
1
0.5
0
0
0.2
0.4
0.6
0.8
1
Directional Change in Firing Rate

Figure 20

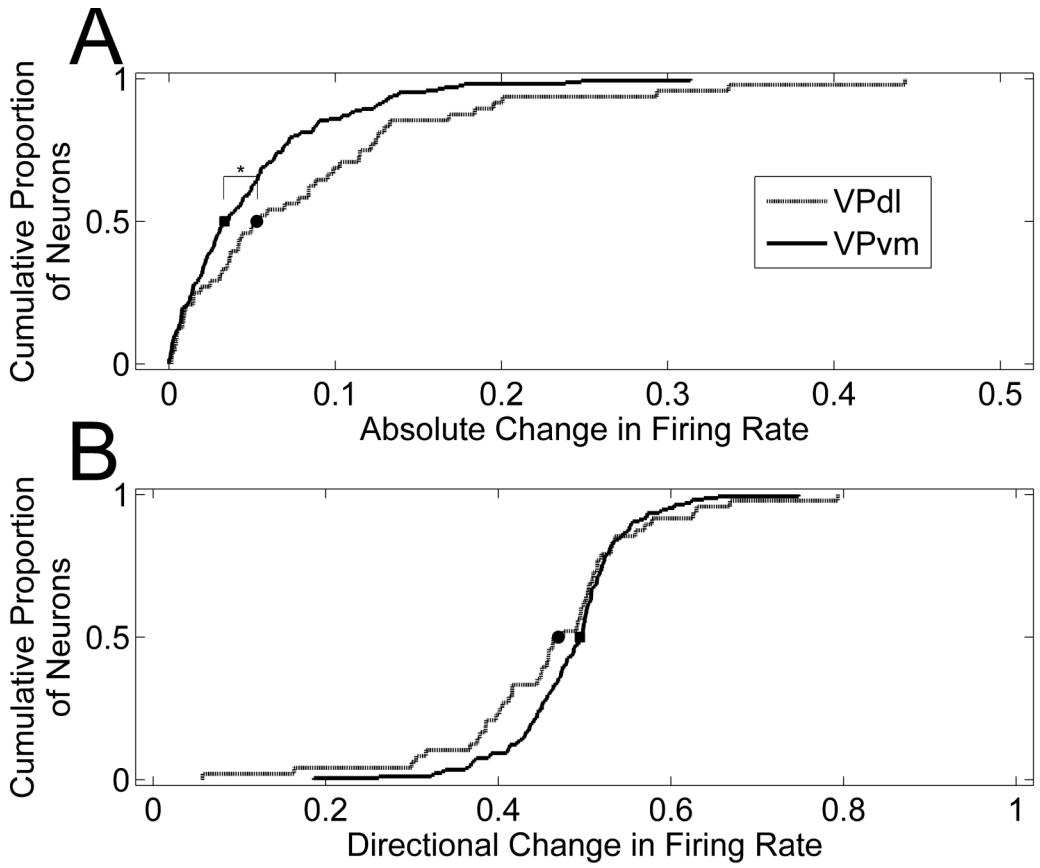
A
Cumulative Proportion of Neurons
1
0.5
0
0
0.1
0.2
0.3
0.4
0.5
Absolute Change in Firing Rate
VPdl
VPvm
*
B
Cumulative Proportion of Neurons
1
0.5
0
0
0.2
0.4
0.6
0.8
1
Directional Change in Firing Rate

Figure 21

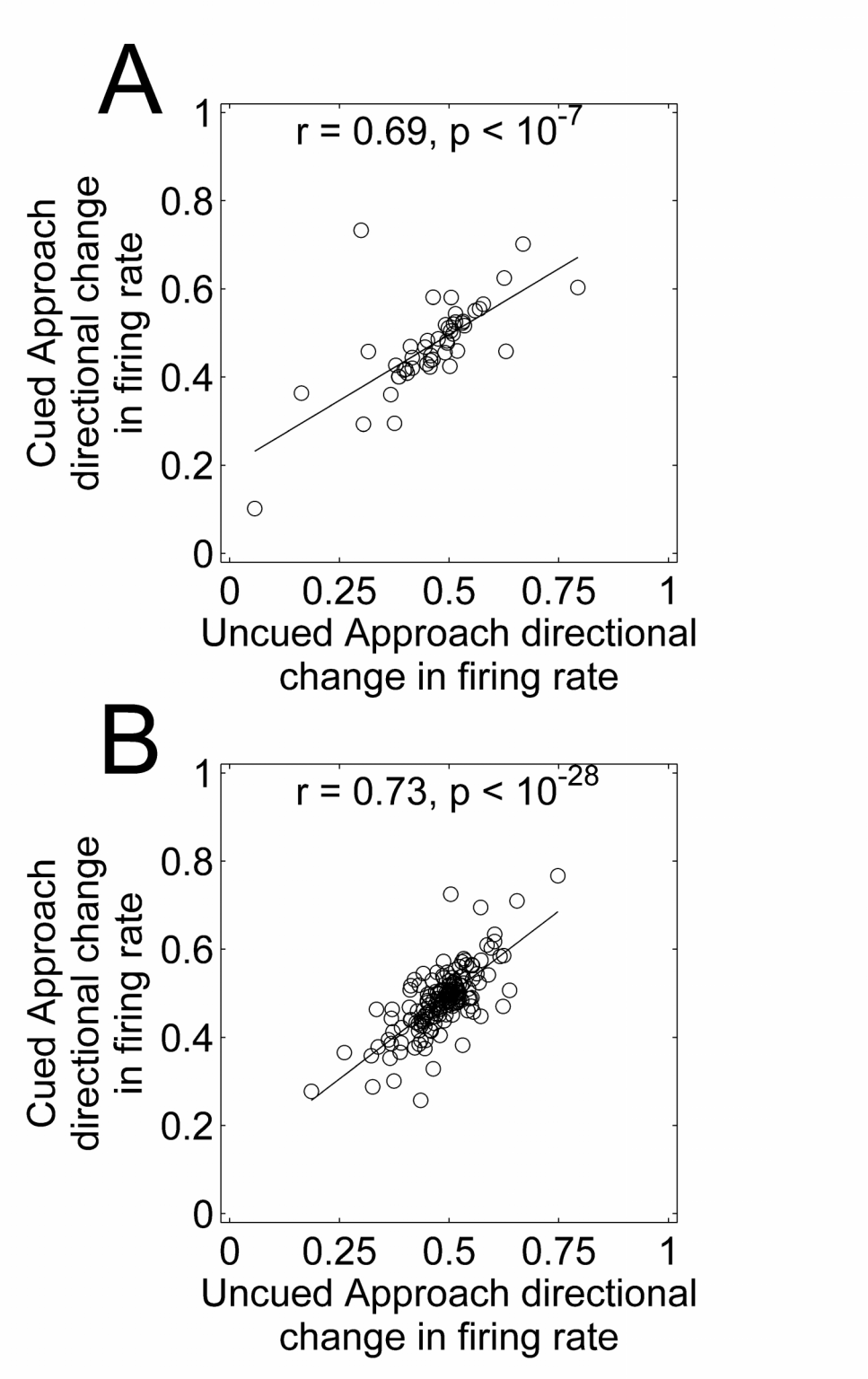
A
r = 0.69, p < 10^-7
Cued Approach directional change in firing rate
Uncued Approach directional change in firing rate
0
0.2
0.4
0.6
0.8
1
0.25
0.5
0.75
B
r = 0.73, p < 10^-28
Cued Approach directional change in firing rate
Uncued Approach directional change in firing rate

Figure 22

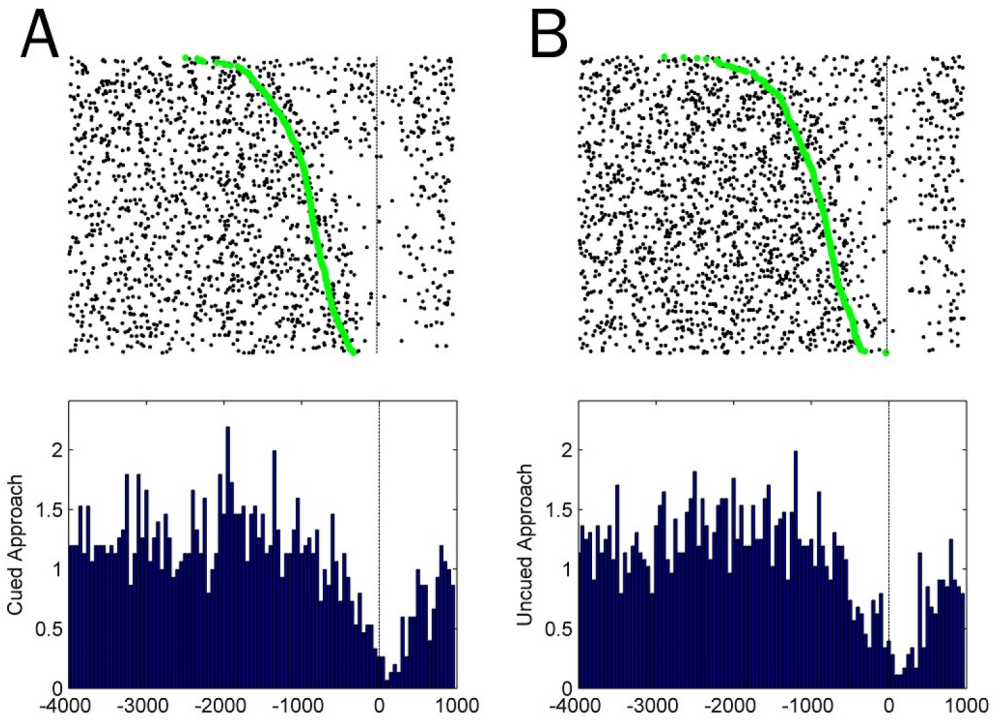
A
B
Cued Approach
Uncued Approach
2
1.5
1
0.5
0
-4000
-3000
-2000
-1000
0
1000

Figure 23

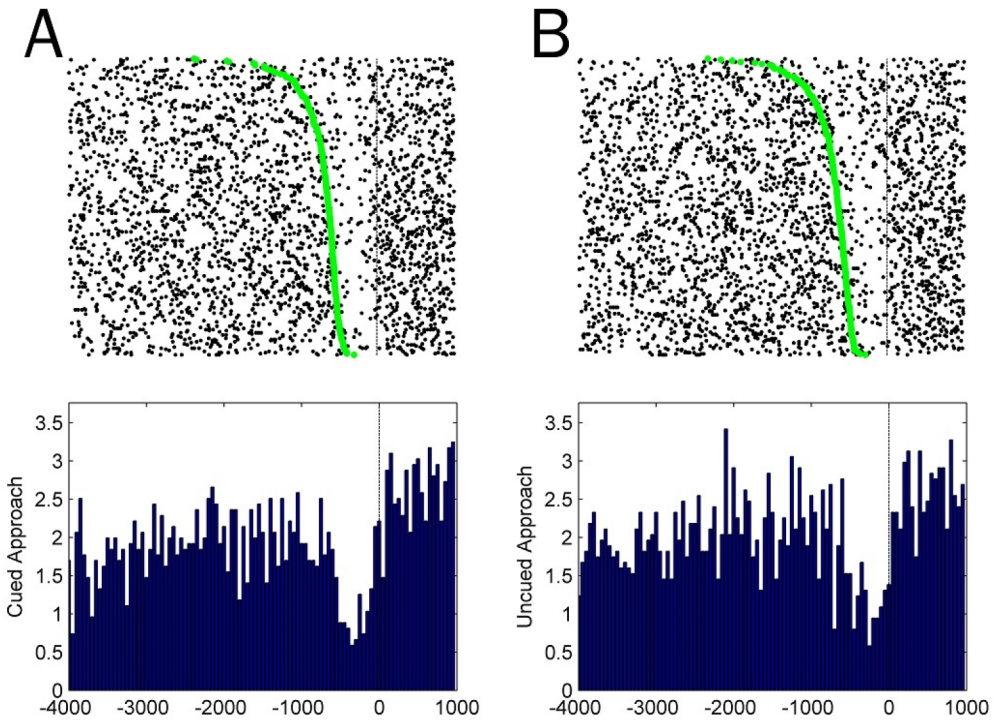
A
B
Cued Approach
Uncued Approach
3.5
3
2.5
2
1.5
1
0.5
0
-4000
-3000
-2000
-1000
0
1000

Figure 24

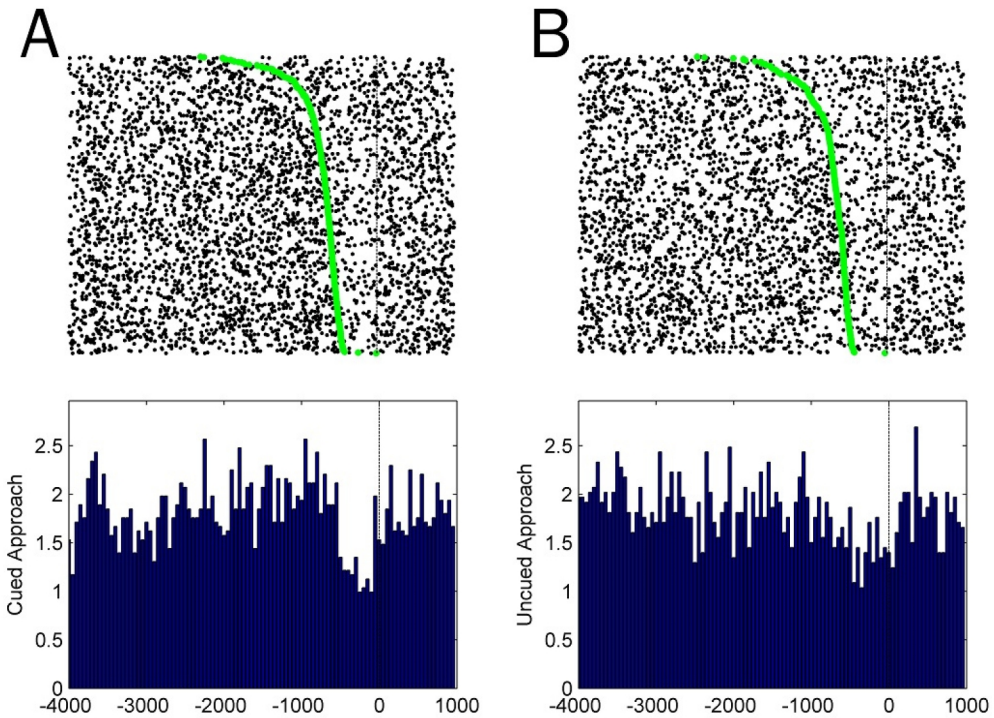
A
B
Cued Approach
Uncued Approach
2.5
2
1.5
1
0.5
0
-4000
-3000
-2000
-1000
0
1000

Figure 25

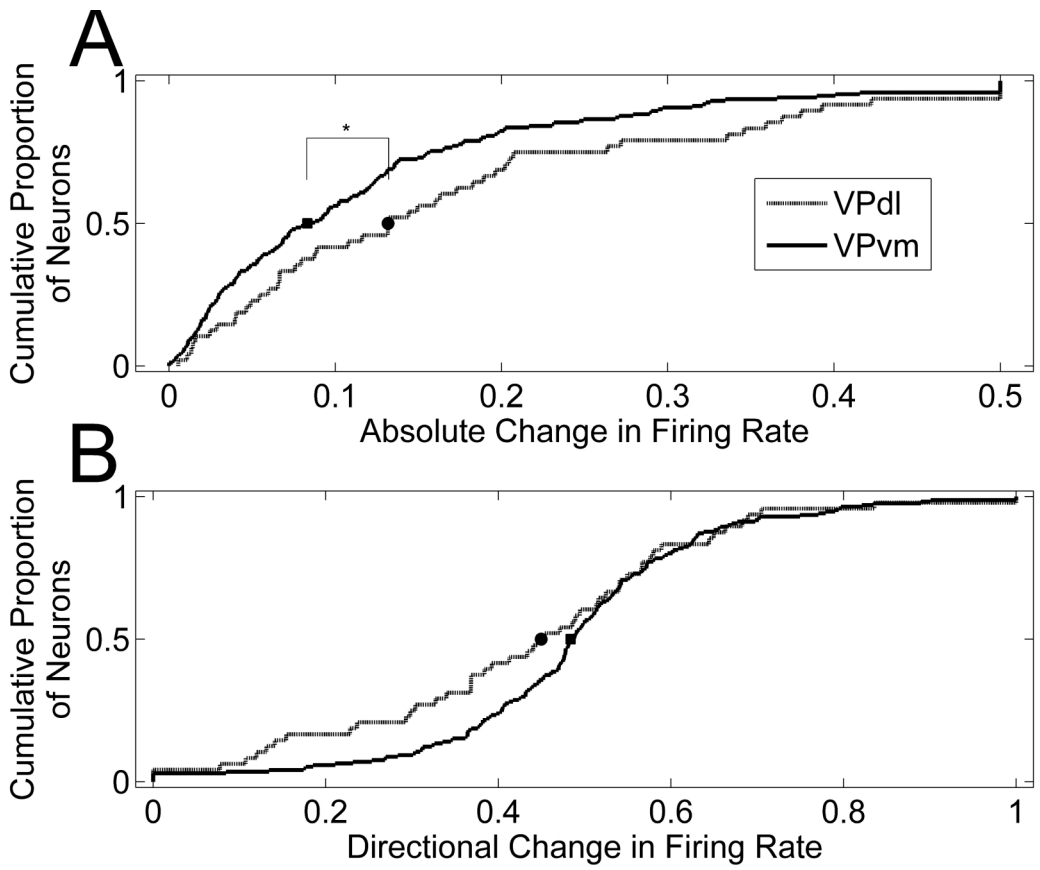
A
Cumulative Proportion of Neurons
1
0.5
0
*
VPdl
VPvm
0
0.1
0.2
0.3
0.4
0.5
Absolute Change in Firing Rate
B
Cumulative Proportion of Neurons
1
0.5
0
0
0.2
0.4
0.6
0.8
1
Directional Change in Firing Rate

Figure 26

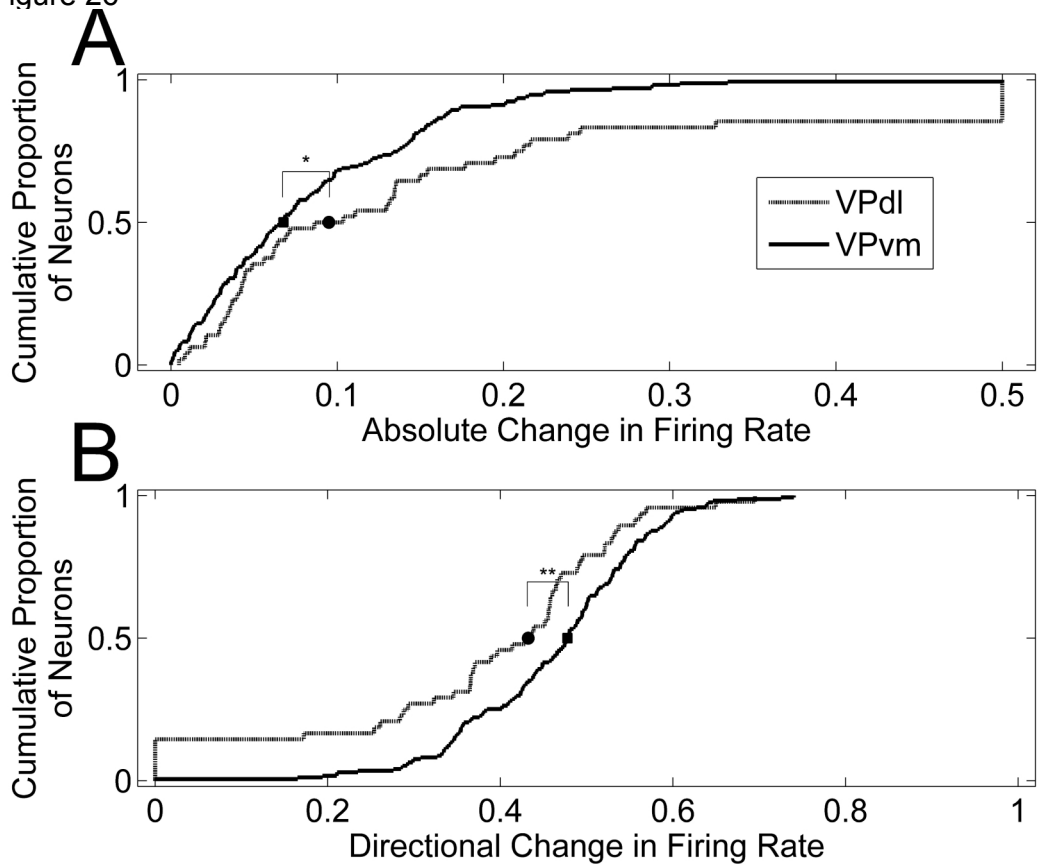
A
Cumulative Proportion of Neurons
1
0.5
0
*
VPdl
VPvm
0
0.1
0.2
0.3
0.4
0.5
Absolute Change in Firing Rate
B
Cumulative Proportion of Neurons
1
0.5
0
**
0
0.2
0.4
0.6
0.8
1
Directional Change in Firing Rate

Figure 27

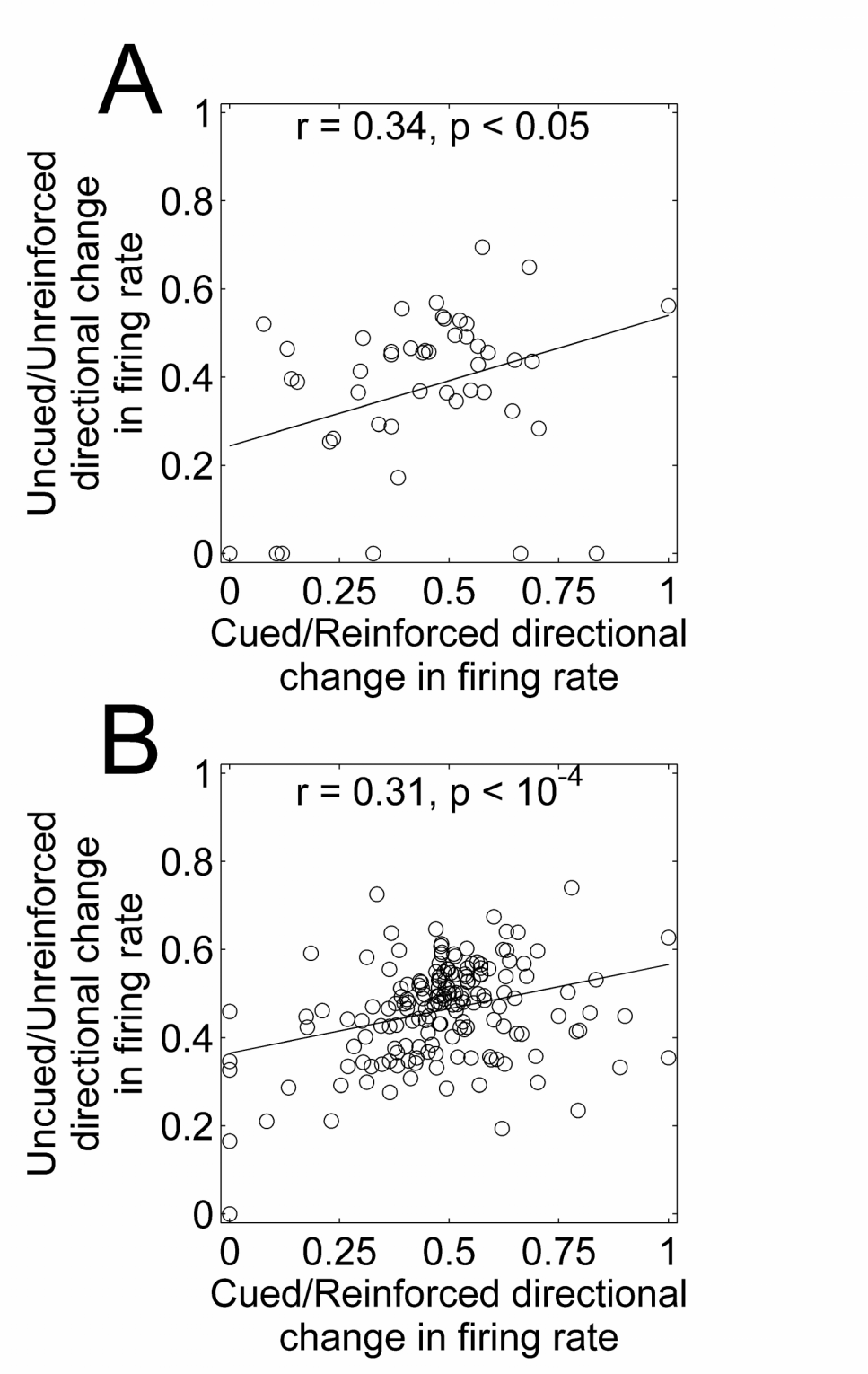
A
r = 0.34, p < 0.05
Uncued/Unreinforced directional change in firing rate
Cued/Reinforced directional change in firing rate
0
0.2
0.4
0.6
0.8
1
0.25
0.5
0.75
B
r = 0.31, p < 10-4
Uncued/Unreinforced directional change in firing rate
Cued/Reinforced directional change in firing rate

Figure 28

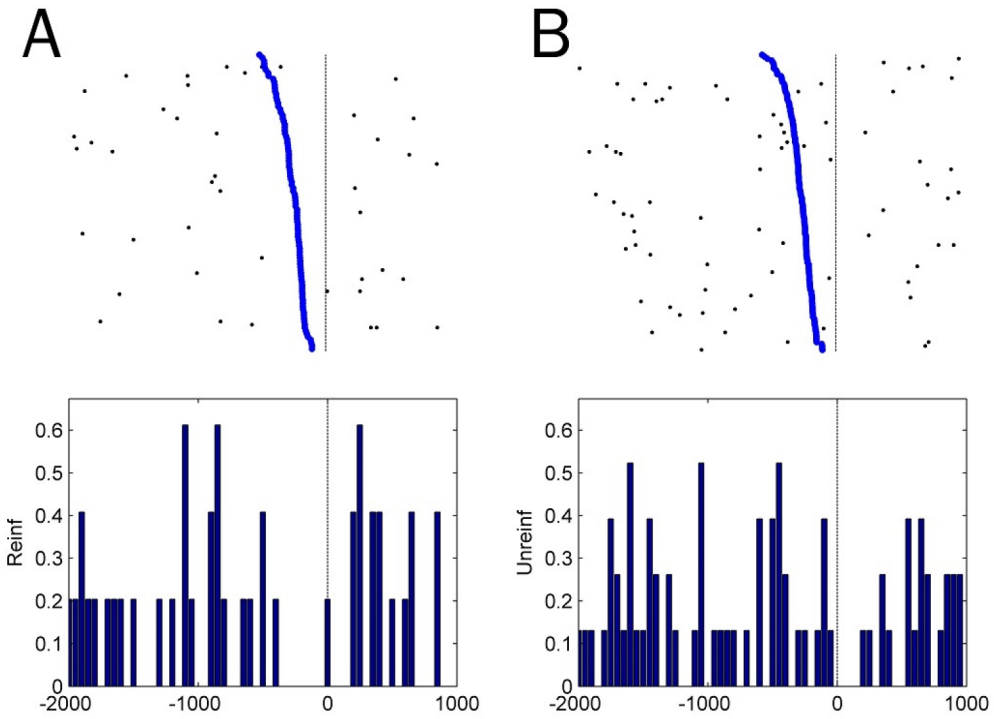

Figure 29

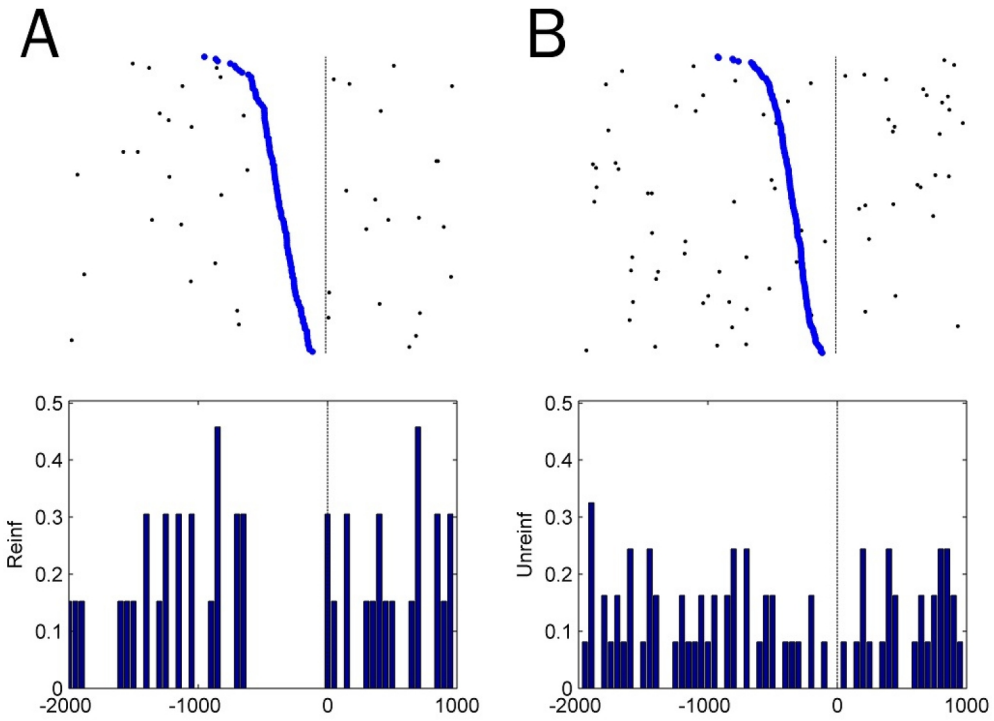

Figure 30

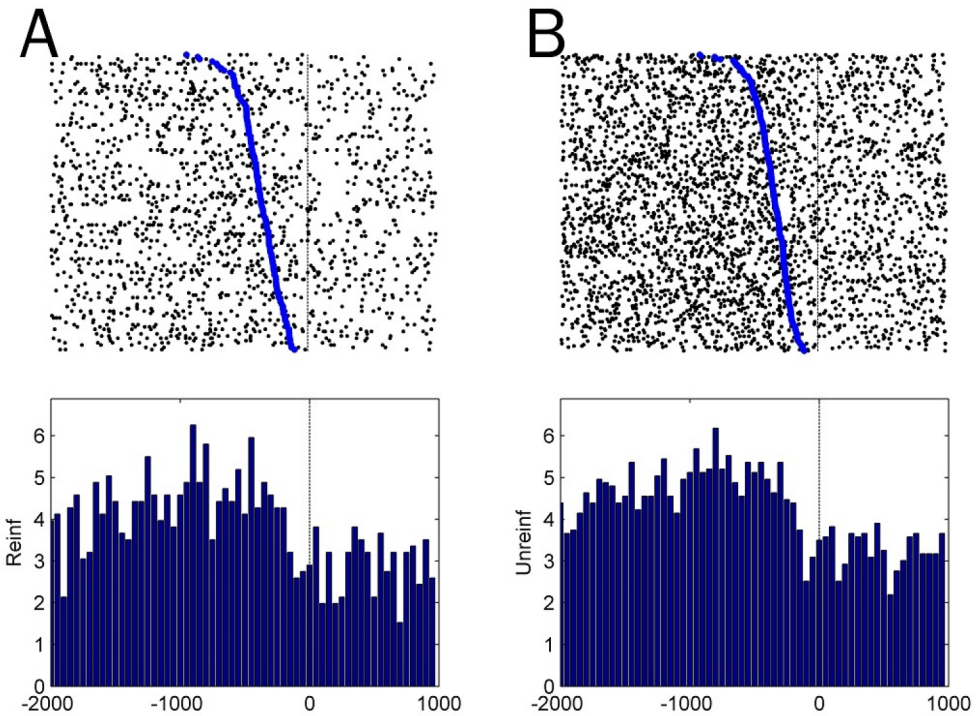

Figure 31

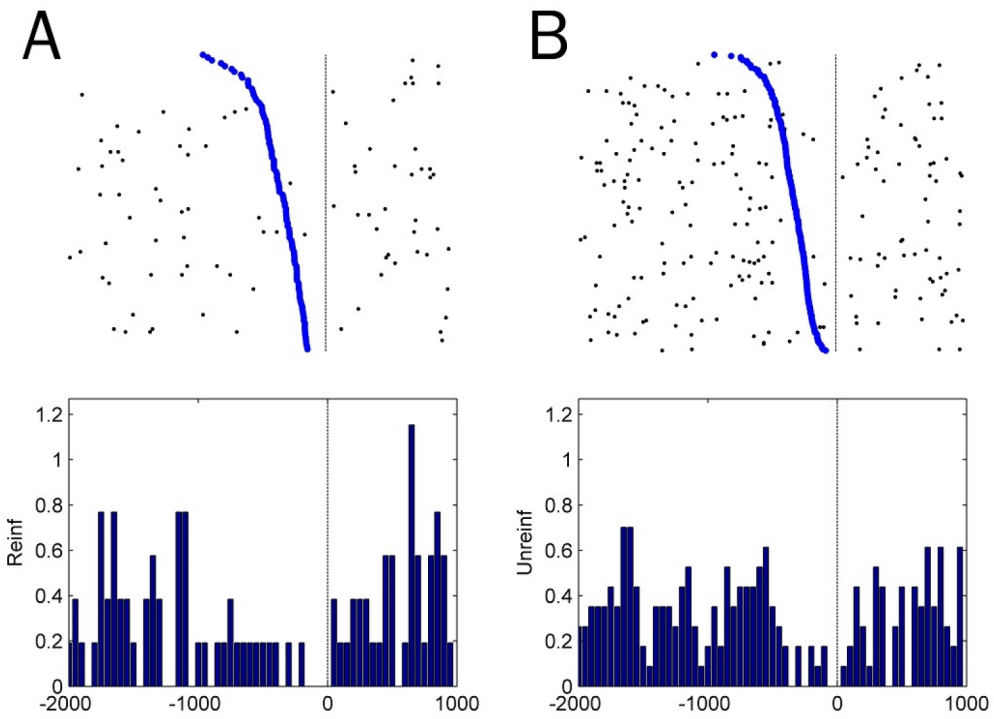

Figure 32

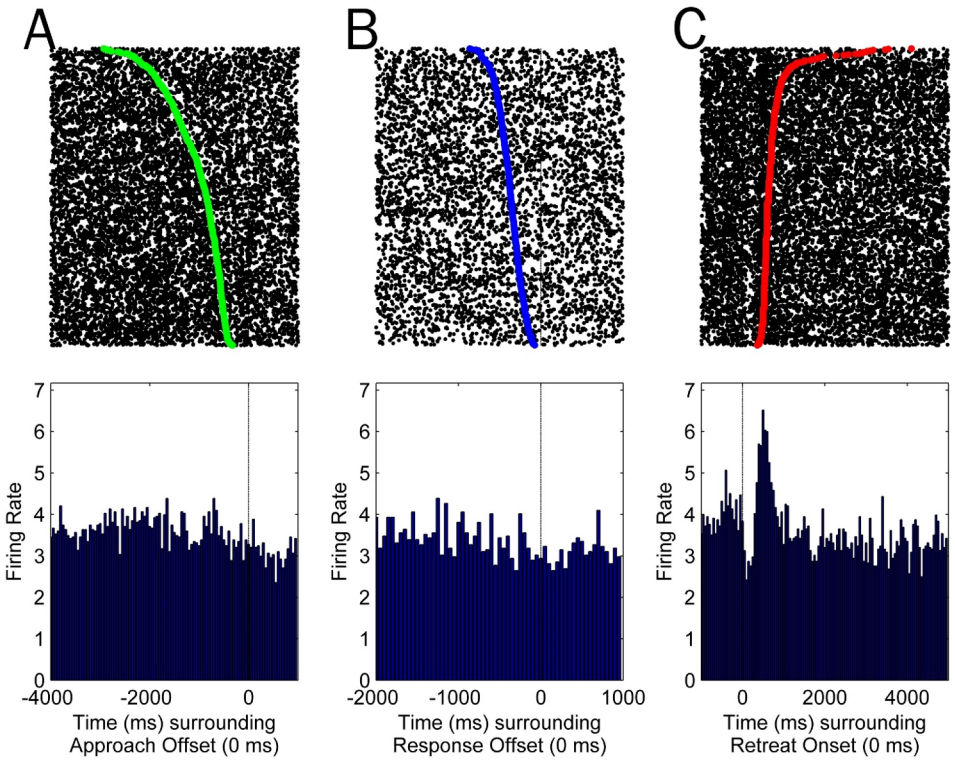
A
B
C
Firing Rate
Time (ms) surrounding
Approach Offset (0 ms)
Time (ms) surrounding
Response Offset (0 ms)
Time (ms) surrounding
Retreat Onset (0 ms)

Figure 33

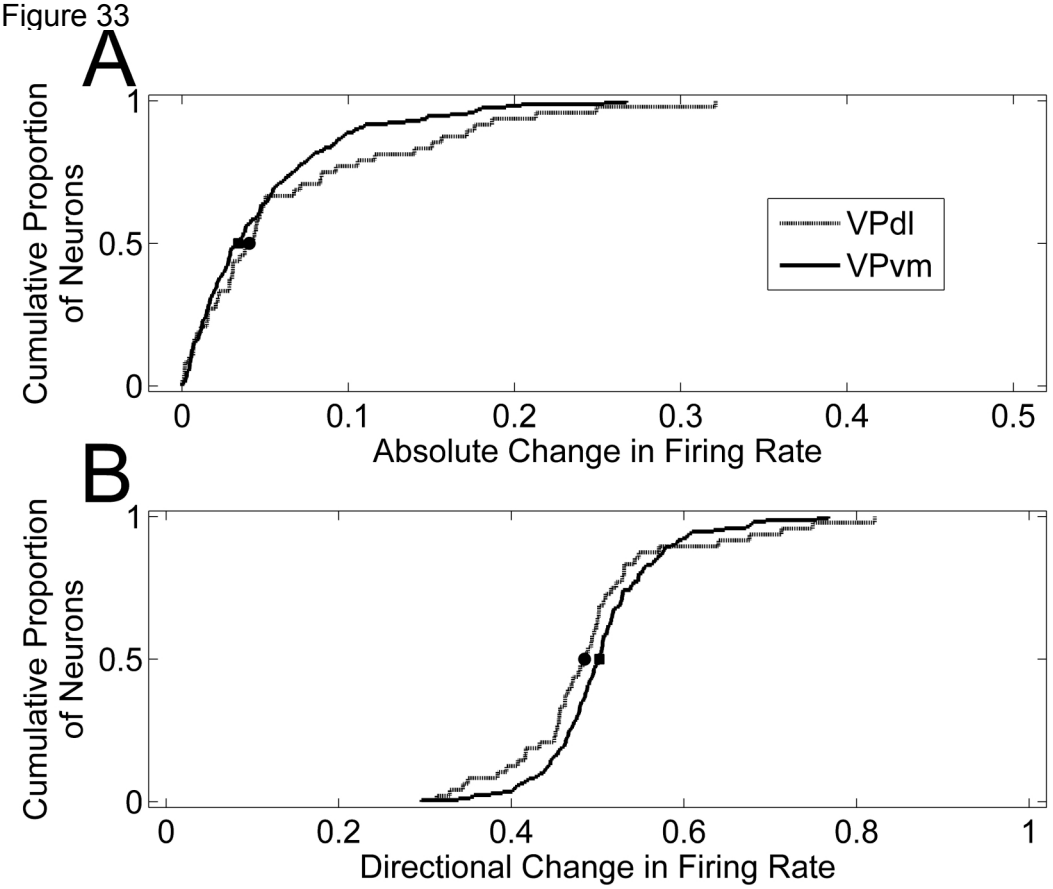
A
Cumulative Proportion of Neurons
1
0.5
0
0
0.1
0.2
0.3
0.4
0.5
Absolute Change in Firing Rate
VPdl
VPvm
B
Cumulative Proportion of Neurons
1
0.5
0
0
0.2
0.4
0.6
0.8
1
Directional Change in Firing Rate

Figure 34

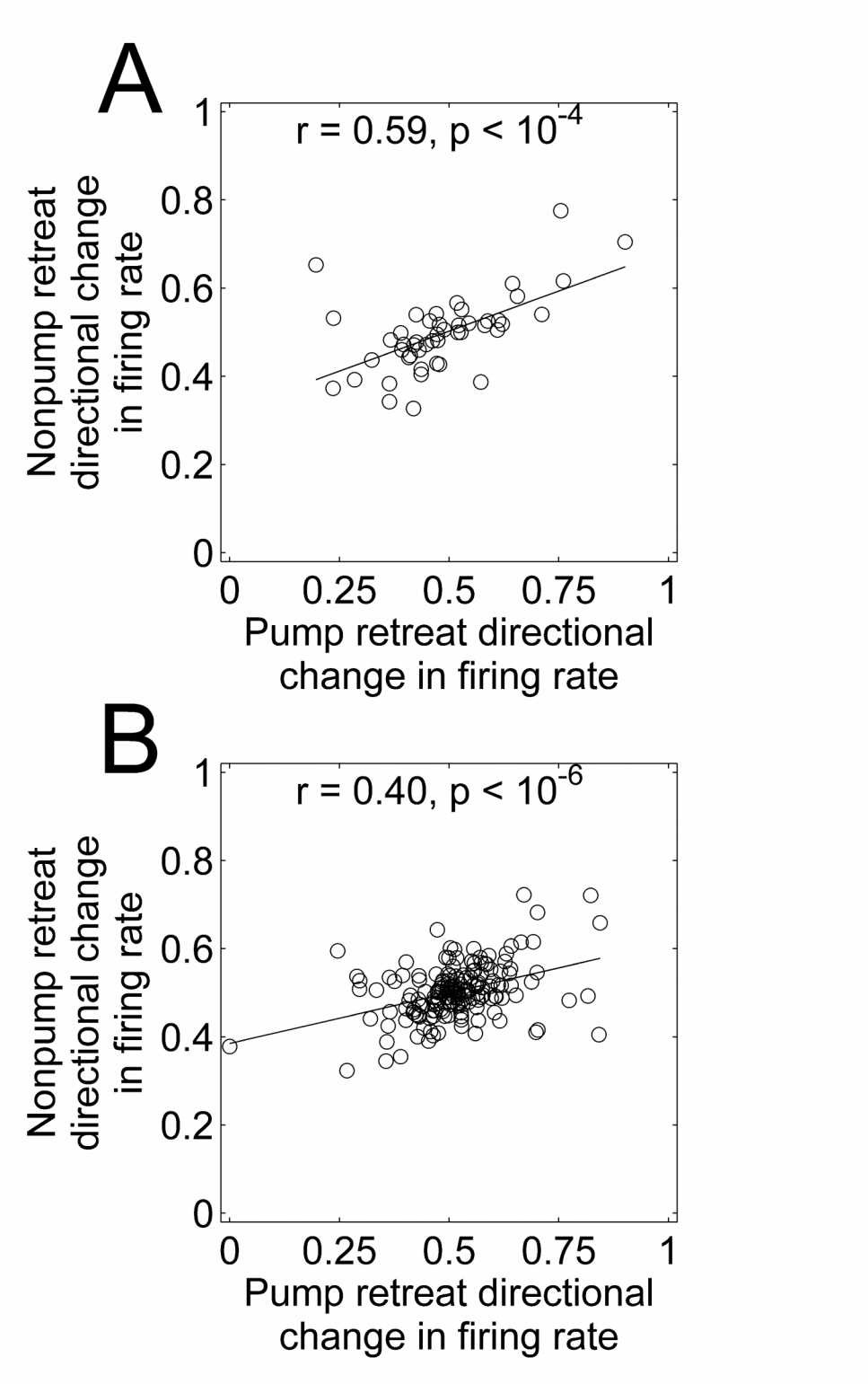
A
r = 0.59, p < 10^-4
Nonpump retreat directional change in firing rate
Pump retreat directional change in firing rate
0
0.2
0.4
0.6
0.8
1
0.25
0.5
0.75
B
r = 0.40, p < 10^-6
Nonpump retreat directional change in firing rate
Pump retreat directional change in firing rate

Figure 35

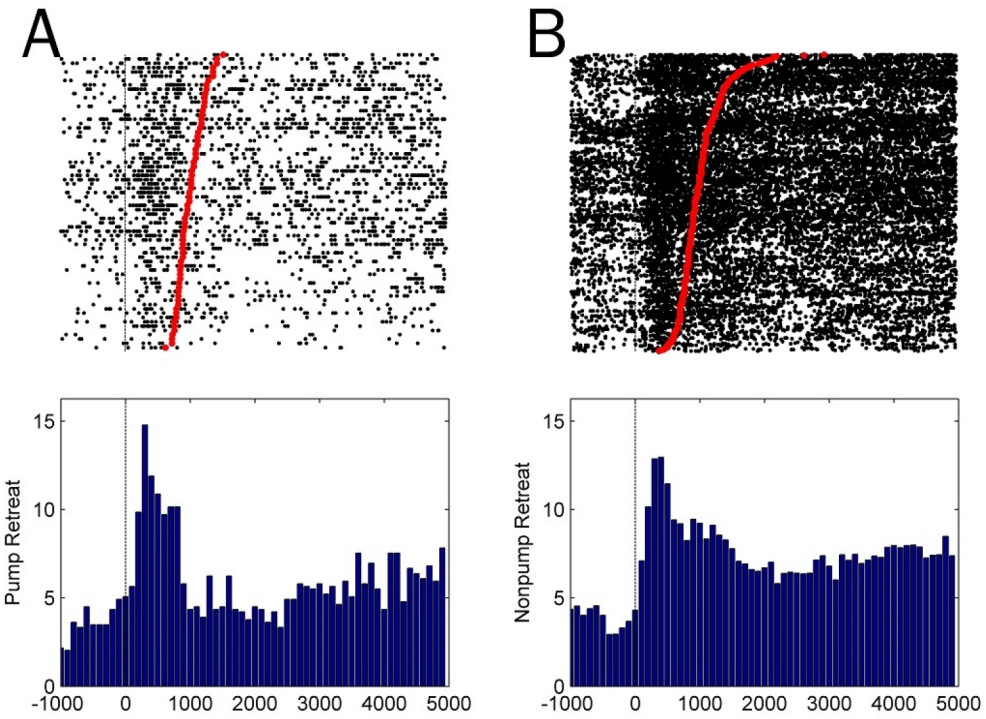
A
B
Pump Retreat
Nonpump Retreat
15
10
5
0
-1000
0
1000
2000
3000
4000
5000

Figure 36

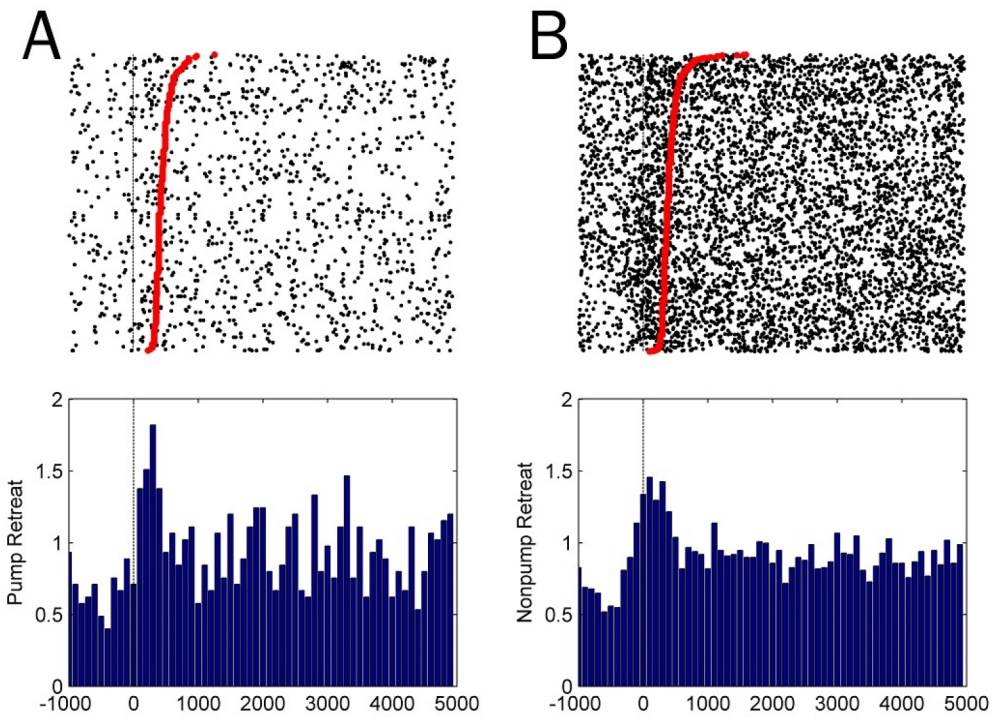
A
B
Pump Retreat
Nonpump Retreat
2
1.5
1
0.5
0
-1000
0
1000
2000
3000
4000
5000

Figure 37

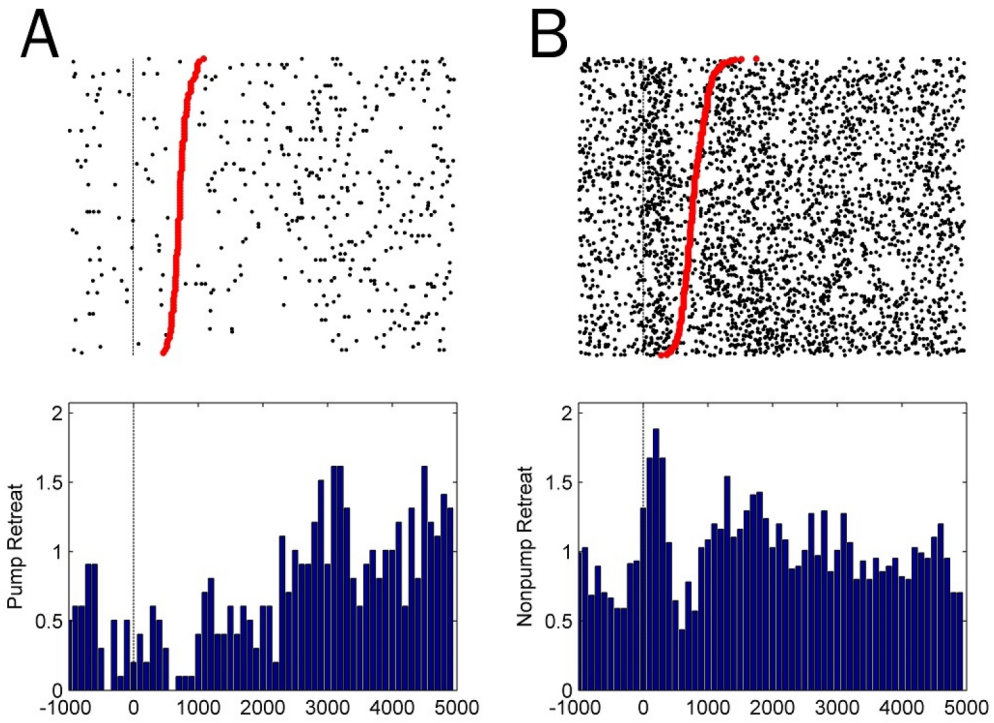
A
B
Pump Retreat
Nonpump Retreat
2
1.5
1
0.5
0
-1000
0
1000
2000
3000
4000
5000

Figure 38

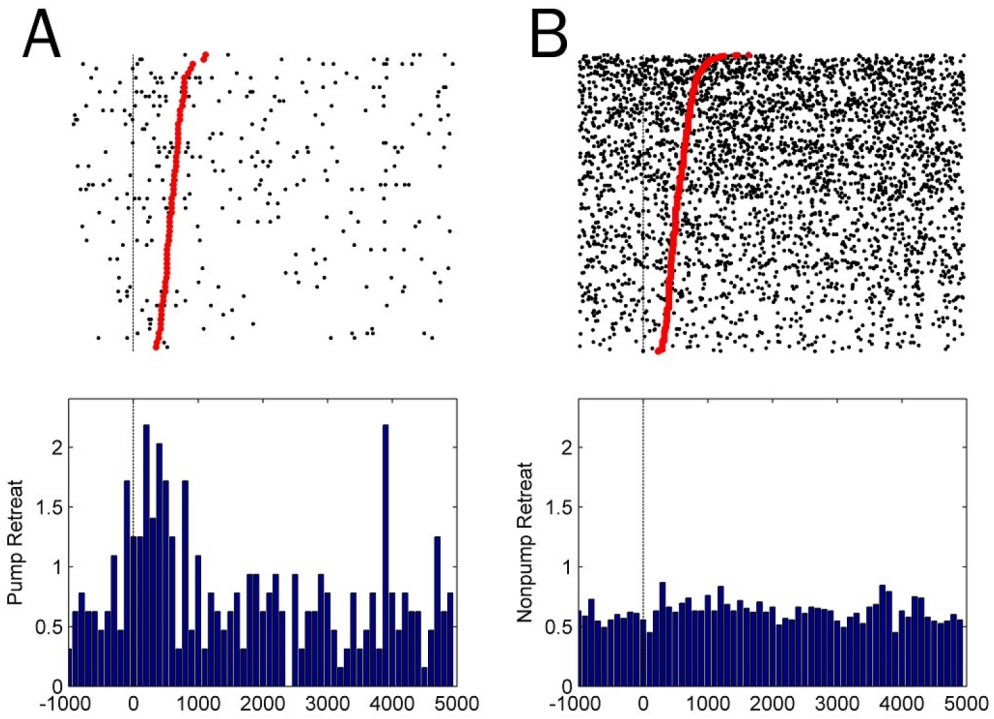
A
B
Pump Retreat
Nonpump Retreat
0
0.5
1
1.5
2
-1000
0
1000
2000
3000
4000
5000

Figure 39

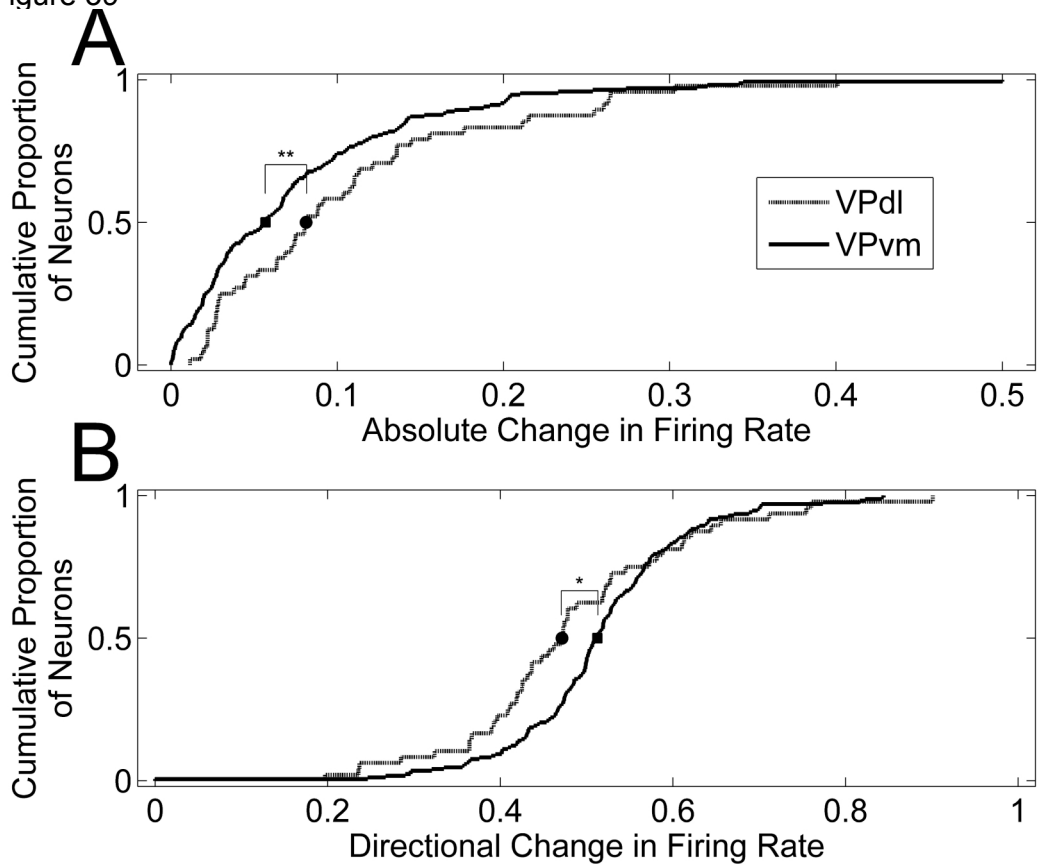
A
Cumulative Proportion of Neurons
1
0.5
0
**
VPdl
VPvm
0
0.1
0.2
0.3
0.4
0.5
Absolute Change in Firing Rate
B
Cumulative Proportion of Neurons
1
0.5
0
*
0
0.2
0.4
0.6
0.8
1
Directional Change in Firing Rate

Figure 40

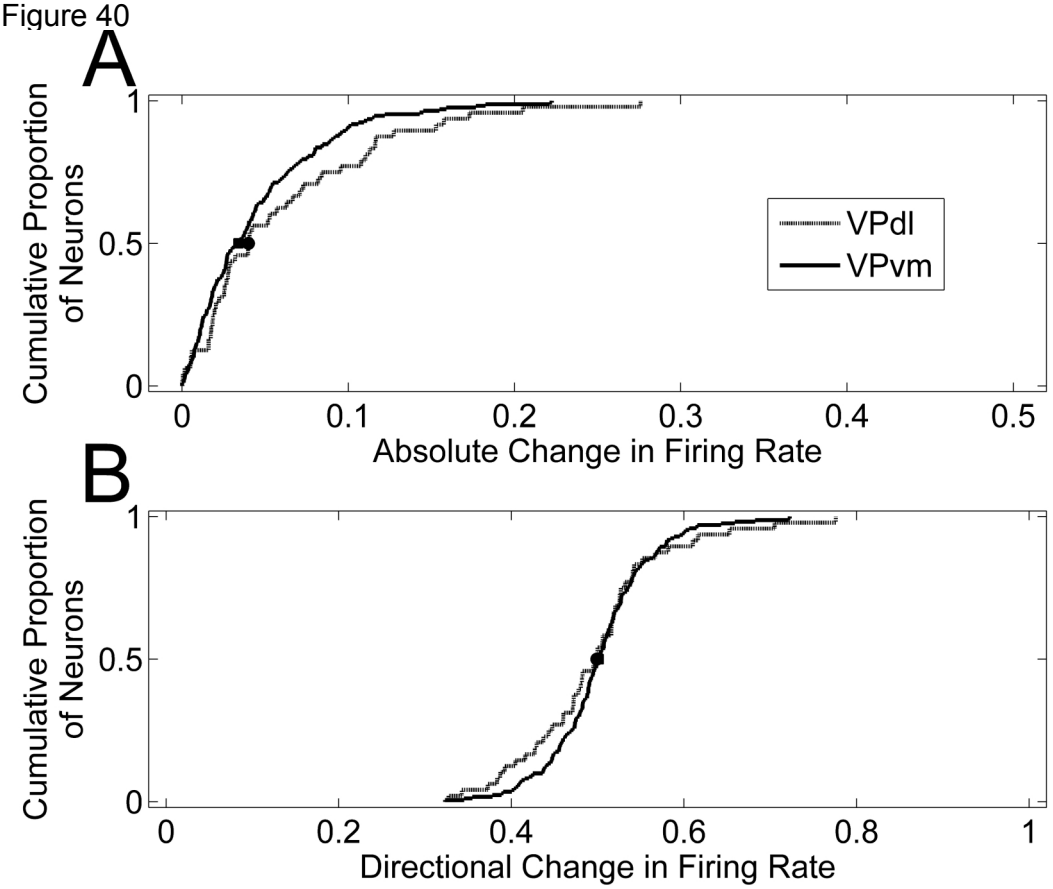
A
Cumulative Proportion of Neurons
1
0.5
0
0
0.1
0.2
0.3
0.4
0.5
Absolute Change in Firing Rate
VPdl
VPvm
B
Cumulative Proportion of Neurons
1
0.5
0
0
0.2
0.4
0.6
0.8
1
Directional Change in Firing Rate

Figure 41

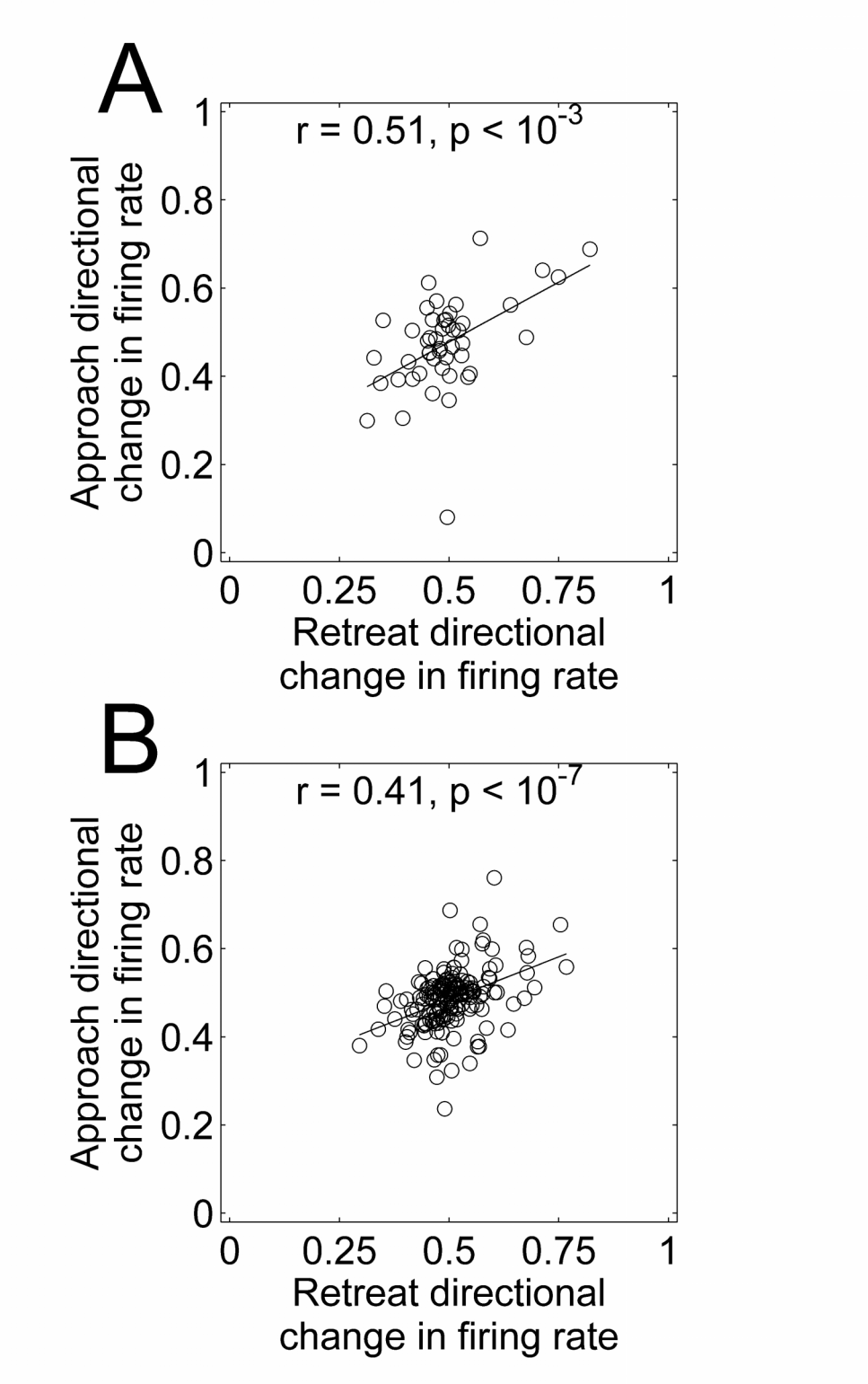
A
r = 0.51, p < 10^-3
Approach directional change in firing rate
Retreat directional change in firing rate
0
0.2
0.4
0.6
0.8
1
0.25
0.5
0.75
B
r = 0.41, p < 10^-7
Approach directional change in firing rate
Retreat directional change in firing rate

Figure 42

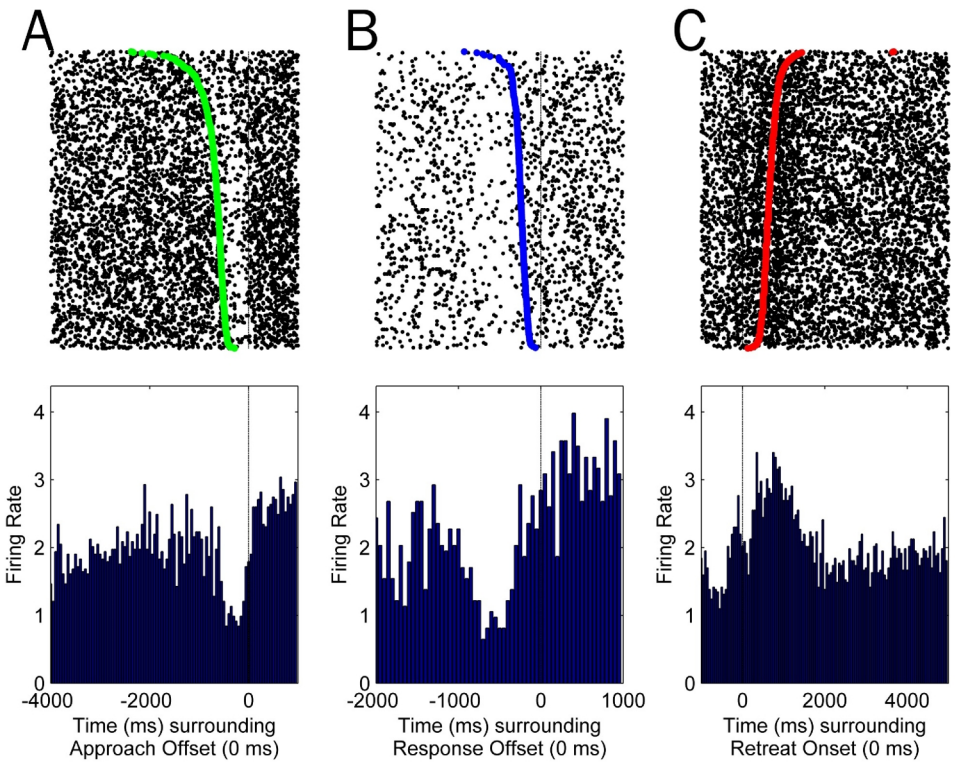
A
B
C
Firing Rate
Time (ms) surrounding
Approach Offset (0 ms)
Time (ms) surrounding
Response Offset (0 ms)
Time (ms) surrounding
Retreat Onset (0 ms)

Figure 43

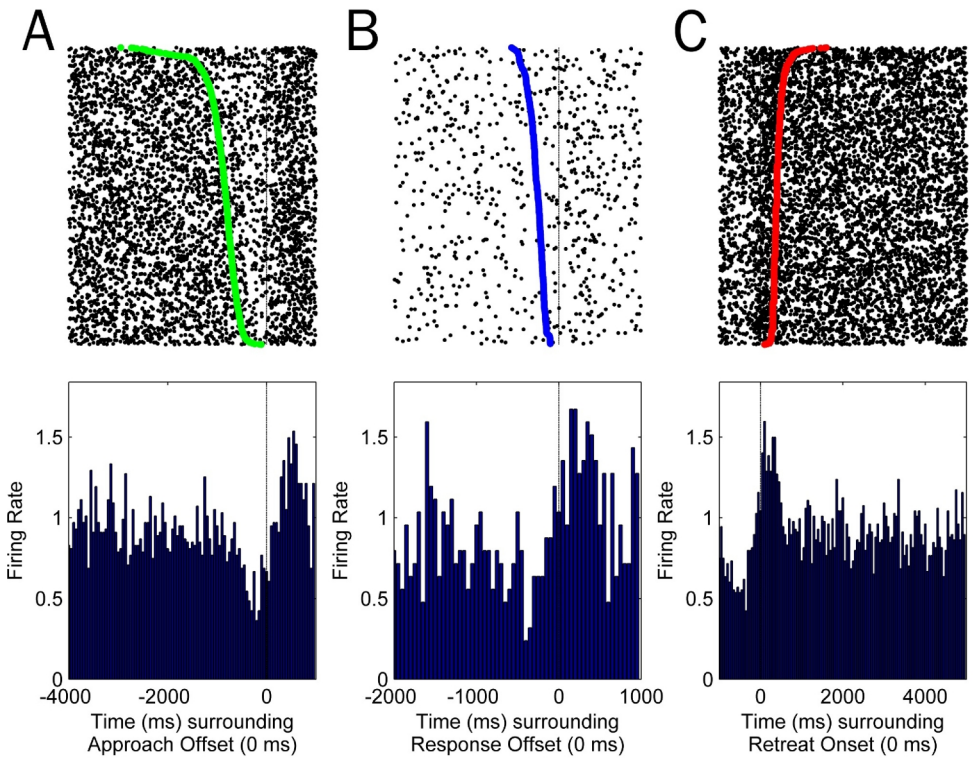
A
B
C
Firing Rate
1.5
1
0.5
0
-4000
-2000
0
Time (ms) surrounding
Approach Offset (0 ms)
-2000
-1000
0
1000
Time (ms) surrounding
Response Offset (0 ms)
0
2000
4000
Time (ms) surrounding
Retreat Onset (0 ms)

Figure 44

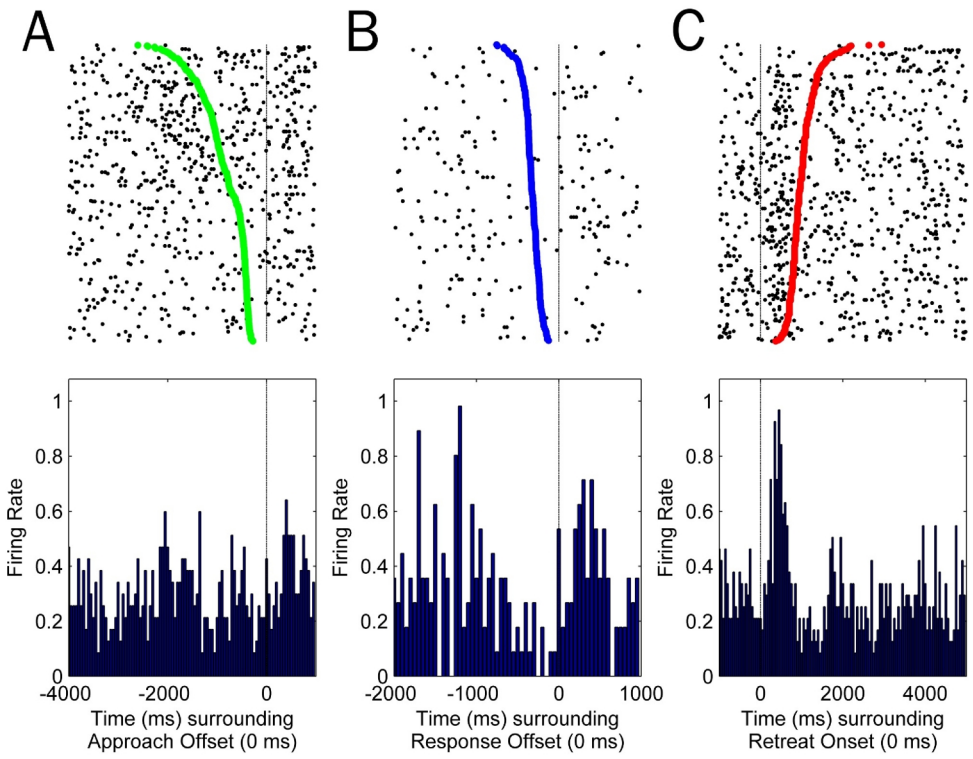
A
B
C
Firing Rate
Time (ms) surrounding
Approach Offset (0 ms)
Time (ms) surrounding
Response Offset (0 ms)
Time (ms) surrounding
Retreat Onset (0 ms)

Figure 45

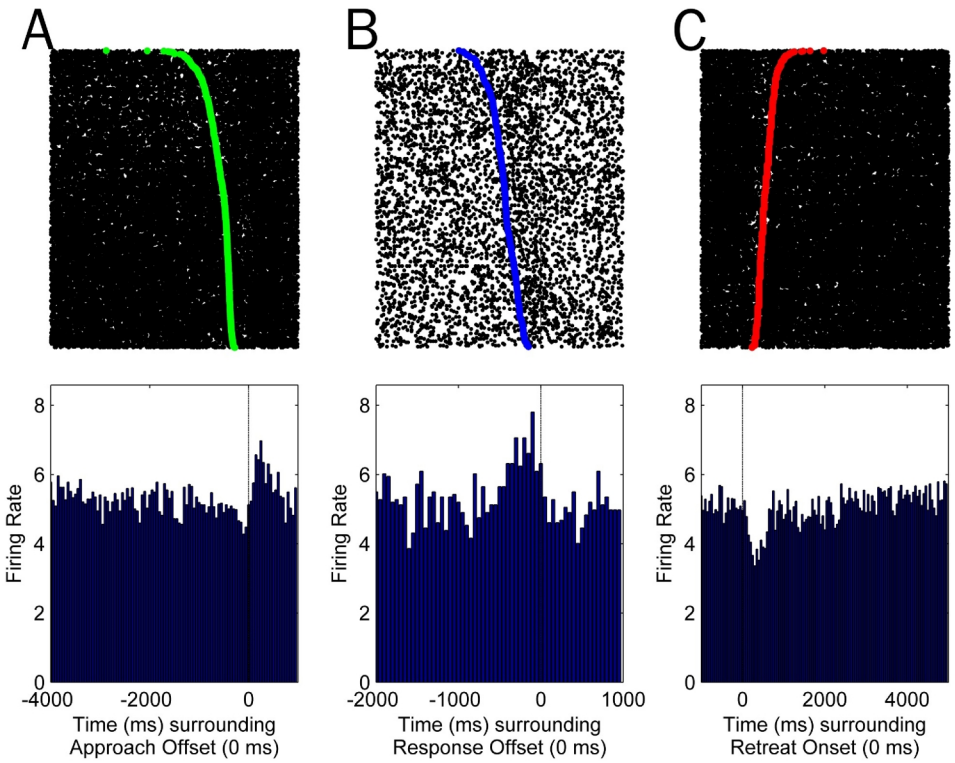
A
B
C
Firing Rate
0
2
4
6
8
-4000
-2000
0
Time (ms) surrounding
Approach Offset (0 ms)
-2000
-1000
0
1000
Time (ms) surrounding
Response Offset (0 ms)
0
2000
4000
Time (ms) surrounding
Retreat Onset (0 ms)

Figure 46

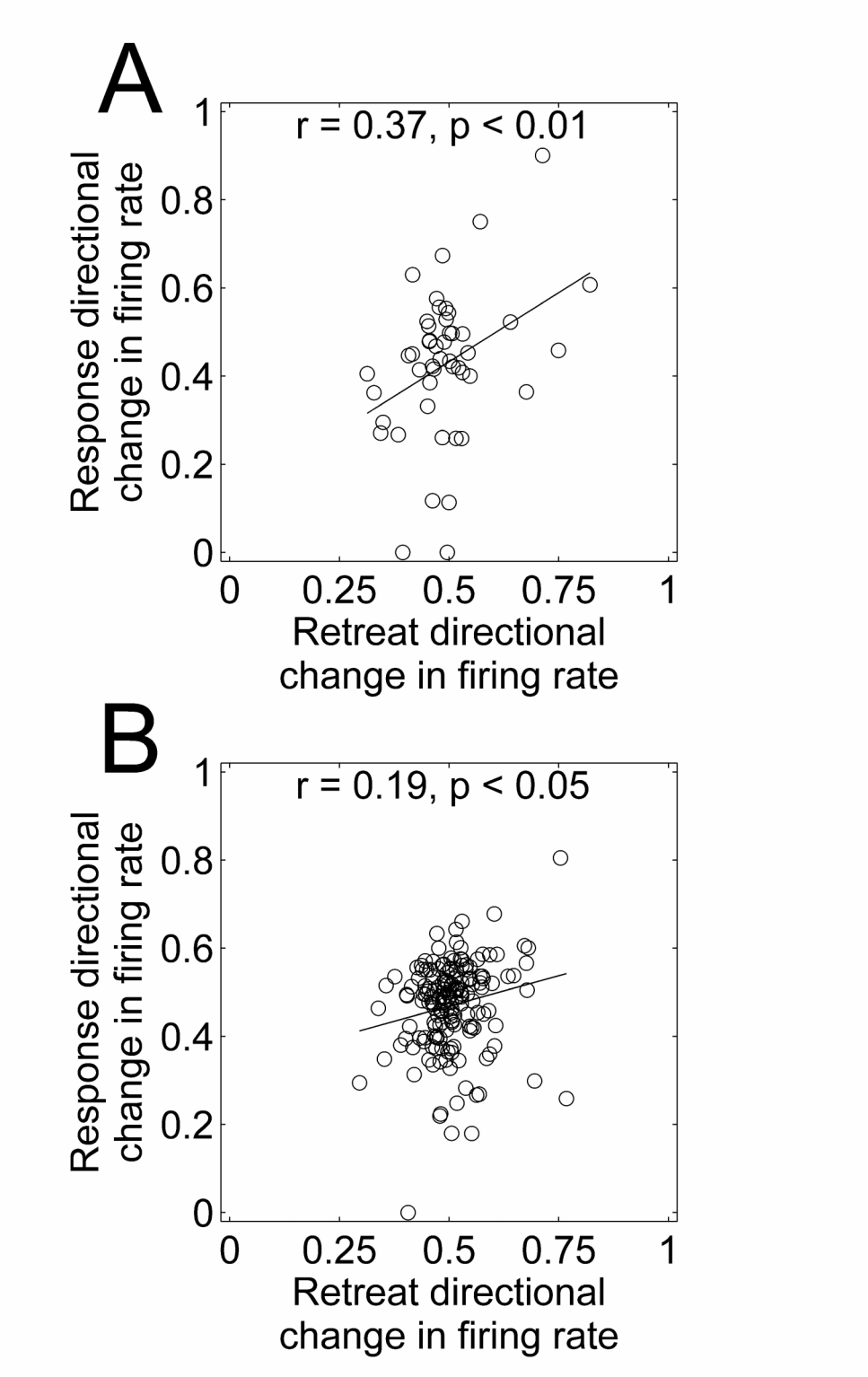
A
r = 0.37, p < 0.01
Response directional change in firing rate
Retreat directional change in firing rate
0
0.2
0.4
0.6
0.8
1
0.25
0.5
0.75
B
r = 0.19, p < 0.05
Response directional change in firing rate
Retreat directional change in firing rate

Figure 47

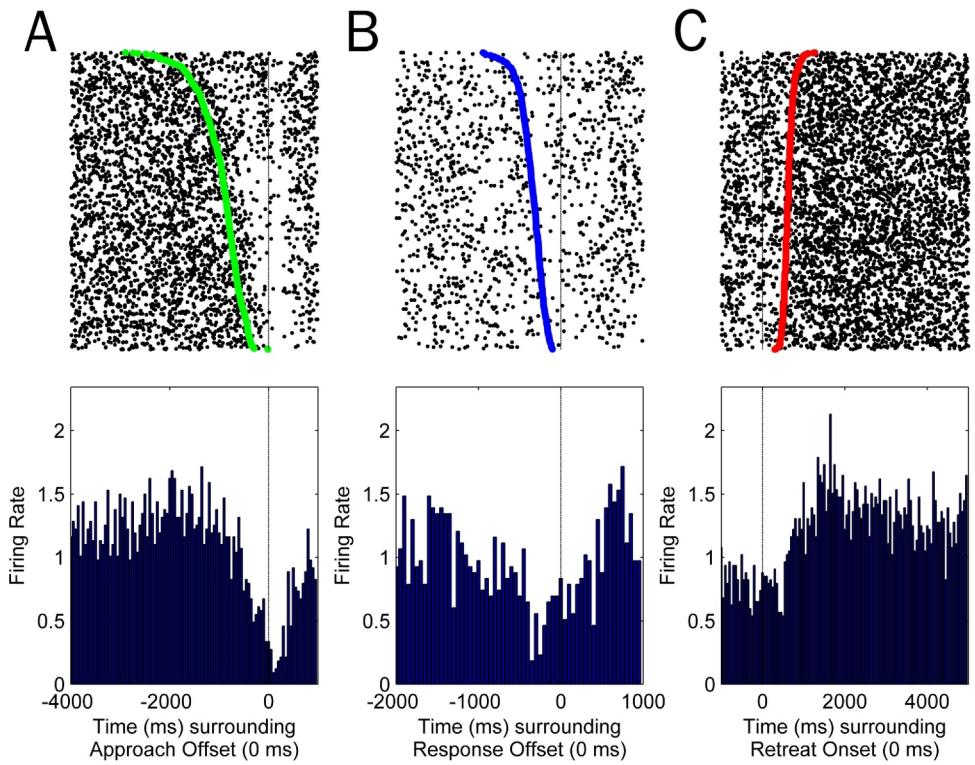
A
B
C
Firing Rate
Time (ms) surrounding
Approach Offset (0 ms)
Time (ms) surrounding
Response Offset (0 ms)
Time (ms) surrounding
Retreat Onset (0 ms)

Figure 48

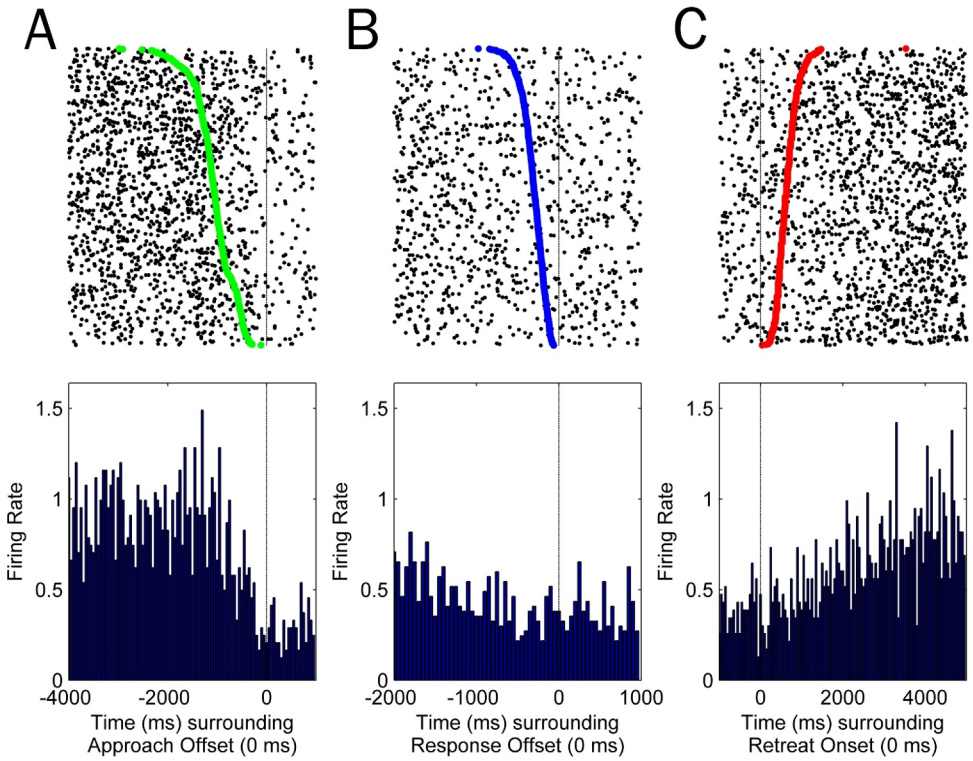
A
B
C
Firing Rate
1.5
1
0.5
0
-4000
-2000
0
Time (ms) surrounding
Approach Offset (0 ms)
-2000
-1000
0
1000
Time (ms) surrounding
Response Offset (0 ms)
2000
4000
Time (ms) surrounding
Retreat Onset (0 ms)

Figure 49

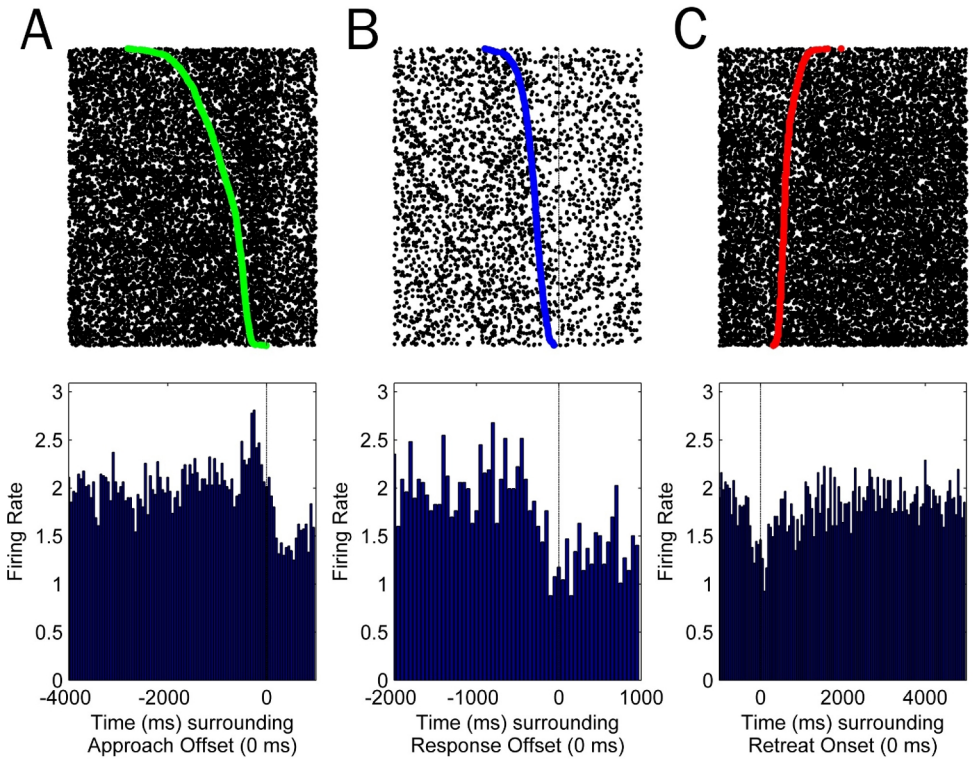
A
B
C
Firing Rate
Time (ms) surrounding
Approach Offset (0 ms)
Time (ms) surrounding
Response Offset (0 ms)
Time (ms) surrounding
Retreat Onset (0 ms)

Figure 50

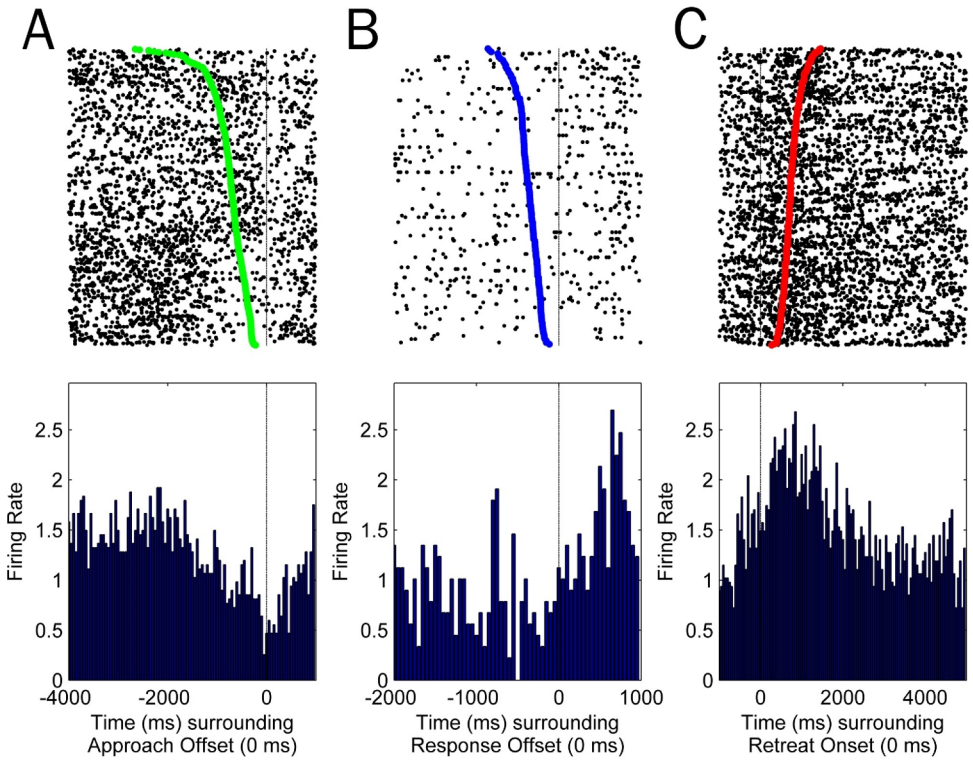
A
B
C
Firing Rate
2.5
2
1.5
1
0.5
0
-4000
-2000
0
Time (ms) surrounding
Approach Offset (0 ms)
-2000
-1000
0
1000
Time (ms) surrounding
Response Offset (0 ms)
0
2000
4000
Time (ms) surrounding
Retreat Onset (0 ms)

Figure 51

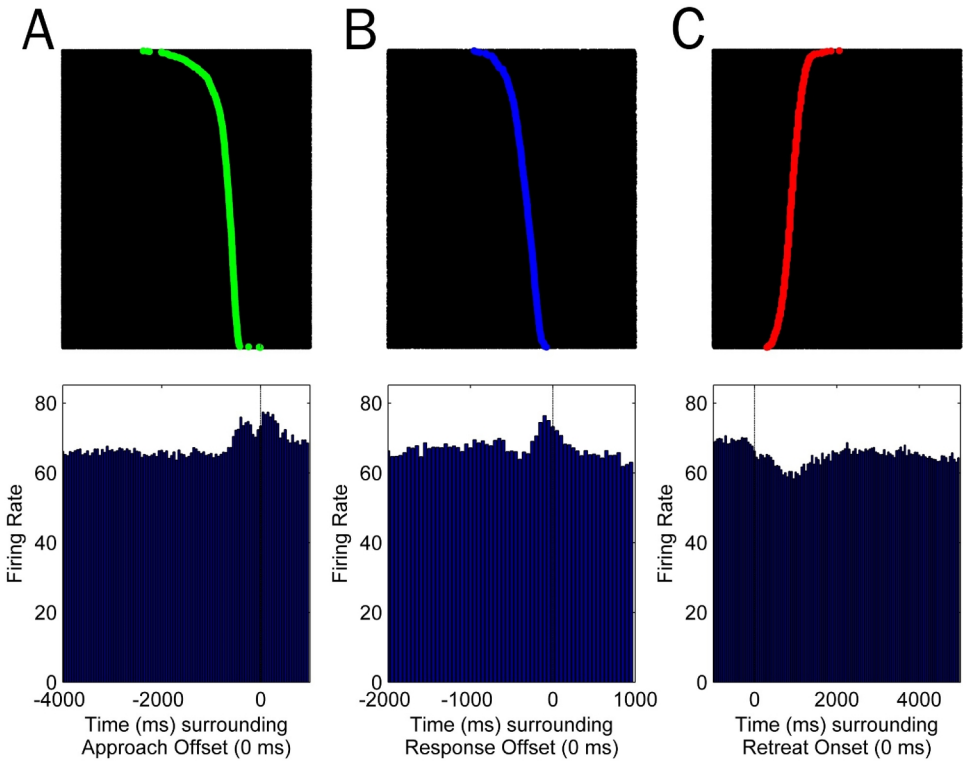
A
B
C
Firing Rate
80
60
40
20
0
-4000
-2000
0
Time (ms) surrounding
Approach Offset (0 ms)
-2000
-1000
0
1000
Time (ms) surrounding
Response Offset (0 ms)
0
2000
4000
Time (ms) surrounding
Retreat Onset (0 ms)

Figure 52

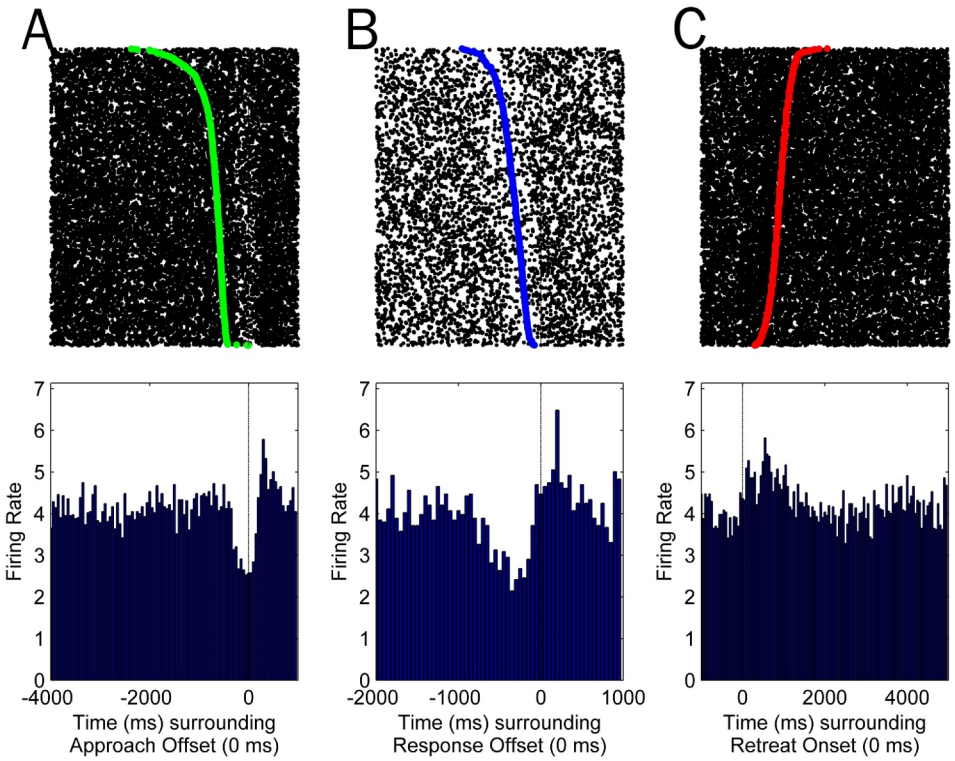
A
B
C
Firing Rate
Time (ms) surrounding
Approach Offset (0 ms)
Time (ms) surrounding
Response Offset (0 ms)
Time (ms) surrounding
Retreat Onset (0 ms)

Figure 53

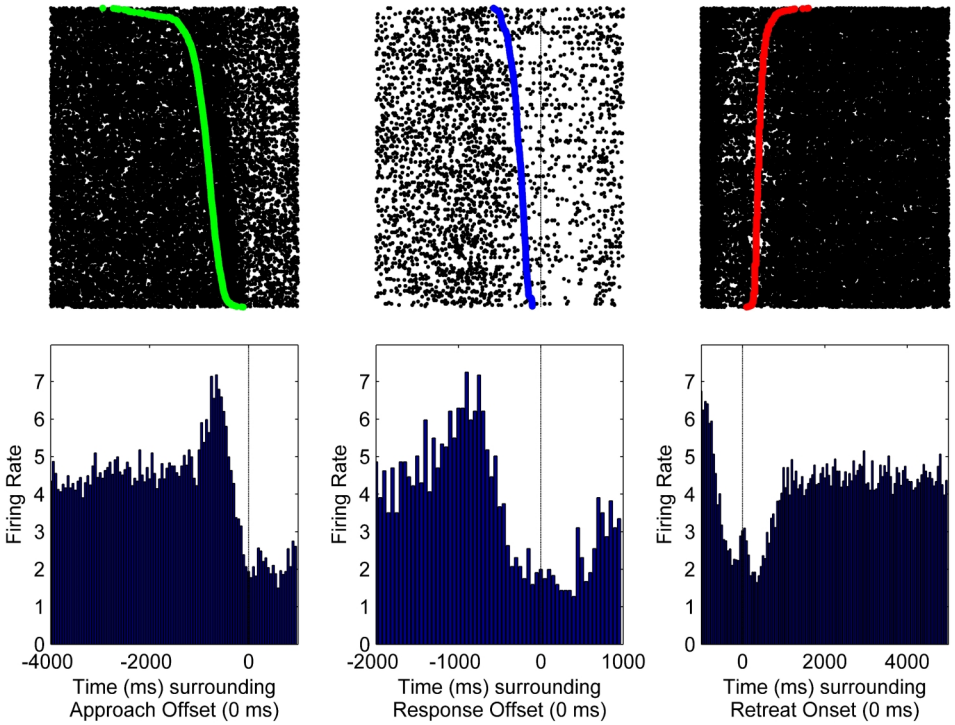
Firing Rate
Time (ms) surrounding
Approach Offset (0 ms)
Time (ms) surrounding
Response Offset (0 ms)
Time (ms) surrounding
Retreat Onset (0 ms)

Figure 54

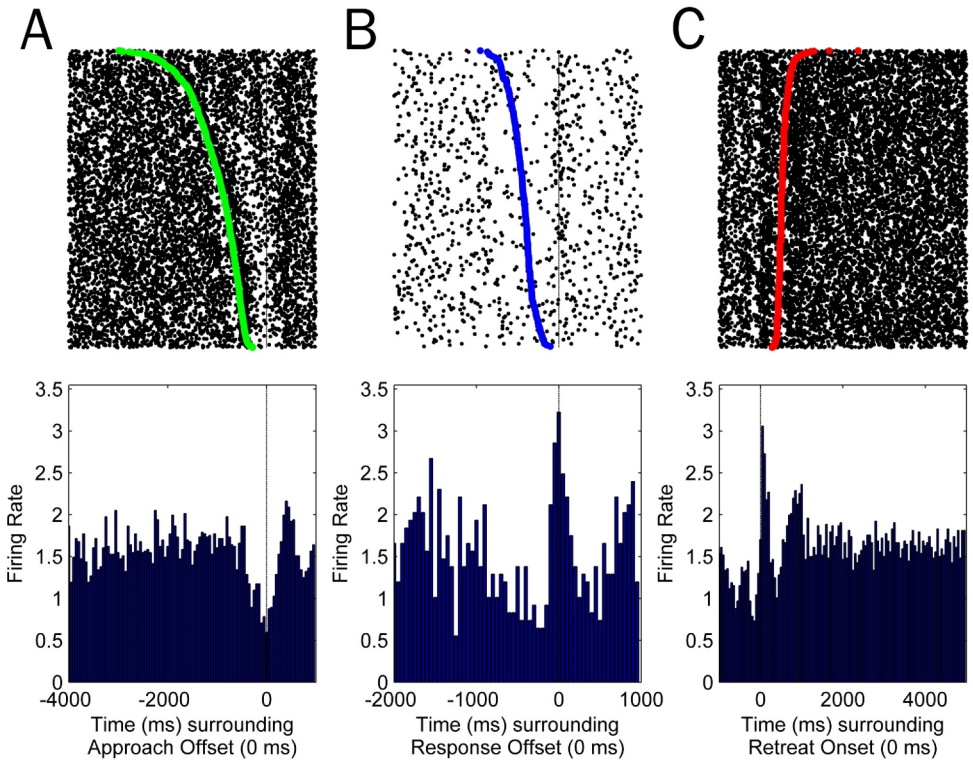
A
B
C
Firing Rate
3.5
3
2.5
2
1.5
1
0.5
0
-4000
-2000
0
Time (ms) surrounding
Approach Offset (0 ms)
-2000
-1000
0
1000
Time (ms) surrounding
Response Offset (0 ms)
0
2000
4000
Time (ms) surrounding
Retreat Onset (0 ms)

Figure 55

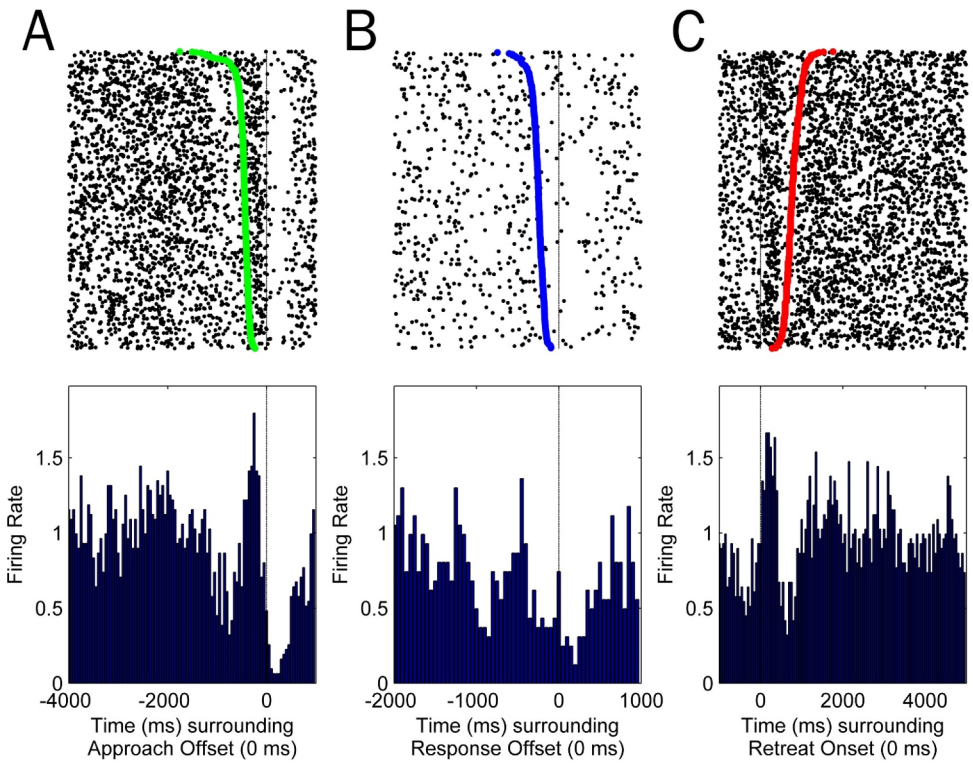
A
B
C
Firing Rate
1.5
1
0.5
0
-4000
-2000
0
Time (ms) surrounding
Approach Offset (0 ms)
-2000
-1000
0
1000
Time (ms) surrounding
Response Offset (0 ms)
0
2000
4000
Time (ms) surrounding
Retreat Onset (0 ms)

Figure 56

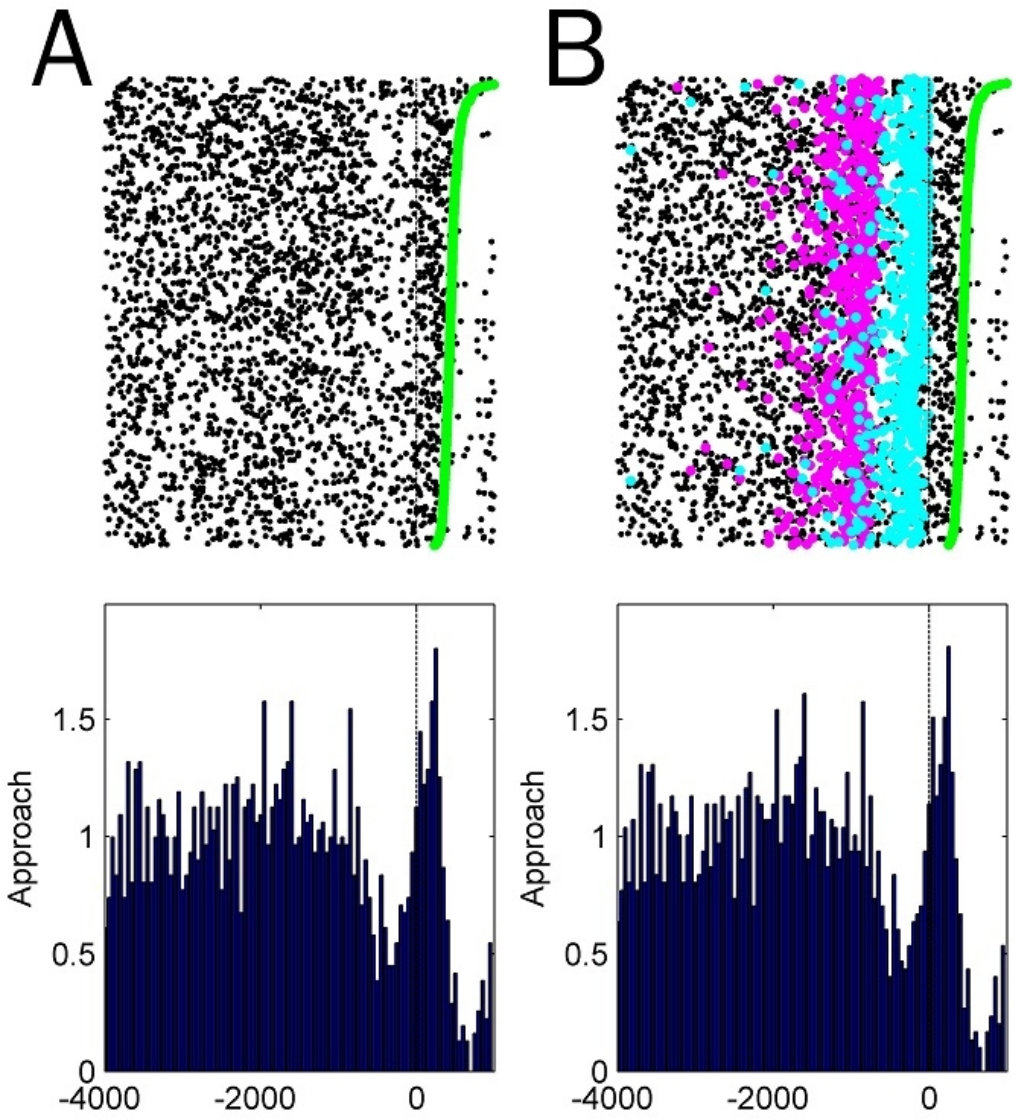

Figure 57

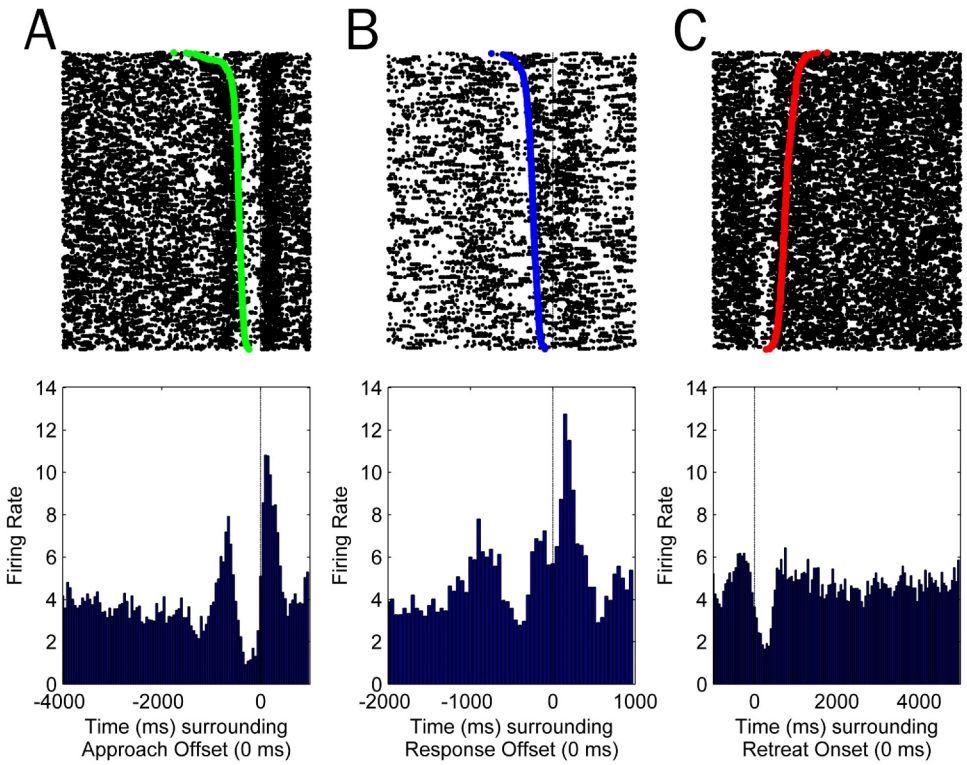
A
B
C
Firing Rate
Time (ms) surrounding
Approach Offset (0 ms)
Time (ms) surrounding
Response Offset (0 ms)
Time (ms) surrounding
Retreat Onset (0 ms)

Figure 58

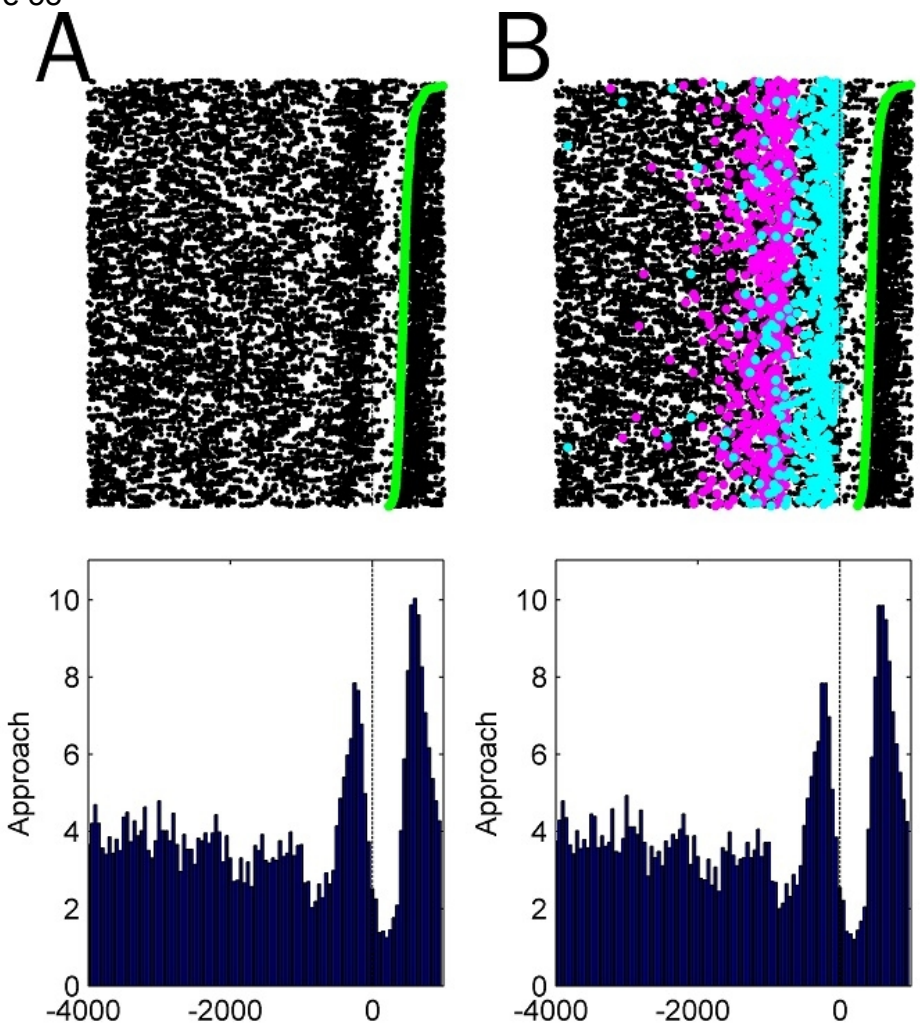
A
B
Approach
10
8
6
4
2
0
-4000
-2000
0
Approach
10
8
6
4
2
0
-4000
-2000
0

Figure 59

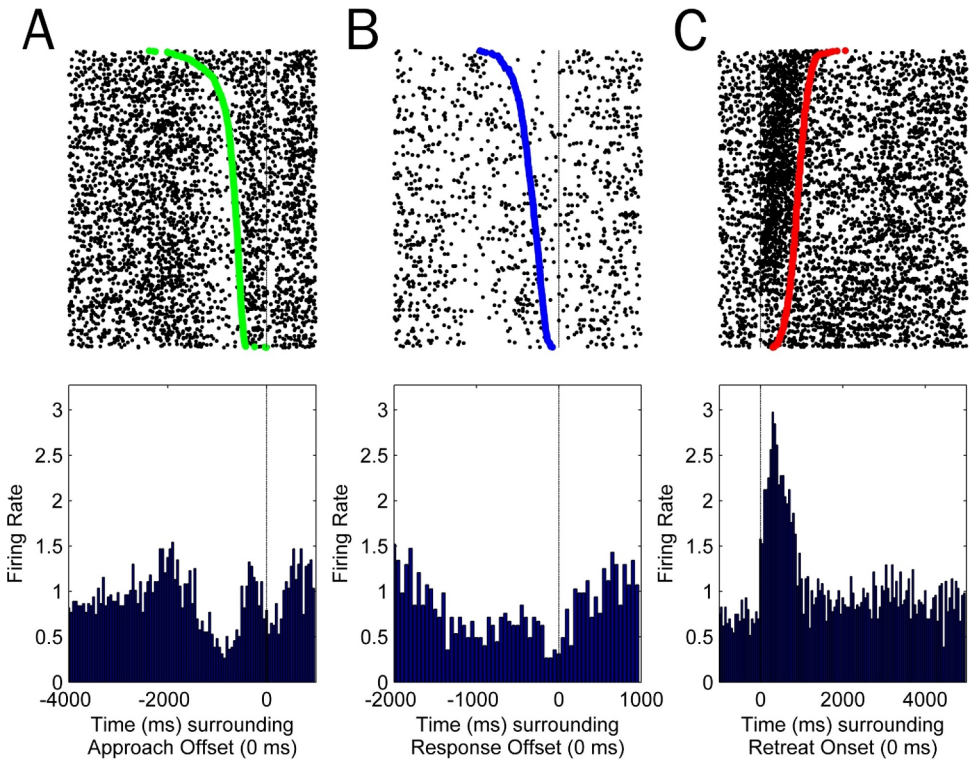
A
B
C
Firing Rate
Time (ms) surrounding
Approach Offset (0 ms)
Time (ms) surrounding
Response Offset (0 ms)
Time (ms) surrounding
Retreat Onset (0 ms)

Figure 60